Surface-enhanced Raman scattering substrates for biomedical sensing

A thesis submitted in fulfilment of the requirements for the degree of

Master of Science (Research)

Jennifer Sarah Hartley

Bachelor of Science (Physics)

Bachelor of Science (App.Sci)(Hons)

Centre for Quantum and Optical Science

Faculty of Science, Engineering and Technology

Swinburne University of Technology

2015

Declaration

I, Jennifer Sarah Hartley, certify:

- except where due acknowledgement has been made, the work is that of the author alone;
- the work has not been submitted previously, in whole or in part, to qualify for any other academic award; and
- to the best of the author's knowledge this thesis contains no material previously published or written by another person except where due reference is made in the text.

Jennifer Sarah Hartley

Centre for Quantum and Optical Science

Faculty of Science, Engineering and Technology

Swinburne University of Technology

Melbourne, Australia

Dated this day,

Acknowledgements

I wish to acknowledge the contributions and support of the following individuals who made it possible for me to complete this body of work.

The most important contribution has to be from my family, especially from my partner Ed, who provided undying support and encouragement. He understood completely the trials and tribulations that a post-graduate student must endure. Thank you for watching and re-watching presentation rehearsals, discussing difficult problems and providing so much motivational support. Huge thanks for training me and giving me access to the material characterisation instruments in the RMMF facility. On that note, I must thank the RMMF facility at RMIT for allowing me to access the large array of material characterisation instruments they have available.

Huge thanks goes to Alex Mazzolini for numerous discussions about my project and all things fibre related. He provided so many useful insights that helped to get me back on track. Alex has been an amazing mentor, both with post-graduate life and for providing the opportunity to teach. Tom Edwards also deserves many thanks for teaching opportunities.

My wonderful Applied Plasmonics group must get credit for listening to all my problems in and out of group meetings and providing some useful bits of information. Some very useful collaborations stemmed from the group to allow breadth to this project. A special thanks to Gediminas for performing contact angle measurements.

A warm embrace for Myintzu, she has been so wonderful and knowledgeable about all those pesky things you don't learn in physics. Thank you so much for training me in the ways of microbiology. You have been a welcome source of companionship.

I would like to thank Kristian for morning chats. Your friendship and understanding was much appreciated, along with your MATLAB wizardry. I would also like to thank Iurii for so many friendly discussions and distractions.

A special thanks to Daniel White, my predecessor, who trained me up on the instruments and gave me a solid grounding of how to complete some initial experiments.

Peter Cadusch created an awesome program for Myintzu which I promptly adopted to use for my work. Thanks for adapting it for me and assisting me with some modelling of fibre mode structures. Your expansive knowledge and skills in modelling optical waveguides was extremely useful. Thank you for all your assistance.

A very big thank you to Andy Moore who made life in the Raman lab so much more enjoyable. You were always there at a drop of a hat to assist when something went terribly and horribly wrong. Thank you for all the interesting discussions, all your help and support.

Finally I must of course thank my supervisor Paul Stoddart for his support and understanding. Together we discovered and solved numerous interesting puzzles. I want to also thank my associate supervisor Saulius Juodkazis for advice, discussions and random detours that helped to further the breadth of my Raman knowledge.

Table of Contents

List of Figures

List of Tables

List of Acronyms

AFM	Atomic force microscopy
BPM	Beam propagation method
CARS	Coherent anti-stokes Raman spectroscopy
CCD	Charge-coupled device
DNA	Deoxyribonucleic acid
EDS	Energy-dispersive spectroscopy
ESEM	Environmental SEM
ETD	Everhart-Thornley detector
FEG	Field emission gun
FRB	Fibre Raman background
HRTEM	High resolution TEM
ICP	Inductively coupled plasma
IR	Infra-red
LHS	Left hand side
NA	Numerical aperture
OAD	Oblique angle deposition
PBS	Phosphate buffered saline
PCF	Photonic crystal fibre
R6G	Rhodamine 6G
RHS	Right hand side
RIE	Reactive ion etching
RMMF	RMIT microscopy and microanalysis facility
RNA	Ribonucleic acid
RSD	Relative standard deviation
SEM	Scanning electron microscopy
SERRS	Surface-enhanced resonant Raman spectroscopy
SERS	Surface-enhanced Raman spectroscopy
STEM	Scanning TEM
TEM	Transmission electron microscopy
TERS	Tip-enhanced Raman spectroscopy
TNT	Trinitrotoluene
UV	Ultraviolet
XPS	X-ray photoelectron spectroscopy

Abstract

This project characterised four potential SERS substrates and then developed these substrates further for application based uses. The first substrate (gold nanoparticles) was deemed unsuitable for most applications due to the strong bands originating from the cross-linker. The second substrate was chosen for suitability with optical fibres. Optical fibres are ideal for remote sensing in biomedical applications as they are biocompatible, minimally invasive, readily available and affordable. Optical fibres can be used as miniaturised probes suitable for in vivo applications. However optical fibres, when coupled with a Raman spectrometer, are a complex optical element which needs to be investigated and fully comprehended in order to determine the ideal parameters needed to address biomedical applications. This project determines those parameters so that future work can be undertaken to customise the probe to sense a specific biological compound of interest.

Standard telecom fibres were investigated as they are readily available and affordable. Multiple fibre types with different numerical apertures (NA), core sizes, mode structure and core/cladding materials were compared as probes. All fibres used in the comparison were manufactured as probes using OAD and thiophenol as a test analyte. Cladding modes were removed by bending each fibre and placing index matching gel on the bend. This was done in an effort to ensure that the mode structure was repeatable for each fibre. Otherwise the cladding modes can interfere with the mode structure in unexpected and random ways, making comparison difficult. This work determined SMF28 had the largest signal to noise ratio when the spectrometer was operated at a wavelength of 514.5 nm with a slit width of 62.5 μm. It was also determined that matching the microscope objective numerical aperture with that of the fibre was not necessary for maximum collection efficiency.

The other two substrates investigated were variations on black silicon (nano-textured, light absorbing silicon) for use as a bacterial identification platform. The substrates were fully characterised for surface chemistry and structure before being implemented as a bacterial sensor. It was determined that the height of the black silicon structures

was not tall enough to fully impale bacteria for reproducible measurements. However, the viability of using an impaling substrate in order to excite the internal constituents of a cell was shown. This will prompt further work into developing an improved technique capable of sensing bacteria.

Chapter 1

Introduction

The overall aim of this research was to develop a miniaturised fibre optic probe and a sensor capable of detecting biological compounds with minimal preparation and fast acquisition times. The currently employed techniques require tagging to identify compounds and thus destroy the sample. A promising alternative is Raman spectroscopy, which does not require tagging. Chapter 1 explores background theory relevant to the project, starting with an explanation of Raman spectroscopy. Surface-enhanced Raman spectroscopy is discussed in detail as this enhancement technique is beneficial for detecting biological compounds. Optical fibres are also discussed as they have potential to be used as remote sensing devices. Finally, some theory on bacteria is presented to tie together all of the necessary information required to understand the research conducted and its significance.

1-1 Raman spectroscopy

Raman spectroscopy is a spectroscopic tool which utilises the process of Raman scattering to identify materials. It is important to first discuss the scattering process before the spectroscopic technique can be explained. Raman scattering describes the inelastic scattering of photons induced by a change in the polarisability of a molecule with respect to its vibrational motion [1]. Raman scattering was first observed by C.V Raman [2] in 1928.

An energy level diagram (Figure 1-1) illustrates the difference between Raman scattering, Rayleigh scattering and infra-red (IR) absorption. During Raman scattering, a molecule absorbs energy (E) from an incoming photon ($E_{incident}$) which excites the molecule from the ground state (g0) to a virtual excited vibrational state ($E_{vibration}$, depicted by the dotted line). The molecule then relaxes to the first excited state (g1) and emits a photon ($E_{scattered}$). The energy of the emitted photon is smaller than the exciting photon as energy was lost during the absorption process [1]. The emitted photon energy reflects vibrational bonds in the molecule that were excited (Equation (1-1)).

$$E_{scattered} = E_{incident} - \Delta E_{vibration} \tag{1-1}$$

The Raman process described above is referred to as the Stokes process and is more commonly occurring than anti-Stokes. Anti-Stokes occurs when a molecule starts in the first excited state, is excited to a virtual excited state then relaxes to the ground state and emits a photon. The Stokes process is of relevance for this project.

During Rayleigh scattering, an incoming photon also excites a molecule from the ground state, to a virtual excited state. However, the molecule relaxes back down to the ground state so the emitted photon energy is the same as the exciting photon. This process of scattering (Equation (1-2)) is more likely than the Raman scattering process.

$$E_{scattered} = E_{incident} \tag{1-2}$$

IR absorption is a direct process which leaves the molecule in the first excited state in contrast to Raman scattering which requires a two-step process of absorption and

emission. This implies causation in IR absorption requiring a much lower energy to reach the first excited state. IR absorption does not scatter, instead all the energy is converted into vibrational energy (Equation (1-3)). IR absorption can occur when there is a permissible change in the dipole moment of the molecule [3].

$$E_{incident} = \Delta E_{vibration} \tag{1-3}$$

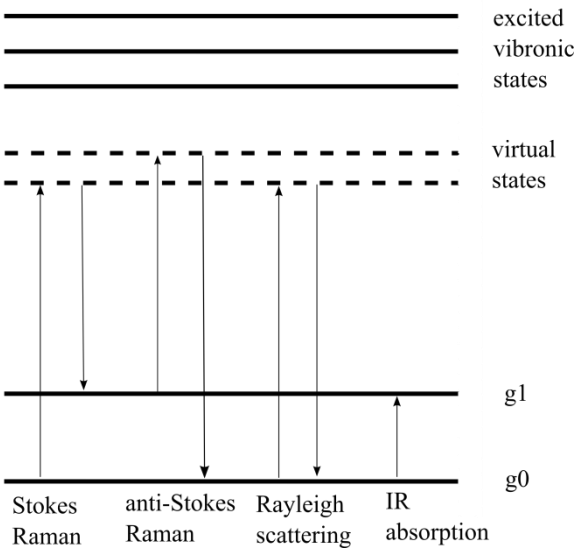

Figure 1-1 Energy level diagram showing various absorption and emission processes.

It is important to note that the Raman process involves a change in the polarisability of the molecule that leads to an induced dipole moment. This is in contrast to IR absorption which directly changes the dipole moment. An induced dipole moment allows transition between vibrational states which form the basis for Raman spectroscopy.

Since its discovery in 1928, Raman spectroscopy has become a widely used vibrational spectroscopy technique, capable of identifying any polarisable molecule and is regarded as a fingerprint analysis technique. This means that every molecule has a unique Raman spectrum, even where the composition is almost identical, as in glucose and galactose (Figure 1-2). This occurs as Raman scattering originates from the bonds in a molecule and each Raman-active vibrational mode is reflected in the Raman spectrum as peaks.

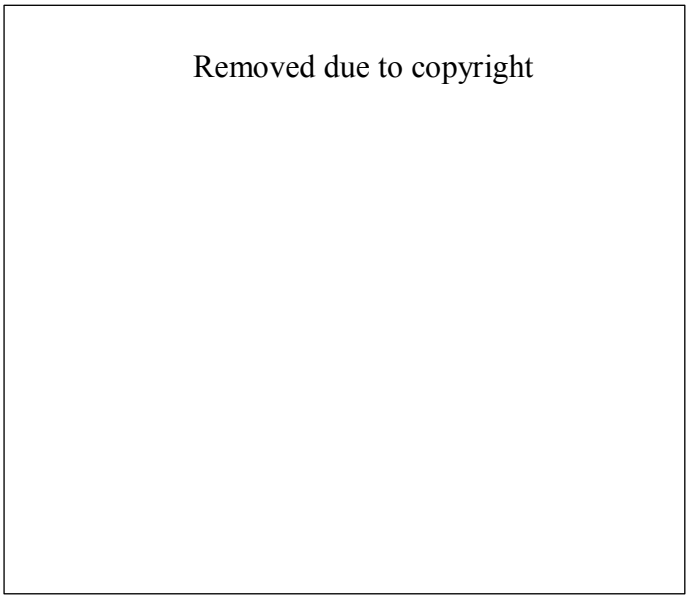

Figure 1-2 Glucose and galactose have almost identical chemical structures; however Raman spectra of the molecules are distinctly different (illumination wavelength of 532 nm).
Reproduced from Lyandres *et al.* [4]

Raman spectroscopy has become a powerful tool since the development of the laser and the implementation of notch filters [5] which remove the strong Rayleigh scattering that otherwise might swamp the Raman signal. The implementation of CCD detectors has also been beneficial due to their increased sensitivity and multiple sensing elements. Raman scattering is a very weak process where approximately 1 in 10 million scattered photons are scattered due to the Raman process. Therefore it can be helpful to enhance the scattering in some practical applications.

Many specialised techniques have branched out, enabling increased sensitivity and signal strength from problematic samples. These include, but are not limited to, Raman optical activity (ROA), surface-enhanced Raman spectroscopy (SERS), tip-enhanced Raman spectroscopy (TERS), coherent anti-stokes Raman spectroscopy (CARS), stimulated Raman spectroscopy, transmission Raman spectroscopy and hyper Raman spectroscopy [6].A notable technique for providing up to 10^8 signal enhancement is surface-enhanced Raman scattering. This technique will be exploited as part of this dissertation.

1-2 Surface-enhanced Raman scattering spectroscopy

SERS is a technique which enhances the Raman scattering cross section by adsorbing the test analyte onto the surface of a nanostructured noble metal [7]. It was originally believed that the enhancement occurred due to additional surface area created by the roughened metal resulting in a greater number of molecules in the area [7]. Later it was discovered that the increase in signal was caused by an interaction between the analyte and the electromagnetic field. The electromagnetic field is increased due to the generation of localised surface plasmon resonances when a molecule is in close contact with a nanoscale metal particle [8]. The metal layer must be nanoscale rough and not a continuous film to allow the generation of localised surface plasmon resonances. Surface plasmon resonance occurs when surface electrons on a material are stimulated by incident light which has the same frequency as the surface electrons. Today, it is widely accepted that the SERS enhancement occurs from two main mechanisms, an electromagnetic and a chemical effect [9].

Smooth surfaces allow non-radiative plasmon waves to propagate in a direction parallel to the surface. In contrast, a roughened metal surface allows a localised resonance that radiates in both a parallel and perpendicular direction. Roughened surfaces allow for incident photons to excite the metal's plasmon resonance which results in scattering. The plasmon excitation caused by incident photons creates a large increase in the electric field within about 2 nm of the metal surface. The adsorbate-electric field interaction is the cause of the increased scattering observed in SERS (Figure 1-3). Hotspots can also occur which are intense localised electric fields formed in the vicinity of nanogaps between particles or protrusions from the metal surface. These localised electric fields are due to a difference in the dielectric constant between the roughened surface and surrounding media. The plasmon field decays exponentially from the metal surface, decreasing to about 10% of its peak value at a distance 2 nm from the surface. The electromagnetic effect is present for all molecules regardless of the adsorption method (chemisorbed or physisorbed).

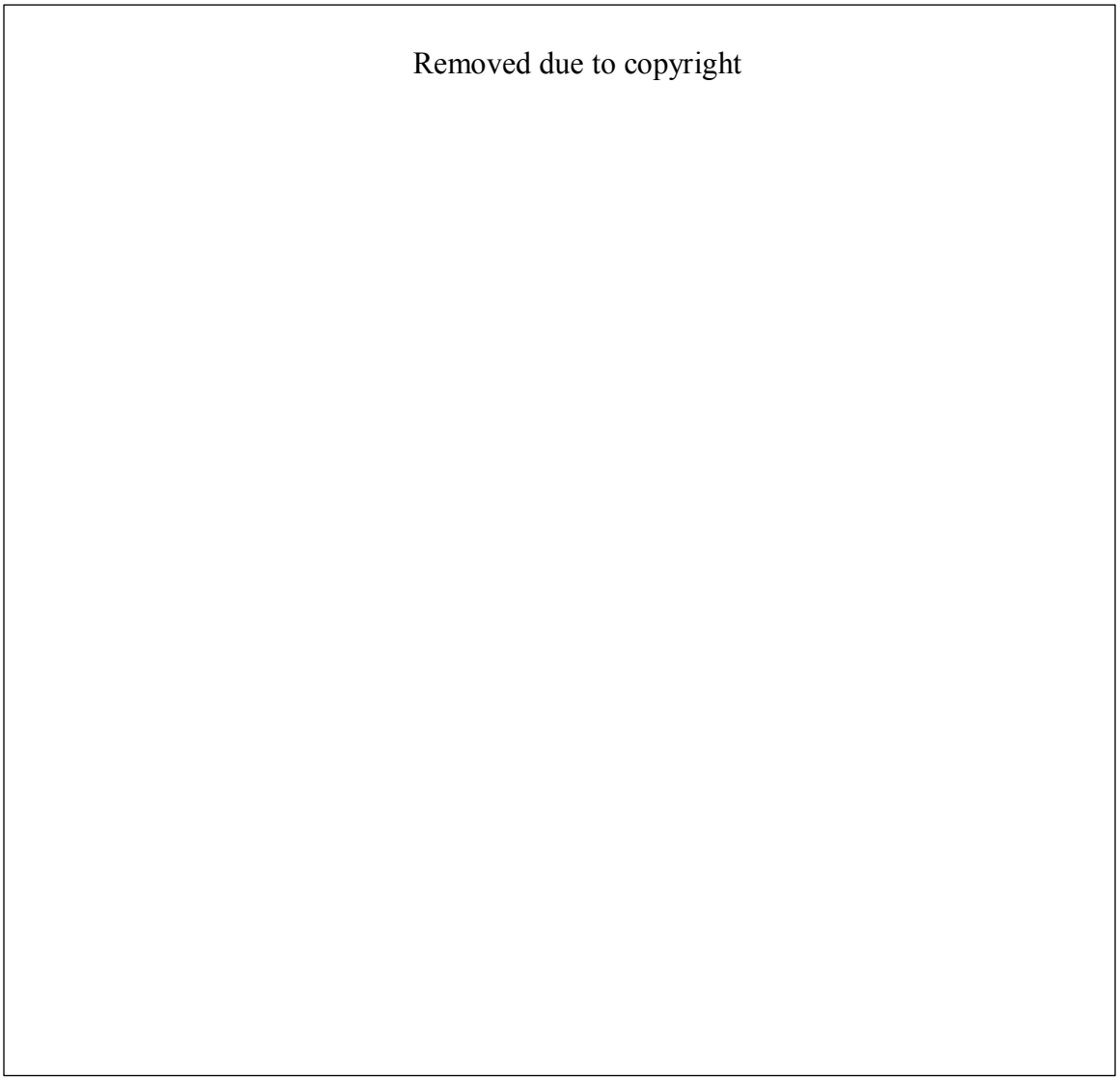

Figure 1-3 Schematic diagram of electromagnetic effect SERS process, reproduced from White [10].

The chemical effect occurs when a molecule is adsorbed by forming a chemical bond directly onto a noble metal surface. The enhancement is not present for all molecules and it occurs alongside the electromagnetic effect. The adsorption produces a larger Raman cross-section than when the molecule was free due to a charge transfer between the molecule and the surface, altering the polarisability of the adsorbed molecule. The molecules adsorb onto the metal surface and create an adsorbate-metal complex which allows for a ready transfer of electrons to and from the adsorbed molecule. This enhancement is dependent on the molecule being adsorbed onto the metal. Therefore the enhancement experienced is reduced exponentially as a function of molecule-metal distance and is confined to a region of about 2 nm.

The electromagnetic and chemical enhancements should be considered when fabricating a substrate. SERS relies on adsorption and scattering from the surface which can be affected by the size and shape of the structures. Raman scattering can only occur from an induced dipole moment, so if the particles are too large they will create multipoles which are non-radiative. On the other hand, if the particles are too small they will not be conductive and hence will not enhance the electric field. A substrate should also be highly uniform and produce a high enhancement. To take advantage of the added chemical effect, the surface should promote binding for the analyte to be tested.

Enhancements to the Raman signal on the order of 10^8 can be achieved with a successfully roughened surface and appropriate metal layer [11]. Gold, silver and copper are the most enhancing metals and a thickness of approximately 100 nm is usually sufficient. These enhancements to the scattering in Raman spectroscopy have allowed for analytes which have a small scattering cross-section to be investigated in greater detail [12]. It has also allowed for low concentrations to be detectable and single molecule detection can also be achieved [13].

1-3 SERS substrates

There are many practical considerations to take into account when designing a suitable SERS substrate [14]. The substrate must be reasonably enhancing yet more importantly it must be reproducible and have limited variability across the surface. Commercial substrates such as Klarite have highly ordered structures yet even they are susceptible to variability [15]. One explanation is that highly ordered structures can create intense localised electric fields which can easily interact with neighbouring structures and cause heating that drives surface diffusion. Randomly roughened surfaces appear to have a higher level of reproducibility and can have similar enhancement factors to highly ordered surfaces [15]. Examples of successful SERS substrate fabrication techniques are:

- Etching a surface to produce pyramids or conical shapes which are then covered with a metal [16];
- Depositing metal over a layer of nanospheres [17];

- Blasting a surface with sand to produce a rough texture before coating [18];
- Depositing metal on a substrate using oblique angle deposition (OAD) [19] which creates metal island films or nanorods depending on deposition time; and
- Using a femtosecond laser, writing a rippled structure [15] onto a substrate and then coating with metal.

When designing a SERS substrate it is important to select a noble metal that will be compatible with the analyte and will create the highest enhancement factor. A theoretical plot modelled by Schatz [20], shown in Figure 1-4, clearly shows the wavelength regions in which various metals are ideally used. Silver has a high enhancement over the visible region (Figure 1-4) and is fairly cheap which is why it is routinely chosen over gold. It should be noted that the model in Figure 1-4 is based on colloidal particles. Although it shows useful trends, they may not translate exactly to nanostructured substrates.

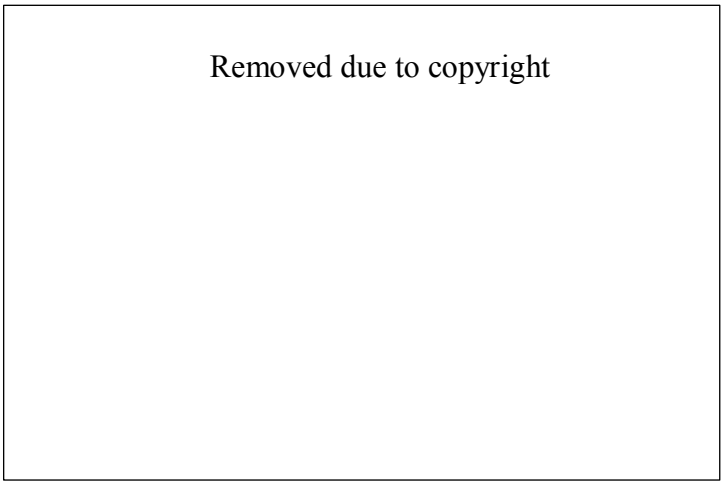

Figure 1-4 Calculated Raman enhancement vs wavelength for various SERS metals. Reproduced from Schatz, Fig 4 [20].

1-3-1 Nanoparticles as a SERS substrate

Strong electric field enhancement near Au nanoparticles is actively employed in SERS to detect and identify biological and chemical species of interest in “in vitro” [21-23] and “in vivo” [24] geometries. However, there is the concern of toxicity for most commonly used fabrication techniques [25, 26]. The toxicity of the nanoparticles

originates from reducing agents used during fabrication which results in surface contamination. This contamination also has contributing Raman bands which can swamp the analyte signal [27]. New techniques for creating nanoparticles are currently underway which do not require the stabilising citrate layer responsible for toxicity. One example of such a technique is ultra-pure laser-ablated nanoparticles[28].

1-3-2 Silver-island films as a SERS substrate

Silver-island films can be created by a few methods; however the most notable is oblique angle deposition [19]. This method relies on evaporation of silver onto a sample where the angle between source and sample is 86°. This causes the growth of nanoscale islands when thicknesses (measured on an equivalent planar surface at normal incidence) of around 100 nm are deposited and nanorods when thicknesses of upwards of 200 nm are deposited. These substrates have proven to be highly repeatable SERS platforms with moderate enhancement factors. The fabrication process is reasonably fast and inexpensive.

1-3-3 Black silicon as a SERS substrate

Black silicon is a by-product of dry etching silicon which results in the surface strongly absorbing visible and infrared light and having low reflectivity, thus appearing black. The dry etching process causes sharp needles to grow from the silicon. As this surface is also a semiconductor, black silicon has been successfully used for sensing techniques. Black silicon has been used for such sensing techniques as surface-enhanced Raman spectroscopy (SERS) [29], terahertz [30] and solar cells [31-34].

Black silicon structures can vary from high aspect ratio needles [29] to small aspect ratio pyramidal shapes [35]. Both of these structures have been used in this work to create SERS substrates by coating them with thin films of gold.

1-4 Optical waveguides

1-4-1 Introduction to optical fibres

Common telecommunication fibres are composed of silica with dopants in the core or the cladding. Generally, the core is doped with germania, phosphorus pentoxide or aluminium oxide which increase the refractive index [36]. Alternatively the core can be kept pure and the cladding doped with either fluorine or boron (this lowers the refractive index of the cladding) or both core and cladding can be doped. This meets the condition of total internal reflection ($n_{co}>n_{cl}$ where n is the refractive index of the core (*co*) and cladding (*cl*)) so that if light is coupled into a fibre, it will propagate along the core (Figure 1-5). Normally, there are some rays that will leak into the cladding and propagate, though these modes will decay given enough distance (typically around 2 m, but up to 20 m may be required to ensure the complete removal of cladding modes).

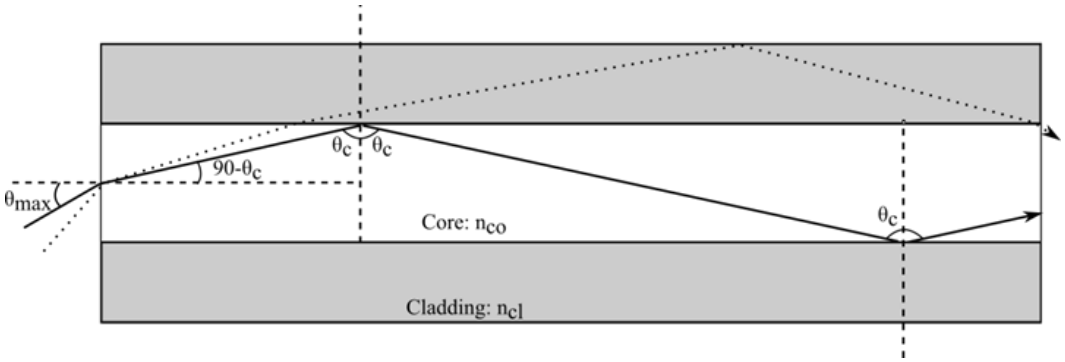

Figure 1-5 Optical fibre schematic showing core and cladding modes.

Optical fibres are attractive for use in Raman spectroscopic probes due to their remote sensing capability, thermal and chemical passivity, and compact size [37]. In order to implement SERS in biomedical sensing applications an optical fibre SERS probe could potentially be used to perform measurements *in vivo* with minimal invasiveness. Optical fibres are ideal candidates for probes due to their ability to analyse compounds remotely. This feature is valuable for the biomedical, security and biohazard industries due to the relatively non-contact and non-invasive nature of an optical fibre probe. Optical fibres are also biocompatible which makes them attractive for biosensors. Optical fibres, when coupled with Raman spectrometers, create a complex optical

element which needs to be completely understood in order to create the most efficient SERS probe. Optical waveguide theory provides the necessary equations to model and explore the complex system in more detail. The main reference for the following discussion is Snyder and Love [38]. Unless stated otherwise, all equations are sourced from Snyder and Love.

1-4-2 Step index weakly-guiding fibres

The refractive index profile of a fibre is a useful way of classifying different fibres based on their structure. Two standard ways of constructing fibres exist; the refractive index can have a sharp discontinuity at the core-cladding boundary (step index) or the refractive index can vary smoothly over the core (graded-index). This is shown diagrammatically for clarity in Figure 1-6 where *r* is the distance across the fibre.

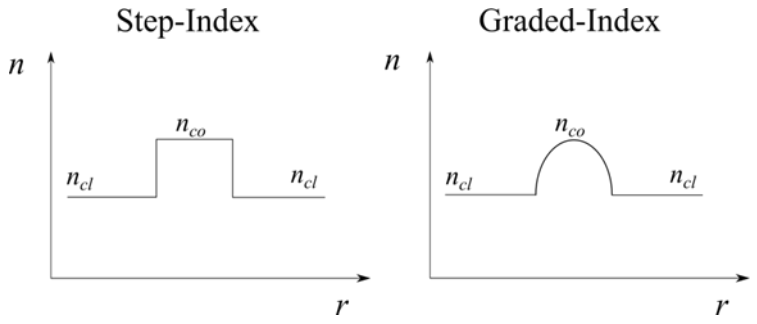

Figure 1-6 Refractive index profiles for step-index and graded-index fibres.

Weakly-guiding step index fibres form the majority of commercial glass fibres. A fibre is weakly-guiding if n_{co} is very close to n_{cl}. This approximation will be used as it greatly simplifies the waveguide analysis for step-index fibres. There are a few important optical fibre parameters that must be defined prior to attempting to solve the wave equations for modal analysis.

Numerical Aperture (NA)

The numerical aperture describes the light gathering capability of the fibre. It can be thought of as a cone of collection angles where any light outside of the cone cannot be propagated in bound modes. The NA can also be defined by the difference in refractive

index of the core and cladding as seen in Equation (1-4) where the incident beam is in a medium of refractive index *n* before entering the core.

$$NA = \sqrt{n_{co}{}^2 - n_{cl}{}^2} = n \sin \theta_{\max} \tag{1-4}$$

Another way of visualising the light gathering capability of a fibre is known as the solid angle. To convert the NA to solid angle (Ω), Equation (1-5) was used with n=1 in air:

$$\begin{aligned} \Omega &= 2\pi(1 - \cos(\theta_{\max})) \\ \theta_{\max} &= \sin^{-1}(NA) \end{aligned} \tag{1-5}$$

Fibre Parameter/Normalised Frequency (V)

The fibre parameter is a measure of the number of allowable modes a fibre can propagate. However, not all light that is accepted into the fibre propagates solely along the core. Some rays leak into the cladding and propagate for 2-20 m before decaying. The fibre parameter (V) is defined in Equation (1-6) where ρ is the core radius and λ is the source wavelength.

$$V = \frac{2\pi\rho}{\lambda} NA \tag{1-6}$$

Modal Propagation Constant (β)

The propagation constant is a fundamental modal property. Every mode l will have its own propagation constant which is determined by solving the eigenvalue Equation (1-7) . In order to determine β_l, Equation (1-7) must be solved either numerically or graphically.

$$\frac{J_{l-1}(U)}{J_l(U)} = -\frac{W}{U}\frac{K_{l-1}(W)}{K_l(W)} \tag{1-7}$$

U and W are transverse components of the wave vector in the core and cladding respectively. $J_l(U)$ and $K_l(W)$ are Bessel functions of the first kind and modified Bessel

function of the second kind respectively. The equation must be plotted as a function of U where the LHS and RHS are plotted separately and the intersect points are solutions to the equation (Figure 1-7). Thus U can be found and then β_l and W can be calculated from Equations (1-8) - (1-11) if V is known.

$$V = \sqrt{U^2 + W^2} \tag{1-8}$$

$$U = \rho(n_{co}^2 k^2 - \beta^2)^{1/2} \tag{1-9}$$

$$W = \rho(\beta^2 - n_{cl}^2 k^2)^{1/2} \tag{1-10}$$

$$k = \frac{2\pi}{\lambda} \tag{1-11}$$

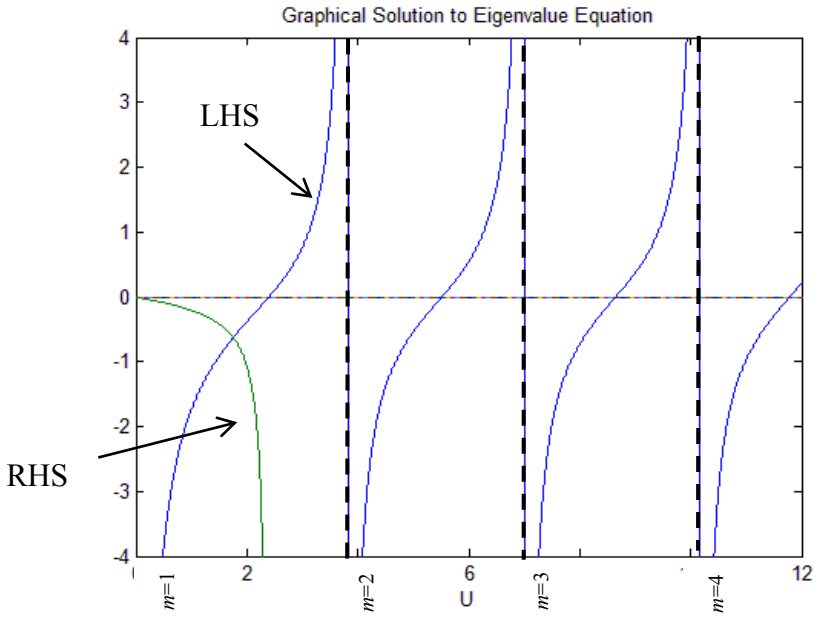

Figure 1-7 An example of graphically solving the eigenvalue equation showing the intersect between the left hand side (blue curve) and the right hand side (green curve) of the equation. Parameters l=0, λ=1.55 μm, NA=0.14, ρ=4.1 μm were input into Equations (1-7) - (1-11). The dotted lines represent the asymptotes. Starting from m=1 in the lower pane, each blue curve represents an integer value of m.

Mode Intensity Patterns

In the weakly-guiding approximation fibre modes are referred to as linear polarization modes (LP_{lm}). Modes are characterised based on the azimuthal and radial distributions l and m respectively. The fundamental mode occurs at LP_{01}. A visual guide to the mode profile of a fibre can be determined by calculating the intensity using Equation (1-12). This representation is useful as it shows clearly the mode structure that would be exciting any sample at the end-face. The intensity must be calculated for each LP_{lm} mode that the fibre can sustain.

$$\begin{aligned} I_{co} &= J_l^2\left(\frac{rU}{\rho}\right)\cos^2(l\phi) \\ I_{cl} &= \left(\frac{J_l(U)}{K_l(W)}\right)^2 K_l^2\left(\frac{rW}{\rho}\right)\cos^2(l\phi) \end{aligned} \tag{1-12}$$

where I_{co} and I_{cl} refer to $r \leq \rho$ and $r > \rho$ respectively.

The mode profile differs greatly for different lm combinations as seen in Figure 1-8. The physical meaning of l and m also become clear: m is the number of maxima along the fibre radius and l is half the number of maxima around the circumference. Visually it can be seen that increasing m means increasing the number of concentric rings, whereas increasing l increases the number of angularly distributed lobes.

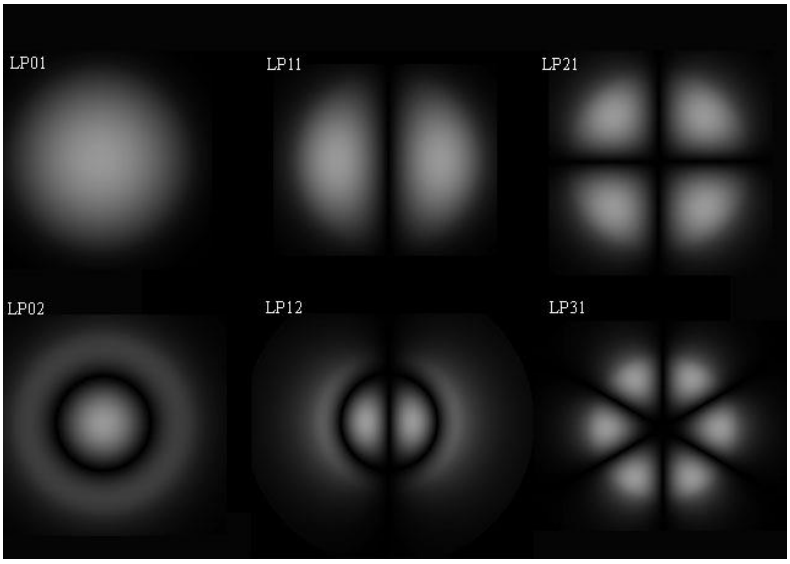

Figure 1-8 Mode profiles showing the differing structure for various *lm* combinations. Profiles simulated using code created by Peter Cadusch.

A standard telecommunication fibre, SMF28, was used as a model for simulating the intensity patterns at non-standard wavelengths. SERS is performed at visible or near infra-red wavelengths, while standard telecommunication fibres are designed to operate in the infrared (1310 or 1550 nm). Therefore, while SMF28 is designated a single mode fibre at 1550 nm, it will not be single mode at 514 nm (common SERS wavelength).

The mode profile for SMF28 was simulated with the following input parameters using MATLAB:

λ= 514 nm

ρ= 4.1 μm

n_{co}= 1.47

n_{cl}= 1.4633

NA= 0.14

The simulation resulted in two modes, LP_{01} and LP_{02} as shown in Figure 1-9. As expected, no cladding modes appear in the simulation due to the assumption of equilibrium in the modal equations and no length dependence. Therefore, this simplistic approach is not suited to short lengths of fibre (25 mm). Simulating short lengths of

fibre to include non-equilibrium modes is beyond the scope of this thesis. The simplistic approach presented here is useful for confirming mode patterns at non-standard operating wavelengths which are relevant to SERS.

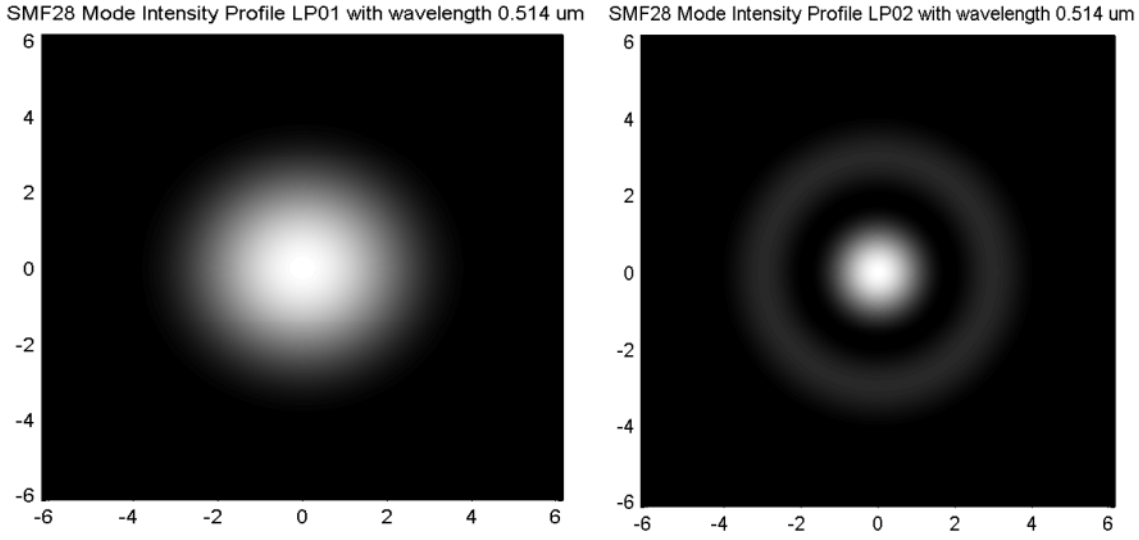

Figure 1-9 Mode intensity profile over the core (distance in μm) for SMF28 using an excitation wavelength of 514 nm.

1-5 Optical fibre SERS probes

1-5-1 Optical fibre selection

In general, the use of optical fibre probes in Raman spectroscopy can be categorized as "extrinsic" or "intrinsic" [39]. Where the fibre is simply used to link the spectroscopic instrumentation to the sampling point, it is referred to as an extrinsic probe. In intrinsic probes, the waveguide itself plays a role in the measurement process. For example, hollow waveguides can be used for the measurement of gaseous or liquid analytes, with long path lengths being possible if the analyte solution has a higher refractive index than the hollow-fibre material [39, 40].

Intrinsic sensing approaches are attractive for SERS, where a nanostructured metal surface is required to generate the enhanced scattering signal. The SERS substrate can be drawn into the core of a hollow fibre [41, 42], or can be deposited directly on the end-face of a solid core fibre in an optrode configuration [18, 19, 37]. In either approach a single fibre can be used for both excitation and collection from the analyte.

These different modes of sensing have a major bearing on the potential for miniaturising Raman probes. Normal Raman scattering is a relatively weak effect that scales with the sample volume. This favours high throughput probes based on large-core, high-NA fibres. However, these fibres generate additional Raman background, which may swamp the signal if it is not removed by bulk optical filters. Consequently the smallest reported extrinsic Raman probe has a diameter of 600 μm [43]. Recent work has shown that the filters can be removed by using a hollow-core photonic-crystal fibre to deliver the excitation with reduced background [44], while fibre Bragg gratings can be used in the collection fibres to remove the Rayleigh scattering [45]. In this way the probe diameter could in principle be reduced to less than 400 μm.

In contrast to normal Raman, SERS can provide significant signal amplification (on the order of $10^6 – 10^8$) for analyte molecules adsorbed on a SERS-active metal surface. When combined with the single-ended optrode sensing approach, the size of intrinsic SERS probes could potentially be significantly reduced. Indeed, the potential for miniaturisation has been demonstrated by the recent progress in tip-enhanced Raman scattering [46]. However, TERS generally relies on high NA microscope objectives to collect externally scattered light and remains a highly specialized technique that is best suited to applications requiring high spatial resolution. Thus there remains a need for robust and alignment-free miniaturised SERS probes in a broad range of chemical and biological trace sensing applications [47]. Miniaturised SERS probes have particular potential for biomedical applications, including remote testing for cancer [48], or for minimally invasive continuous glucose measurements [49].

Despite these important potential applications, there have been relatively few studies on the optimal characteristics of optical fibres for SERS optrodes. The relationship between SERS intensity and fibre NA, core size and material must be optimized to achieve the best sensing performance. The importance of matching the source area and solid angle (étendue) to the spectrometer entrance slit has been appreciated for extrinsic Raman probes [50]. Recent work on the collection efficiency of an intrinsic SERS probe based on multi-mode telecommunication fibre has suggested that the numerical aperture of a fibre should be matched to the NA of the excitation/collection objective (Figure

1-10), while the fibre core size should match the projection of the spectrometer slit onto the fibre [51]. The throughput of the combined optical fibre-spectrometer system can be described by:

$$\frac{I_{rem}}{I_{dir}} \propto \left(\frac{\Omega_{fib}}{\Omega_{obj}}\right) \int_0^{\infty} \int_0^{2\pi} \int_0^{\alpha} f(r,\theta,z) r dr d\theta dz \qquad (1\text{-}13)$$

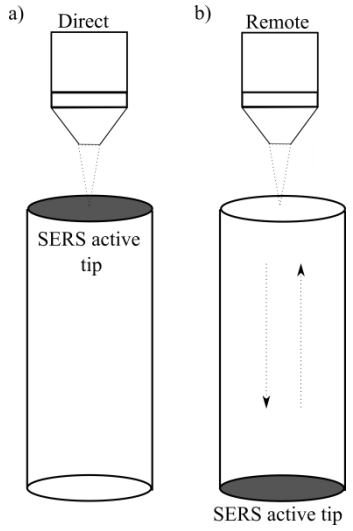

Figure 1-10 Fibre collection geometries: a) direct and b) remote SERS measurements.

where I_{rem} is the intensity of the scattered light collected through the optical fibre, I_{dir} is the intensity collected directly from the SERS substrate, with both quantities normalized against the respective excitation powers at the SERS substrate; Ω is the solid angle of the fibre/objective, α is the radius of the spectrometer entrance pinhole projected onto the fibre core of radius ρ (the source) and the integral of $f(r, \theta, z)rdrd\theta dz$ defines the overlap between the collection region of the objective and the distribution of scattered light [51]. The cylindrical coordinates (r, θ, z) represent the radial, azimuthal and vertical coordinates of the fibre, with positive z inside the fibre. However, this model does not explicitly account for out of focus rays which can broaden the cone of signal collected from the sample. This must be considered in the optical fibre case as the sample is transparent. Therefore the integral must be altered to account for these out-of focus components in the z plane [52] as follows.

$$\int_0^{\infty}\int_0^{2\pi}\int_0^{\alpha} f(r,\theta,z)\,r\,dr\,d\theta\,dz = \left(\frac{\alpha}{\rho}\right)^2 \int_0^{\infty} g(z)\,dz \tag{1-14}$$

$$\frac{I_{rem}}{I_{dir}} \propto \left(\frac{\Omega_{fib}}{\Omega_{obj}}\right)\left(\frac{\alpha}{\rho}\right)^2 \int_0^{\infty} g(z)\,dz \tag{1-15}$$

The integral of *g(z)dz* is the signal contribution from out-of-focus rays. This modified version of the model is more suited to the applications in this project involving transparent substrates. In principle this ratio can exceed unity, due to the additional enhancement that arises in reverse excitation due to the recently proposed Fresnel mechanism, where boundary matching conditions cause an increase in the electric field for excitation through the dielectric [53].

In previous studies of extrinsic probes [43, 54, 55], the spectrometer slit was made sufficiently large that the fibre core projection was not restricted. However, these large slit sizes may reduce the resolution of the spectrometer and are not indicative of the slits used in practical applications.

From the preceding discussion, there is a lack of reliable data regarding fibre selection for miniaturised SERS optrodes. Therefore, this work explores the SERS collection efficiency of silica-based fibres with core sizes ranging from 3.0 to 62.5 µm. Although it is known that silica fibres tend to produce less background than other fibre materials, this hasn't been systematically tested for smaller core fibres in the SERS optrode configuration [18, 43]. Therefore, a comparison of low- and high-doped fibres will be presented. Furthermore, to investigate the relationship between core size and fibre Raman background, this work used a slit width that is relevant to practical applications (i.e. corresponding to 1 cm^{-1} spectral resolution). This allows fibres that have a range of different NAs to be characterized with a range of microscope objectives in order to confirm the effects of fibre NA and core size on SERS probe performance.

1-5-2 SERS substrates

Optical fibres also provide a unique challenge for creating appropriate SERS substrates. If the substrate is on the tip of the fibre in the optrode configuration, only one fibre is

required for both excitation and collection, which eliminates any alignment issues [37]. However, the substrate must be reasonably transparent otherwise it may act as a mirror and the analyte will not be excited efficiently [37].

There have been many different methods explored for fabricating nanostructured surfaces on the tip of an optical fibre. Viets and Hill [18] have attempted a range of techniques to determine the most enhancing substrate available on optical fibres. They compared an evaporation method, dry coating method and sandblasting method for durability, enhancement and repeatability. The parameters and results are shown in Table 1-1. Fibres were cleaved and no cleaning was performed prior to substrate preparation as this was shown to have no effect. The enhancement was similar for each method, although the evaporation technique had the lowest relative standard deviation (RSD) and the highest ratio of remote to direct signal collection. This method therefore proves to be the superior choice for performance and convenience.

Table 1-1 Comparison of fibre optic SERS substrate techniques from Viets and Hill [18].

Technique	**Method**	**RSD**	**Durability**	**Remote/Direct**
Evaporation	5 nm silver deposited on tip at a rate 0.006 $nm.s^{-1}$	20 %	Island films easily detachable	5 × enhancement in remote geometry
Dry coating	Dip coated in alumina nanospheres. 2 nm chromium (0.03 $nm.s^{-1}$) then 75 nm (0.2 $nm.s^{-1}$) silver evaporated directly on alumina.	42%		
Sand blast	Silicon sand blast for 1 min, diameter 135 µm, pressure of 4 bar. Chromium and silver deposition as above.	38%	Highest durability	3.6 × enhancement in remote geometry

Jayawardhana *et al.* [19] also investigated using an evaporation method to create SERS substrates on the tips of optical fibres. The procedure consisted of a 2 nm chromium layer sputtered directly onto the tips, and then 100 nm of silver was deposited using oblique angle deposition (deposition rate of 0.05 $nm.s^{-1}$), where the angle between the tips and the source was 86°. This angle provided the largest enhancement factor and 100 nm was chosen as it created metal island films instead of rods. Rods occurred at larger thicknesses, which resulted in reflection losses when exciting remotely.

Optical fibres, due to their unique structure, have the added benefit of exploring angle substrates simply by polishing the tip at an angle prior to substrate fabrication. This has been shown to increase the enhancement by up to 20 times [56]. Viets and Hill tested multiple angles with the same three techniques as shown in Table 1-1 and determined that the largest enhancement occurred at 40° with the dry coating technique. They show good reusability and durability and can even be used to sense thiophenol with a fibre length of up to 17 m [56].

Conically etched tips [57] take the angled tip idea one step further by etching steep sides on either side of the core. An angle of 10° provided the highest enhancement due to laser light reflections within the cone. The tips were etched with 40% hydrofluoric acid. Then the substrate was prepared by depositing 75 nm of silver onto the core. These fibre probes are reusable and the angle of 10° makes these fibres more enhancing when compared to non-angled tips (three times enlarged signal).

Another technique of preparing a SERS substrate on a fibre tip is photochemical modification [58]. A fibre is dipped into a silver salt solution and light from a 514 nm laser is coupled into the polished core. Silver nanoparticles form on the dipped end of the core in concentric rings, thereby creating the SERS substrate. The laser power, exposure time and area illuminated all contribute to the final pattern. The largest enhancement, comparable to silver island films, occurred after a short deposition time of 4.5 mins. This makes the photochemical modification technique a fast, cheap and controlled method of deposition.

Nanoimprinting the tip of an optical fibre is a novel way of creating a SERS substrate [59]. The method involves imprinting a pattern from a shim onto a fibre using a curable polymer layer on the tip. This technique could be implemented with a wide range of patterns. A promising new pattern has been created using black silicon [29] which could be transferred to a shim and then an optical fibre tip.

Optical fibres have been shown to be highly flexible platforms for creating SERS substrates. A single fibre could be used to remotely detect biological and chemical agents in a safe non-invasive and non-contact controlled environment. They are highly

enhancing when used remotely due to the Fresnel near field effect [53] and have a reasonable repeatability. It is for these reasons that optical fibres have been investigated in this project as a potential application-based sensing probe. The OAD technique was implemented in this work due to high repeatability, cheap production and reasonable enhancement.

1-6 Bacterial identification

Unless otherwise stated, the following discussion refers to the text *Bacteria and Viruses* [60].

1-6-1 Introduction to bacteria and bacterial identification

There are two basic cells which are the basis for all living organisms: eukaryotic, which contains plants and animals, and prokaryotic, which contains bacteria and archaea. The main distinction between the two types of cells is the location of the genetic material; eukaryotic cells separate the genetic material from the rest of the cell by enclosing it in a nuclear membrane, where as prokaryotic cells have no separation. Prokaryotic cells are simpler in design than eukaryotic cells (Figure 1-11). They do not require specialised structures to perform functions (i.e. organelles to store genetic information, to convert light and chemicals to energy and to digest nutrients). The genetic information in prokaryotic cells is simpler and their ribonucleic acid is an exact copy of the genes (not modified). This simpler design and lack of specialised structures allows for fast growth and division of cells.

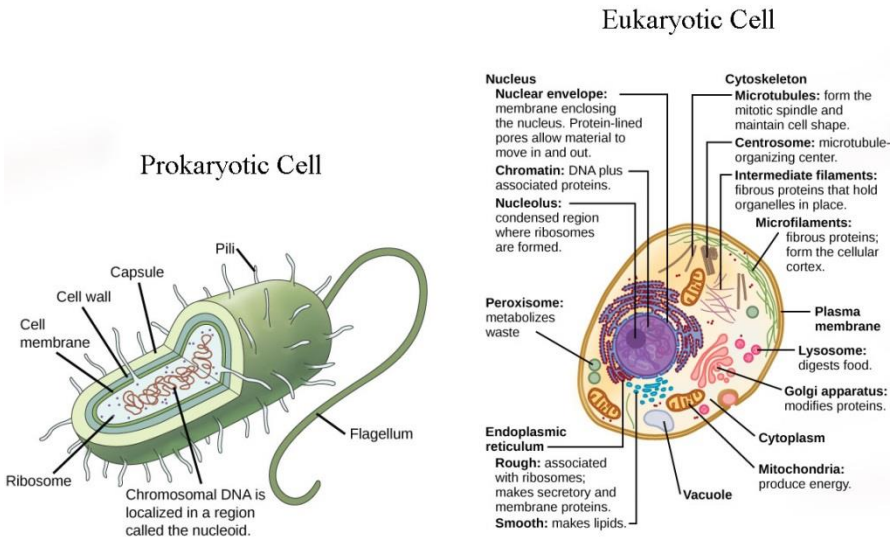

Figure 1-11 Schematic of prokaryotic and eukaryotic cells. Reproduced from Boundless [61, 62].

Bacteria are prokaryotic microorganisms which can be either symbiotic or pathogenic. Most bacteria are useful and can aid in digestion, protect the intestine from invasions by pathogenic bacteria, protect skin from infections, break down waste material and provide nutrients for soil. There are pathogenic bacteria which cause harm to the host resulting in food poising and wound infections. As bacteria are unicellular they will often group together and form a biofilm that is able to protect the cells from attack. Bacteria are extremely diverse, from their shape, what they eat, where they live and their effect on plants or animals.

The identification of bacteria species is important for a range of fields, including medicine and food safety. Routine tests are performed to check and control for bacterial infections in hospital patients, GP clinics and the agriculture industry. Contamination in food production can have dire consequences, potentially infecting thousands of consumers. Quick and accurate identification is sought after to ensure the safety of produce and water supplies. The following sections describe the common identification techniques currently used, techniques that could be more beneficial when identifying bacteria and a model bacterium for study (*Escherichia coli*).

1-6-2 Differential testing

A common method for identifying bacteria is differential testing. This involves a range of culture-based techniques aimed to eliminate and narrow down the possible species. It usually takes at least 24 to 72 hours to prepare a sample and run through the possible tests to gain a positive identification.

The first test normally undertaken is a *gram stain*. There are two types of cells: gram positive and gram negative. When cells are dyed with crystal violet, treated with iodine and decolourised, only positive cells retain the dye. The cells are then counter-stained with safranin which will only stain negative cells. The difference between gram positive and negative cells is the thickness of the cell wall, which is made of the molecule peptidoglycan. Gram positive cells have a thicker wall which retains crystal violet even after washing. However the gram negative cell wall is very thin and does not retain the dye.

Bacteria can have rod, spherical or curved shapes which can be used to further narrow down species. The way cells group is also an indication of the species; some species group in pairs, cubic structures or chains.

Other stains can also be used for identification such as capsule stain, flagella stain, acid-fast stain and spore stain. These stains will highlight differences inherent to certain types of bacteria.

Another test can be performed by growing the bacteria on different types of media. Bacteria species prefer specific food and growing conditions so this can be used to see which media promoted growth.

As it can be seen, there are many culture based tests to be utilised to determine which bacteria is present. This can require growing bacteria to view the colony formation and the environment they prefer. Growing the bacteria prior to testing also ensures that they are in a specific life state. Spore forming bacteria only reach the spore state after a specific life time. Also, it is important to have live healthy cells as the dyes may not work correctly if the cell is damaged. This results in long preparation times and multiple

procedures needing to be undertaken for identification. Once cells have been dyed it is difficult to perform other tests. Due to these issues, faster and non-destructive techniques are sought after.

1-6-3 Alternative identification techniques

Alternative bacterial identification techniques exist which promise to provide faster results with less preparation time. Some examples of rapid microbiological analysis [63] are gas chromatography, mass spectrometry, Fourier transform infrared spectroscopy, Raman spectroscopy, polarised light scattering and fluorescence lifetimes. This thesis focuses on the use of surface-enhanced Raman spectroscopy as it promises to increase sensitivity and identify bacterial species in a non-contact, non-destructive environment with limited sample preparation required.

Raman spectroscopy has been used to identify bacteria [64]. During excitation, the laser beam is focussed on an entire cell. Due to the inherent scattering volume and penetration associated with Raman spectroscopy, the signal collected originates from the entire cell. This includes the RNA/DNA, lipids, proteins and carbohydrates, which allows for fingerprint identification as each bacterium has slightly different internal concentrations and compositions of these components.

However, surface-enhanced Raman scattering only obtains signal from analytes that are adsorbed or very close to the roughened metal surface. If a bacterium is on a SERS surface, the spectrum obtained would be characteristic of the cell wall. This would not result in a reliable identification as the cell walls between bacteria are relatively similar in composition. In order to use SERS to distinguish between bacterial species the roughened metal surface must be inside the cell, allowing for excitation of the RNA/DNA, lipids, carbohydrates and proteins which can provide a more precise "fingerprint" identification.

1-6-4 Model bacterium: Escherichia coli

Escherichia coli (*E. coli*) are a gram negative rod-shaped bacterium generally measuring 2 μm in length and 0.5-0.8 μm in diameter. *E. coli* is present in the intestines

of most warm-blooded organisms. They are normally harmless and aid in digestion and protecting the gut from pathogenic bacteria. However, some pathogenic strains of *E. coli* exist and are normally consumed from undercooked or contaminated food.

Some *E. coli* strains are used as a laboratory standard as they are well characterised, have lost their ability to thrive in the intestine, can be used to pass genetic information to other bacteria and can represent food borne illness bacteria. They are routinely used in microbiology laboratories as a standard bacterium. Some laboratory strains are still able to create biofilms and are used in the study of biofilm production.

E. coli is identified in differential testing by testing positive for indole and methyl red tests. *E. coli* tests negative for Voges-Proskauer, citrate, hydrogen sulphide, urease and phenylalanine deaminase tests [65].

1-7 Applications

This project will investigate two SERS substrates which can be used for specific applications. The next two sections discuss some examples of the types of application each substrate can be used for.

1-7-1 Optical fibre SERS probe applications

The miniaturised probe design used in this project is ideal for areas that are difficult to access and where space is a priority or where minimal invasiveness is preferred. A probe with a maximum diameter of 125 μm is ideal for biomedical applications as well as assessing dangerous and possibly volatile situations. For example, TNT is a commonly used substance in explosives. SERS has been shown to be a successful technique for label-free detection of TNT [66, 67]. If a miniaturised probe is utilised, the sample can be measured by insertion through a small opening.

Biomedical applications are important to discuss further as they impact a large percentage of the population. Miniaturised probes could be utilised during operations to identify unknown growths or bacterial infections. SERS has been shown to successfully identify cancerous tissue without the use of radioactive labels [68]. A miniaturised

probe would allow minimally invasive procedures to test a suspicious growth and determine if it is cancerous prior to removal.

A potential application that could be used on a daily basis and impact millions of people would be a continuous glucose sensor. Currently the standard glucose meter uses a chemical reaction on a test strip that is inserted into an electrical meter. This method relies on the patient pricking their finger multiple times a day to administer the test. This results in low compliance and often a patient will only test their glucose levels a few times a day or if they feel unwell. Ideally, a continuous measuring device should be used which can warn the patient when their glucose levels are rising high or dropping low before they reach dangerous levels which result in them feeling unwell. It should be noted that continuous glucose monitoring devices do currently exist [69]. They utilise interstitial fluid to obtain readings which classes them as minimally invasive. However, interstitial fluid is much slower to react to changes in glucose levels than blood. Also, the currently available systems may only be used for up to a week at a time and require daily calibration with standard finger prick tests.

1-7-2 Black silicon applications

Black silicon is a versatile platform to use as a SERS substrate for sensing. It can simply be used as a platform for adsorption of test samples [35]. It could also be incorporated into a microfluidic chamber for testing of fluids [70]. Most impressively, it has been shown to impale bacteria [71], which could provide an exciting method of introducing SERS-active spots inside cells for internal and hence differential identification. SERS originates from an analyte-metal interaction; normally cells residing near a hotspot would only provide a SERS signal from the cell wall. Bacterial cell walls tend to be relatively similar whereas the internal composition allows for differential identification.

1-8 Motivation for the project

A complete understanding of optical fibre properties when used as an intrinsic sensor is required to design and implement a successful miniaturised SERS probe. Previous work has appreciated NA matching between fibre and objective, but a thorough investigation was not undertaken [51]. Miniaturisation is important for biomedical applications (see

Applications section). Confidence in the repeatability and reliability of a probe must be high if it is to be successfully used in the medical industry. Therefore, an understanding of the underlying mechanisms is a highly important first step in creating a miniaturised SERS probe.

SERS probes are a useful avenue to explore due to the wide breadth of applications that could benefit from their implementation. SERS is a promising technique to identify molecules in the chemical and biological world due to its chemical sensitivity and specificity. Not only is SERS a fingerprint analysis technique, but it is also non-destructive, does not need labels added and is not hindered by the presence of water. This results in a spectroscopic technique that can measure samples in their natural state with no preparation and has potential to measure *in vivo*. Miniaturisation of SERS probes enables the technique to be used in difficult-to-access regions. This adds to the viability of using SERS to identify compounds in vivo without the need to remove and prepare the sample.

Understanding the complex nature of optical fibres will provide the necessary insight required to advance the probe design to a state where they can accurately measure low concentrations of target molecules.

Bacterial identification conventionally requires long preparation times and destructive measurement techniques. The ability to quickly and easily identify bacteria without destroying the sample would be beneficial to the medical community. If an optical fibre can be used to remotely measure bacterial infections on implants, this might avoid the need to remove the implant to treat the infection.

The work presented in this thesis involves the characterisation of a range of substrates and a discussion on their suitability to be used as SERS probes. The substrates considered here include laser-ablated metal nanoparticles, oblique angle deposition and two forms of black silicon. Then two applications were applied to the two platforms selected for further investigation. OAD was chosen to characterise a range of optical fibres due to its ease of deposition on fibre tips and its repeatability.

Black silicon was chosen for SERS bacterial identification due to its ability to create hotspots inside the bacteria.

The methodology and instruments used to collect the experimental results are first described in Chapter 2. Chapter 3 presents the characterisation of substrates, while Chapter 4 shows a comparison of ten different optical fibres which were created into SERS probes using OAD and thiophenol as a test analyte. A range of collection objectives were used to determine if NA matching to the fibre core provides a benefit to signal collection. Chapter 5 presents bacterial identification using black silicon pyramids to pierce the cell and introduce gold nanostructures inside the bacteria. This allows for a SERS signal to originate from inside the cell and this potentially allows for a new method to analyse bacteria. Chapter 6 provides conclusions of the work presented and describes further work which can build on this thesis.

Chapter 2

Experimental Methods

This chapter describes the methods implemented when preparing and characterising samples. The standard operating procedures followed when using instruments are also summarised, along with common instrumental parameters. Experiment specific parameters are outlined in the appropriate chapter. Optical fibre handling and preparation, SERS substrate thermal evaporator procedures, scanning electron microscopy, transmission electron microscopy, energy-dispersive X-ray spectroscopy, X-ray photoelectron spectroscopy, atomic force microscopy, chemical handling and Raman spectrometer operation are presented. Where SERS substrates have been supplied by other researchers, a brief description of the procedures used has been provided. All experimental procedures, sample preparation and sample characterisation were performed by the author, unless otherwise stated.

2-1 Optical fibre preparation

Optical fibres are composed of glass and consequently care must be taken when cleaving fibres as shards of glass can fly in any direction. It is advisable to always wear protective eye wear and gloves when handling fibres. Ensure that the location of fibres and off cuts is known and be careful to check clothing for shards when leaving the laboratory.

Table 2-1 List of fibres used in the project and the associated suppliers.

Fibre model	**Supplier**
S405	ThorLabs
Hi 1060 Flex	Corning
780HP	ThorLabs
Hi 980	Corning
Pure Silica Core	Sumitomo
F-SBC	Newport
SMF28	Corning
SM1500	Corning
MMF (62.5)	Corning
MMF (50)	Corning

The fibres (see Table 2-1) were stripped of their protective jacket using 125 μm fibre strippers (Clauss, Fiberoptic stripper, CFS-2). Lens tissue paper with a small amount of ethanol was used to remove any remnants of the jacket and to ensure the fibres were clean. A fibre optic cleaver (Fitel model number S323, the Furukawa Electric Co. Ltd, Figure 2-1) was modified to include a micrometer attachment (Mitutoyo, Figure 2-2) which allowed the length of the fibres to be set to 25 ± 0.5 mm. A uniform length was desired to ensure measurements were comparable between fibres as the mode pattern differs with length. The cleaver operates by clamping a fibre in place, then a blade is used to nick the surface and tension is applied to create a flat break. The fibres were cleaved at both ends and retrieved carefully.

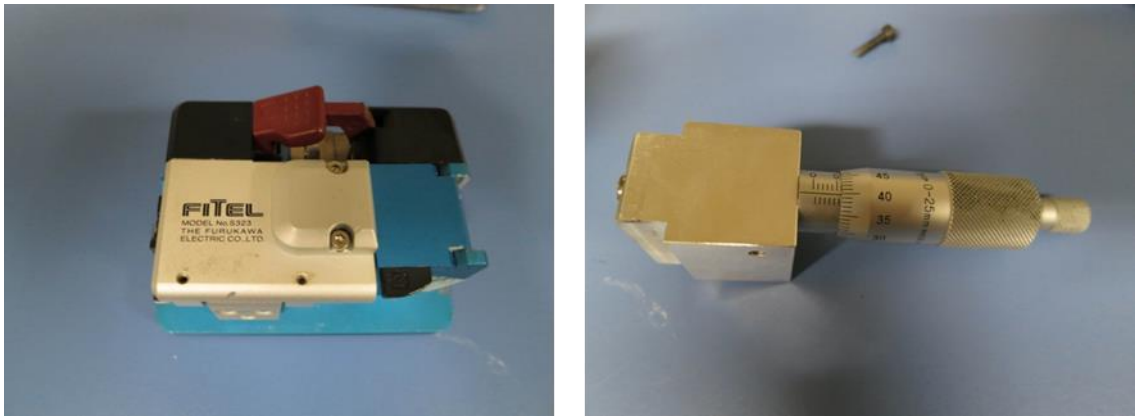

Figure 2-1 Left: Fitel cleaver. Right: Cleaver micrometer attachment.

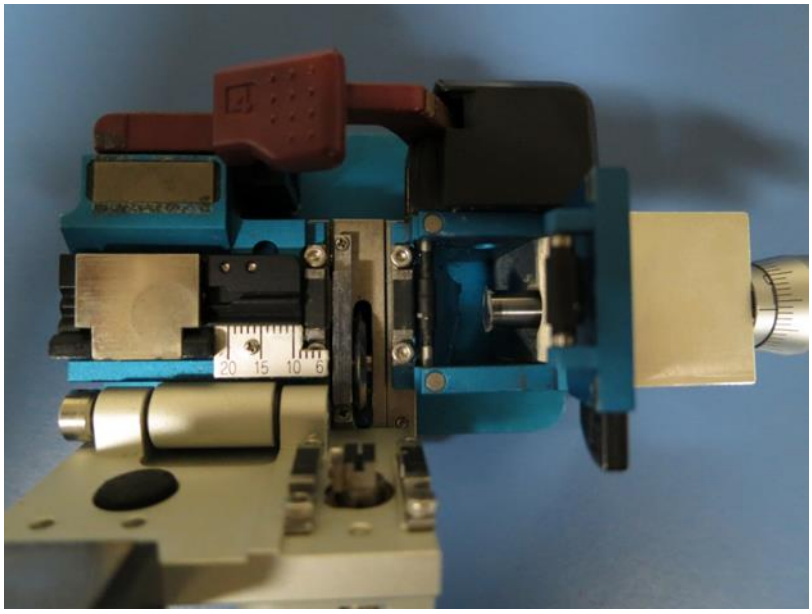

Figure 2-2 Fitel cleaver with micrometer attachment connected. The micrometer can be set to the desired length. A fibre is then placed in the channel and butted up against the end of the micrometer. After the fibre is clamped in place and nicked with the blade, the micrometer must be wound out. This ensures that the fibre does not press hard into the micrometer and become damaged when tension is applied.

Each section of fibre was imaged using a microscope to inspect the end-face for unsatisfactory cleaves. The core must remain clear and the surface reasonably flat. A thermoplastic adhesive (Crystalbond, 509) was melted across the width of a mounting block and the fibres were carefully mounted ensuring that 1 mm of fibre protruded from

the block at both ends (Figure 2-3). The block was then immersed in ethanol and placed in an ultrasonic bath for 1 minute to ensure that the ends were clean.

Figure 2-3 Aluminium block with channels used for mounting 25 mm length fibres. The mounting block base is at an angle of 4° so that when the block is placed under the evaporation source, there is an angle of 86° between the fibre tip and the source (see Section 3-2).

2-2 Thin film deposition

The Emitech K975X (Figure 2-4) is a deposition system which can create silver-island films with SERS functionality. There are two deposition modes available in the system, sputtering and evaporation. Sputtering occurs when a metal target is bombarded with Ar^+ ions and metal atoms are consequently ejected or sputtered onto a substrate. Sputtering requires a partial vacuum and argon gas is normally bled into the chamber to provide the bombarding atoms. Evaporation is the process of heating a wire basket that contains metal shots until the metal becomes so hot it evaporates and then condenses on the substrate. Evaporation can only occur in a vacuum as this allows a free path for the metal to reach the substrate and condense. The system has a removable glass chamber that must be cleaned after each deposition. When replaced it must be centred so the lid can form a seal to create a vacuum. An implosion guard is attached around the front of the chamber.

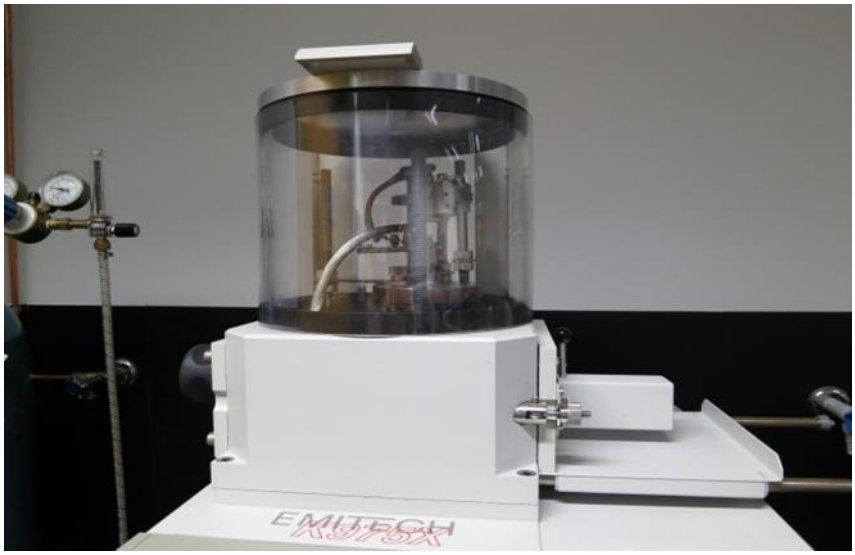

Figure 2-4 Emitech K975X evaporator system.

The sputtering mode is first used to coat a 2 nm thick film of chromium onto the tips of the fibres. The fibres are mounted vertically directly under the target head and the distal end of the fibres was covered in aluminium foil to prevent any stray metal vapour from contaminating the surface. The system evacuates the chamber and pumps down to a vacuum of approximately 8×10^{-3} mbar. Argon gas is then bled into the chamber using a valve at the back of the system until the pressure reaches 7×10^{-3} mbar. The target head is connected to a high voltage supply which provides a negative potential while the sample is grounded. The argon ions accelerate towards the target and the ejected metal particles are sputtered onto the fibre tips below. The tips were 30 mm below the target head. In order to deposit a 2 nm thick film of chromium the system was set to have a current of 60 mA for a total of 60 s.

The sputter head was removed by unscrewing point 1 and unplugging the high voltage at point 2 in Figure 2-5. The fibres were then placed horizontally at an angle of 4 degrees beneath the evaporation basket so the tips were directly in line with the basket. The basket was filled with silver shots (Sigma Aldrich, >99.99% 1-3 mm shots) and a shield placed around the source. A shutter was manoeuvred into position under the source. The chamber was pumped down to a vacuum of 1×10^{-4} mbar and then the current was manually increased until the metal basket was heated enough that the metal

started to melt. The shutter was removed to start the evaporation process at a rate of 0.05 nm/s.

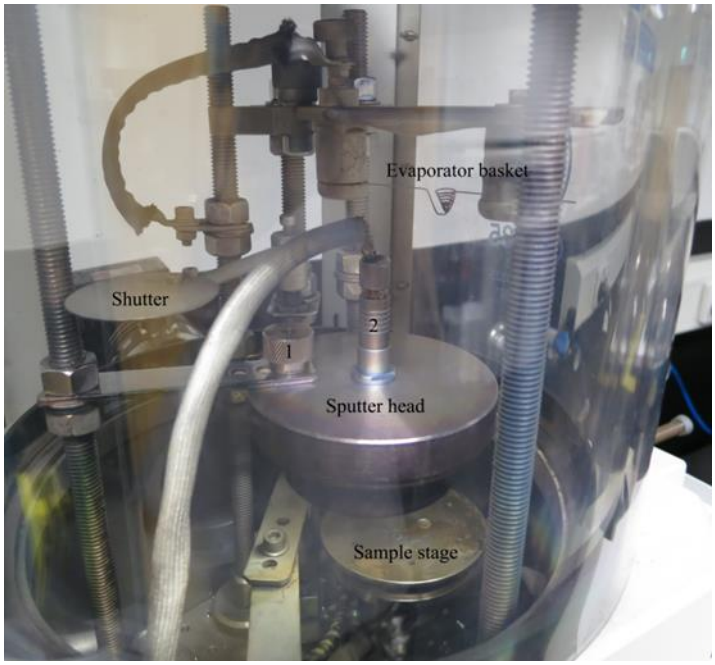

Figure 2-5 Evaporator annotated to show main components.

The thickness of the metal was monitored using a quart crystal microbalance. As the microbalance was positioned away from the sample (Figure 2-6) a tooling factor was used to calculate the effective thickness read on the microbalance for a specific substrate thickness (Equation (2-1)). Once an effective thickness was reached the current was turned to zero and the deposition system vented to atmosphere.

$$TF = \left(\frac{L_m}{H}\right)^2 \times \left(\frac{1}{\sin(\theta)}\right) \tag{2-1}$$

where TF is the tooling factor, L_m is the distance from the source to the film thickness monitor, H is the height from the source to the sample and $\theta = sin^{-1}(z/L_m)$ where z is the distance from the source to the stage. The actual thickness can then be determined by Equation (2-2),

$$T_A = T_m \cdot TF \tag{2-2}$$

where T_A is the thickness that would be measured on an equivalent planar surface at normal incidence and T_m is thickness recorded on the microbalance.

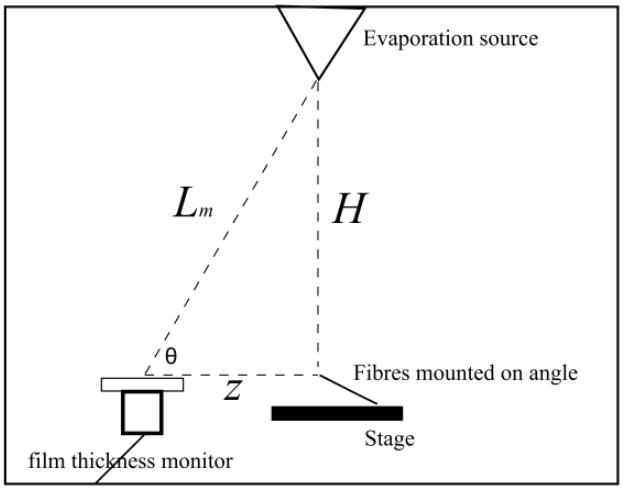

Figure 2-6 Diagram of film thickness monitor in relation to source and sample.

2-3 Scanning electron microscopy

A scanning electron microscope (SEM) is able to produce images of nanoscale samples as it utilises a focused electron beam to raster across the surface. The resolution of an SEM is typically better than 1 nm. An image is produced when the electrons interact with the atoms in the sample, producing secondary electrons and back-scattered electrons. An SEM can be run in high or low pressure mode which allows wet (non-conducting) samples to be imaged.

Optical fibres are made from a dielectric material (glass) which is not conducting. Therefore the samples were prone to "charging". Charging occurs when the electrons have no path to ground and hence build up charge on the surface of the material. This results in the image appearing saturated, out of focus and the sample seems to move. This limited the magnification that was viable for imaging the silver island film used for SERS fibre probe studies.

2-3-1 Zeiss Supra 40VP

The fibre tips were imaged using a Zeiss Supra 40VP SEM (Figure 2-7). This instrument was operated in high vacuum mode with an Everhart-Thornly detector

(ETD). The accelerating voltage was set to 3 kV. The tips were imaged directly so the silver-island film could be seen in detail. Silver is a conducting material, though as the thickness was less than 20 nm and the film was not continuous there were still charging issues due to the underlying dielectric material. Therefore, a magnification of 50,000-90,000 × was used with a working distance (distance from sample to bottom of the SEM column) of 6 mm. The fibres were imaged immediately after the deposition process to limit oxidation. Once there was confidence in the metal film repeatability between fibres the SEM was no longer used. This was to limit the amount of adventitious carbon contaminating the silver film and oxidation of the film prior to chemical functionalization.

Bacteria samples used the same settings as above. Bacteria samples were sputter coated with gold using the Emitech K975X immediately after incubation as the Zeiss Supra 40VP was not set up for variable pressure mode. Gold was sputtered using a current of 35 mA for 30 s with the stage rotating at 138 rpm. Images were collected with and without a stage tilt.

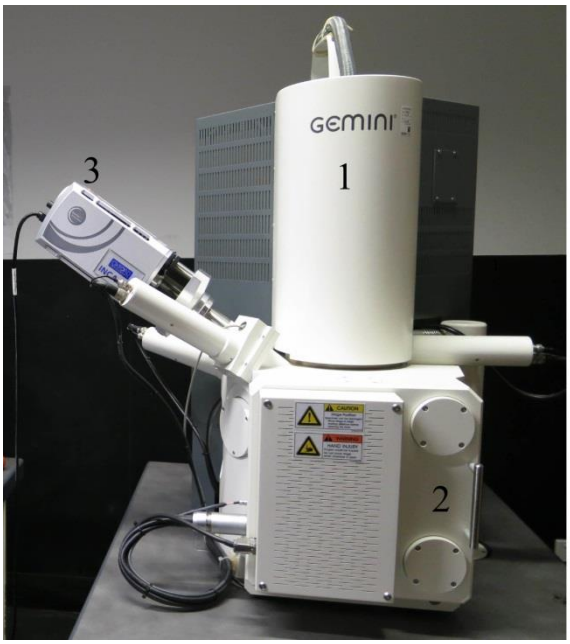

Figure 2-7 Zeiss Supra 40VP SEM where numbers are indicating 1: electron column, 2: sample chamber, and 3: EDS detector.

2-3-2 Nova NanoSEM

The Nova NanoSEM (Figure 2-8) was used to obtain images of black silicon as it was available at the RMIT microscopy and microanalysis facility (RMMF) to use in conjunction with other characterisation techniques. The Nova NanoSEM is able to operate in partial vacuum mode, which can help to eliminate charging of non-conducting samples by adding pure water vapour. It also has a field emission gun (FEG) which provides high resolution image so the curvature of the black silicon tips can be estimated. The SEM was operated in high vacuum with a working distance of 5 mm and the ETD installed. Surface charging was a slight issue, but high vacuum mode was used regardless, as it provides a higher resolution than partial vacuum mode. In general, the spot size was 3.5 and an accelerating voltage of 5 kV was used as this produces less surface penetration. Operating the instrument at 15 kV initially resulted in ghostly looking structures due the deep surface penetration. The stage was tilted to provide images from different angles so the structure could be fully appreciated.

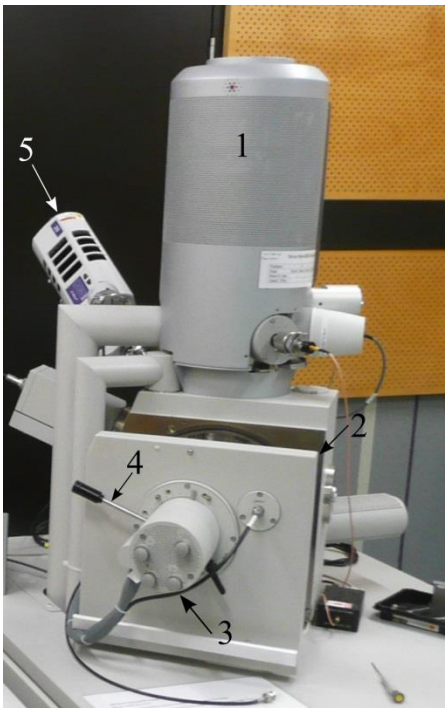

Figure 2-8 FEI Nova NanoSEM in the RMMF where numbers are indicating 1: electron column, 2: sample chamber, 3: stage controls, 4: stage tilt, and 5 EDS detector.

2-3-3 FEI Quanta 200 ESEM

The FEI Quanta 200 (tungsten filament) ESEM (Figure 2-9) is an environmental SEM and a part of the RMMF. This SEM was able to be used in low vacuum mode which is ideal for imaging bacteria without sample preparation which has the potential to damage samples. In a conventional SEM the bacteria must be chemically fixed, dry and gold coated prior to imaging which destroys the sample for other characterisation techniques. Low vacuum mode operates by allowing pure water vapour into the chamber to lower the pressure after pump down. Images were collected with and without stage tilt. Working distance for this instrument is 10 mm, an accelerating voltage of 10 kV was used with a spot size of 3.5.

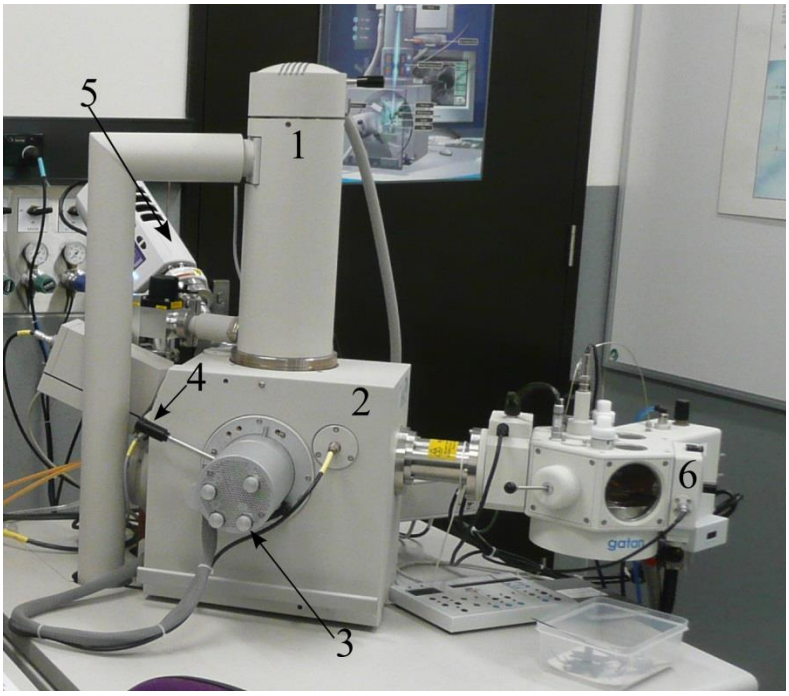

Figure 2-9 FEI Quanta 200 ESEM in the RMMF where numbers are indicating 1: electron column, 2: sample chamber, 3: stage controls, 4: stage tilt, 5 EDS detector, and 6: cryoSEM sample prep.

2-4 Transmission electron microscopy

Transmission electron microscopy (TEM) is a microscopy technique where electrons pass through samples of less than 100 nm thickness. The transmitted electrons create an

image of the sample as they interact with the sample when passing through. TEM can also be used to obtain diffraction patterns of thin samples.

The emission source in TEM can be either a tungsten filament or a lanthanum hexaboride (LaB_6) source (small single crystals). High voltage is applied to the filament which creates an electron beam. A TEM requires a high-vacuum to ensure there are no collisions with particles and to prevent arcing. The electron beam is focused using magnetic fields to create a lens.

TEM grids are used to hold samples. The grids are normally a ring of diameter 3 mm with a thin meshed grid (<100 μm) in the centre (Figure 2-10). Copper is a common grid material. Samples can be investigated using bright field imaging, electron energy loss spectroscopy, high resolution imaging or mapped with energy dispersive spectroscopy (EDS). This project utilised bright field and high resolution imaging and EDS mapping.

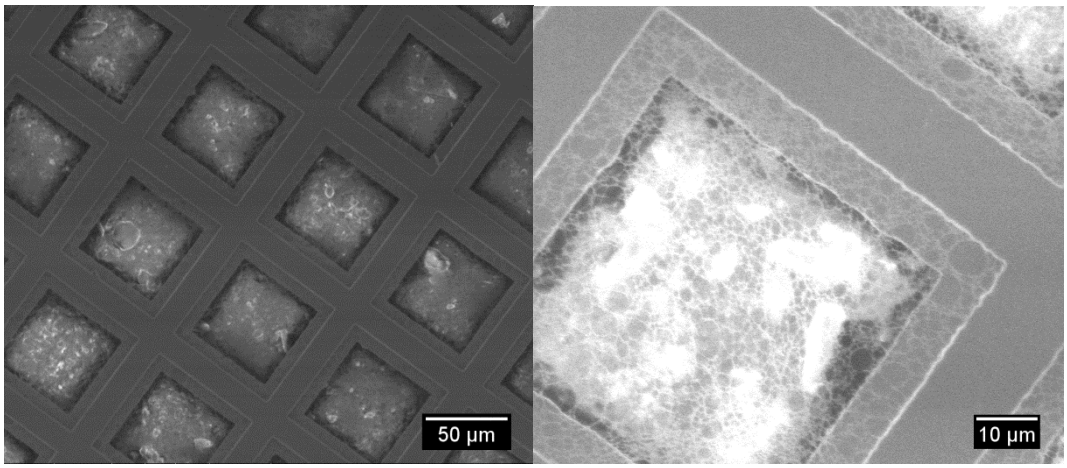

Figure 2-10 TEM grid viewed under SEM.

Bright field imaging occurs when electrons pass through a sample and the transmitted electrons are collected by a detector. As the electrons must pass through the sample, the brighter portions of the image originate from thin sections of the sample while dark portions originate from thick areas of the sample. Bright field was the basic technique used to collect transmission images.

Scanning transmission electron microscopy (STEM) is a mode of operation that collects images by using a small focus point to raster scan across the sample. This mode makes EDS mapping possible on the TEM.

High resolution TEM (HRTEM) is capable of atomic level resolution. This allows the crystal structure of a sample to be determined provided that the sample is uniform in thickness. The instrument is operated under TEM mode with a large field detector inserted.

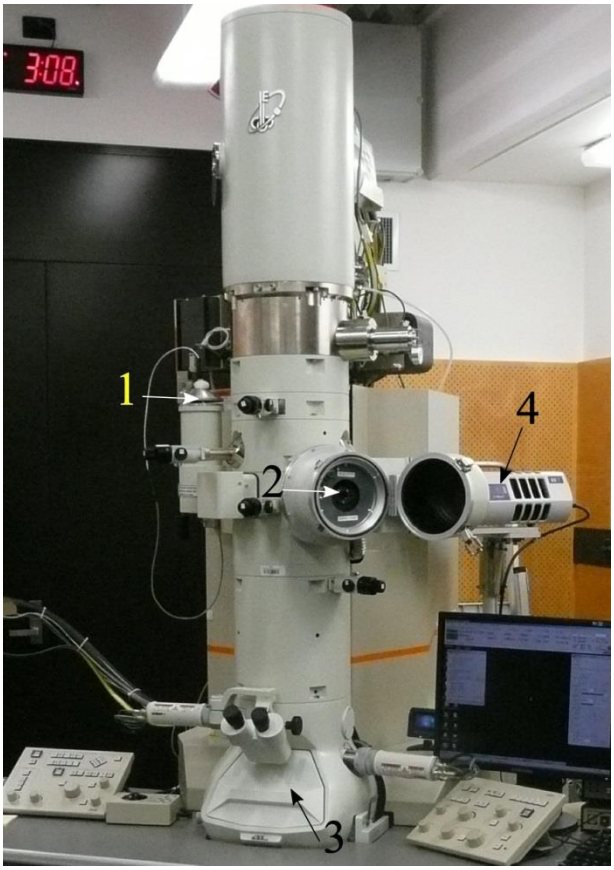

Figure 2-11 Jeol 2100F TEM in the RMMF where numbers are indicating 1: cold trap, 2: sample load lock, 3: viewing screen, and 4: EDS detector.

The Jeol 2100F (Figure 2-11) is a part of the RMMF and uses a field emission gun with 200 kV accelerating voltage. The sample must be inserted into the sample load lock and then pre-pumping occurs before the sample can be fully inserted into the chamber. Samples and the sample holder must be handled with gloves to prevent

contaminants from entering the chamber. The TEM requires liquid nitrogen for a cold trap. The cold trap is connected to a copper ring that is near the sample which causes any contaminant to be attracted to the ring as opposed to the column. The voltage is increased using a controlled ramp over a period of 45 mins until it reaches the desired value of 200 kV. Then the filament is slowly wound up until a green glow of emission is seen. Alignments must be undertaken involving positioning apertures, correcting shifts, tilts of the electron beam, removing astigmatism and several other lens alignments. Then the system is ready to obtain images.

Black silicon samples were investigated in the TEM. Sample preparation consisted of scraping off a small section of the sample into a beaker with a few drops of ethanol (Sigma Aldrich, 200 proof, anhydrous, >99.5%.). The solution was extracted with a pipette and placed on a mesh copper TEM grid. Standard TEM mode was used to collect bright-field images. High resolution TEM mode was used to determine crystal structure.

TEM measurements were obtained with assistance from Edwin Mayes, duty microscopist for the RMMF.

2-5 Energy-dispersive spectroscopy

Energy dispersive spectroscopy (EDS) is a spectroscopy technique capable of determining elemental composition of a sample. EDS has a deep interaction volume of approximately 3 μm and is used for bulk sample analysis. EDS is normally coupled with an SEM (Section 2-3) or a TEM (Section 2-4). However the spatial resolution of EDS is approximately 1 μm. EDS measures the number and energy of X-rays emitted from a sample after excitation with an electron beam source. Collisions can cause an inner shell electron to eject and leave an electron hole. If an outer shell electron fills the hole, an X-ray can be emitted from the energy difference between shells. The X-ray energy is characteristic of the element's atomic structure and can be used to determine the element. It can be difficult to detect low atomic weight elements (anything below boron), especially in low concentrations.

Figure 2-12 Philips XL30 SEM with EDAX attachment for EDS where numbers are indicating 1: electron column, 2: sample chamber, 3: stage controls, 4: stage tilt, and 5 EDS detector.

The Philips XL30 SEM (Figure 2-12) is located in the RMMF. The XL30 was used to determine elemental composition of the core and cladding of test fibres. The XL30 is equipped with a LaB_6 filament and an EDAX attachment for EDS. EDS is most efficient if the sample is at a working distance of 10 mm. The focus was set to 10 mm and then the sample was brought into focus using the height control on the stage door. A dead time percentage of 25 -35% is optimal for collecting EDS spectra. Dead time is the time after each count where the system is not able to record another count. This is altered by the spot size, accelerating voltage, gun tilt and the count amplify time. This instrument has an infrared camera which is used to view the chamber. This must be turned off prior to EDS otherwise it will interfere with measurements.

A backscatter detector was used in order to clearly differentiate the core and the cladding of each fibre for correct positioning of the sample widow. An accelerating voltage of 30 kV was used with a spot size of 5.7. Once a spectrum is collected, peaks can be assigned from a list of possible elements. EDS requires prior knowledge of the sample composition to correctly assign peaks as many peak positions overlap. The composition can be quantified from the peaks but this is not always reliable. There are

issues with beam spread, so the sample area can be larger than anticipated. If the electron beam drifts due to sample charging, the selected area can change position, possibly to an unwanted area. Charging itself can also cause errors which will affect quantitative measurements. This can be checked by ensuring that spectra decay to zero at the excitation energy (30 kV). EDS, under ideal conditions may provide reliably quantitative results. Boron sensing is also problematic as the detector has a boron window.

The theory and procedure for EDS is similar for the other SEM and TEM used in this project. The Nova (Section 2-3-2) was operated in EDS mode (Oxford SDD EDS detector model X-max^n) to map the contaminants of the black silicon samples (same operating parameters used as during image collection). The Jeol 2100F (Section 2-4) collected elemental maps of black silicon in scanning TEM mode using an Oxford SDD EDS detector model X-max^n with an electron probe size of 1.5 nm.

2-6 X-ray photoelectron spectroscopy

X-ray photoelectron spectroscopy (XPS) is a semi-quantitative technique used to identify chemical elements. XPS is surface sensitive with a probe depth of approximately 0-12 nm. Therefore, it is a useful technique to analyse elemental surface composition and possible contaminants with atomic numbers larger than 3 (lithium) at parts per thousand sensitivity. XPS provides complementary elemental composition information to EDS. However, where EDS quantifies elemental composition, XPS can analyse bonds and hence determine species.

An XPS spectrum is a plot of the number of electrons hitting the detector against the binding energy of the electron. Every element has its own characteristic binding energy determined by the electron configuration. Therefore the peaks in a spectrum represent the chemical species formed by specific elements. Ultra high vacuum is used to eliminate error as the detector is positioned relatively far from the sample. As the energy of the electrons is measured it is necessary to eliminate any collisions with residual gases that could alter the energy before the electrons reach the detector.

XPS can only obtain data from the surface of the sample. X-rays irradiate the sample and photoelectrons must escape from the sample to reach the detector. The photoelectrons can have inelastic collisions, combine or become trapped inside the sample which limits the number that can escape. Escape becomes unlikely from depths greater than 10 nm but it is dependent on the element.

Figure 2-13 The Thermo Scientific KA XPS system in the RMMF.

The Thermo Scientific K-Alpha system (Figure 2-13) is a part of the RMMF. It has an aluminium K-alpha X-ray (AlKα) source which has photon energy of 1487.6 eV and 15 eV pass energy. The AlKα X-rays are created by diffracting and focusing a beam of X-rays onto a thin disc of natural crystalline quartz with a <1010> crystal orientation. High resolution scans can obtain peak widths of 0.4-0.6 eV. The spot size available on the system is 400 μm and the measurement area can be chosen for multiple samples (plate size 60×60 mm). A depth profile can also be obtained by ion milling the sample during collection (ion gun energy range 100-4000 eV).

The system has a flood gun which can provide the target area with a steady flow of low-energy electrons and Ar^+ ions which remove charge build up on the surface. The

flood gun option can be used depending on sample charging effects. If the sample is prone to charging it is necessary to use the flood gun.

Samples are loaded onto a plate (Figure 2-14) and locked down with pins. Gloves must be used to handle samples and plates as finger grease can contaminate the ultra-high vacuum system. The plate is inserted into the load lock which is pumped to a rough vacuum before a valve is opened to the main ultra-high vacuum chamber, into which the sample plate is transferred. The sample is focused by control software which alters stage height until counts are detected and then the height is optimised for maximum counts. Areas to be investigated can be chosen and a queue of measurements can be set to run automatically. Survey scans run the full energy range to find elements or specific ranges can be selected to scan at higher resolution to obtain chemical binding information.

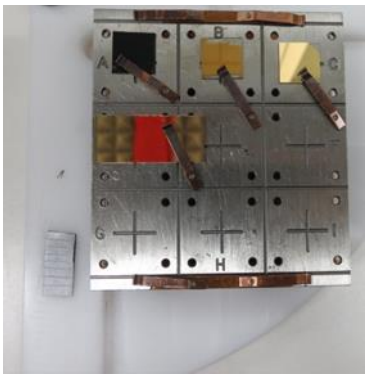

Figure 2-14 Sample plate for XPS with samples loaded.

2-7 Atomic force microscopy

An atomic force microscope (AFM) can be used to image and measure a surface at the nanoscale. It can have a resolution on the order of fractions of a nanometre. This type of scanning probe microscope can provide vital topographical and roughness measures of a surface, which is useful to characterise SERS substrates.

An AFM operates by probing the surface with a sharp tip attached to a silicon or silicon nitride cantilever. The probe tip usually has a radius of curvature on the order of nanometres. When the tip probes the surface it is deflected according to Hooke's law. This deflection is measured with a laser spot which is reflected from the top surface of

the cantilever. There is a feedback mechanism which adjusts the distance between the tip and the sample. This protects the tip/sample from damage and keeps the force applied constant across the sample. An AFM can be used in contact mode or tapping mode (non-contact where the cantilever is vibrated). In contact mode the tip is dragged across the sample to map the surface contours directly. In tapping mode the tip is oscillated at the fundamental resonance frequency. Changes in the oscillation frequency are used to map the sample's contours.

AFM does have limitations which can affect the image. Artefacts can occur when the topography is steep or overhanging. Artefacts can make structures appear wider if the tip has a large radius of curvature compared to the structure. Very tall structures (few microns) can also be problematic. The structure or the tip can break while attempting to probe tall needle structures.

Figure 2-15 Nanoscope D3100 AFM in the RMMF where numbers are indicating 1: sample stage, 2: scanning head, and.3: optics for alignment.

The Veeco Nanoscope D3100 (Figure 2-15) is a part of the RMMF. It was operated in tapping mode with a TAP300-G tip with a resonant frequency of 300 kHz and force constant of 40 N/m. This AFM uses a laser to deflect off the cantilever and provide deflection measurements. The sample is loaded under the tip and the sample is slowly

brought into focus. Once in focus a tuning check is performed. This ensures that the tip is mounted correctly and aligned. A scan area can be chosen and the scan size determines the resolution of the image. The same number of points is collected regardless of area, so a smaller area will result in higher resolution.

2-8 Analyte preparation

2-8-1 Thiophenol

Thiophenol was used as a standard test analyte for characterising SERS performance for different optical fibres. It was chosen as it forms a stable monolayer [18, 19] on silver, which allows for a quantitative comparison between samples. It is also effective in displacing adventitious carbon on the surface. A monolayer is essential as this ensures that the same volume of analyte will be present on each sample. A non-monolayer forming analyte would have an unknown concentration present and so changes in intensity of SERS signal could not be attributed to the substrate alone. Thus the use of thiophenol allows comparison of samples that have the same metallic surface area; i.e. share the same preparation conditions.

A 10 mM thiophenol solution was used during all SERS measurements. As thiophenol is a potentially carcinogenic substance, care was taken during handling. A well-ventilated fume hood, a lab coat, splash goggles and nitrile gloves were used during all handling procedures.

The solution was prepared by diluting 103 μL of thiophenol (Sigma Aldrich, >99%) in 100 mL of high purity ethanol (Sigma Aldrich, 200 proof, anhydrous, >99.5%). Glass beakers and bottles were used as thiophenol can react with plastic. Used gloves and pipette tips were placed in a sealed plastic bag prior to being disposed.

Immediately after the fibres were coated with silver-island films, the fibre tips were carefully placed in the 10 mM thiophenol/ethanol solution for 10 mins. Next they were placed in pure ethanol for 10 mins and lastly they were left to dry in a well-ventilated fume hood for 1 hour. Leaving them to dry for an hour minimised the fumes let off during SERS measurements.

2-8-2 Rhodamine 6G

Rhodamine 6G (R6G) is a red dye commonly used as a test analyte in Raman spectroscopy. A stock solution of 10 mM R6G in water was diluted using milliQ water to concentrations of 1 μM or 4.3 μM as required. Nitrile gloves, lab coat and glasses were worn as protection. Fortunately, R6G does not produce fumes though care should be taken to not allow skin or clothing contact as it will stain and be difficult to remove.

2-8-3 Escherichia coli

The culture of *E. coli* was prepared by collaborator Mya Hlaing due to her expertise in microbiology, using the following procedure for growing *E. coli* cultures:

1). *E. coli* ATCC 25922 from -80 °C stock was isolated on a nutrient agar plate (Becton Dickinson, Difco nutrient broth) for approximately 12 hours.

2). A single *E. coli* colony was then inoculated from the plate into 20 ml of nutrient broth media and then incubated at 37 °C, with orbital shaking at 200 rpm overnight.

3). The total biomass of overnight culture was detected using optical density measurements at λ= 600 nm with a spectrophotometer (Agilent, Varian, Cary 50).

4). The overnight culture of *E. coli* was adjusted to approximately 1.4×10^9 cells/ml (OD600 nm ~ 1.4) with fresh sterile nutrient broth.

When incubating *E. coli* on substrates, the following procedure was used:

1). Overnight culture was adjusted to have OD600 nm of 0.3.

2). The *E. coli* planktonic cells were washed three times by centrifugation at 12,000 rpm (Centrifuge 5804 R, Eppendorf) for 2 min).

3). The washed calls were then resuspended in low strength minimum medium (Dulbecco A, phosphate buffered saline (PBS)).

4). 100 μL of solution was pipetted onto substrates and left to incubate for 1 hour on the bench or covered in solution and incubated at 37 °C overnight for 18 hours.

For SEM imaging of the bacteria, the substrates were washed 3 times with milliQ water, allowed to dry and then immediately sputter coated with gold using the Emitech K975x (operating current 35 mA, sputter time 32 s, stage rotate 138 rpm and vacuum of 1×10^{-2} mbar). Substrates were stored in a desiccator cabinet until imaging was performed.

For SERS or normal Raman analysis, the substrates were washed 3 times with milliQ water and allowed to dry prior to spectrum collection. Substrates stored in PBS at 4 °C while not in use.

2-9 Live/Dead staining and fluorescence microscopy

In order to determine the live/dead state of bacteria, live/dead staining was implemented. Live dead staining relies on two fluorescent dyes which interact with the cells in very specific ways. The first dye (SYTO 9) is able to penetrate all cells and stain them to emit green fluorescence. The second dye (propidium iodide) is only able to pass through compromised membranes associated with dead cells. The dye is then able to interact with the DNA where it emits red fluorescence. Appropriate ratios of the two dyes provide green/red fluorescent images indicative of the live/dead state of the sample.

The culture and incubation procedures described in Section 2-8-3 were used. After the incubation was completed the staining procedure was implemented with Invitrogen Live/Dead BacLight Bacterial Viability Kit L7012. This kit contains SYTO 9 dye (green fluorescence) 3.34 mM and propidium iodide (red fluorescence) 20 mM. The staining procedure was as follows:

Equal volumes of both dyes were mixed thoroughly in a tube.

1) A ratio of 3 μL of mixed dye to 1 mL of bacterial suspension was used. The mixed dye was added to the bacteria sample on the substrate and mixed.

2) The substrate was incubated at room temperature in the dark for 15 minutes.

3) The staining solution was pipetted off the substrates and then a 10 μL drop was placed on a microscope slide. A cover slip was placed over the drop and then the slide was mounted cover slip side down over the objective for imaging. The slide was not allowed to dry. The solution was stored at 4 °C when not in use.

4) Substrates were washed 3 times with milliQ water then mounted upside down on a microscope slide for imaging with epifluorescence. The substrates were not allowed to dry. Samples were stored in PBS at 4 °C when not in use.

An Olympus epifluorescence microscope (IX71 inverted microscope) was used to collect live/dead images of substrates. A water immersion 60× magnification objective was used to collect images. A droplet of water was placed on the objective prior to placing the sample on top. There are two filters used to collect live/dead images with a mercury lamp source; U-MNIBA2 blue excitation narrow band gives green emission (live) and U-MWIG2 green excitation wide band gives red emission (dead). Images were collected in quick succession between filters to limit sample drift. The same exposure time was used so the strength of fluorescence could be compared between live and dead stains.

2-10 Raman Spectroscopy

The Renishaw inVia system (Figure 2-16) is comprised of the system unit, which is a lockable section which houses all the sensitive optics; a Leica microscope used to focus on the sample to be investigated; and a CCD camera. There are also multiple lasers coupled into the system unit to provide excitation of the sample.

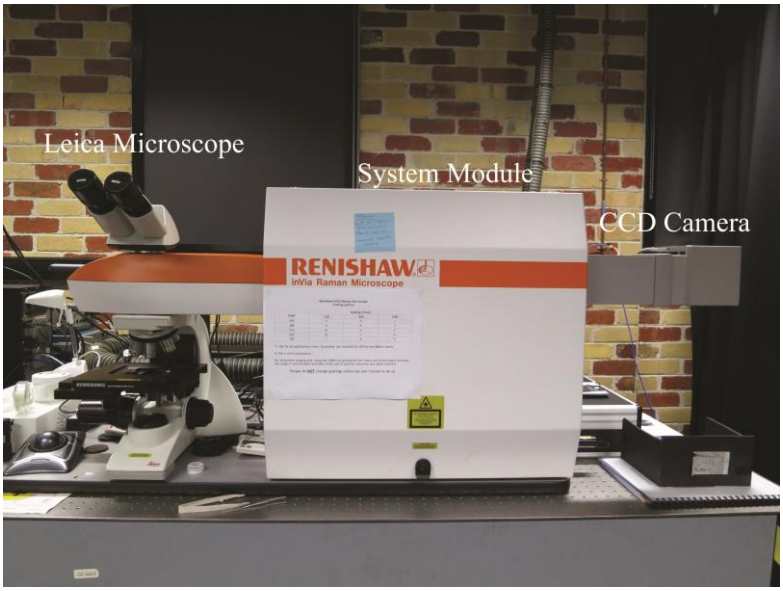

Figure 2-16 Renishaw inVia system.

There are 5 distinct wavelengths available on the system. Each wavelength must be paired with a compatible grating as shown in Table 2-2. The grating determines the resolution of the spectrum, the more lines per millimetre (l/mm) the higher the resolution. This may result in slower acquisition times as the more l/mm the shorter the wavenumber range (static scan) available to acquire over without rotating the grating (extended scan).

Table 2-2 Renishaw inVia Raman laser/grating compatible combinations.

Wavelength (nm)	1200 l/mm	1800 l/mm	2400 l/mm
457	×	×	yes
488	×	×	yes
514	×	×	yes
633	×	yes	×
785	yes	×	×

Prior to using the instrument an appropriate laser/grating combination must be setup and a Rayleigh filter must be inserted that matches the laser line. A schematic of the optical components is shown in Figure 2-17. Only the Rayleigh filter and gratings should be changed, altering the alignment of any other component is not advisable. The

highest resolution available for the laser is recommended. If time is a factor the low resolution 1200 l/mm grating can be used to accelerate data collection. This can be beneficial when collecting numerous points to map a surface. Mapping is possible as the sample stage is fully automated and coordinates can be programmed in for line and area scans.

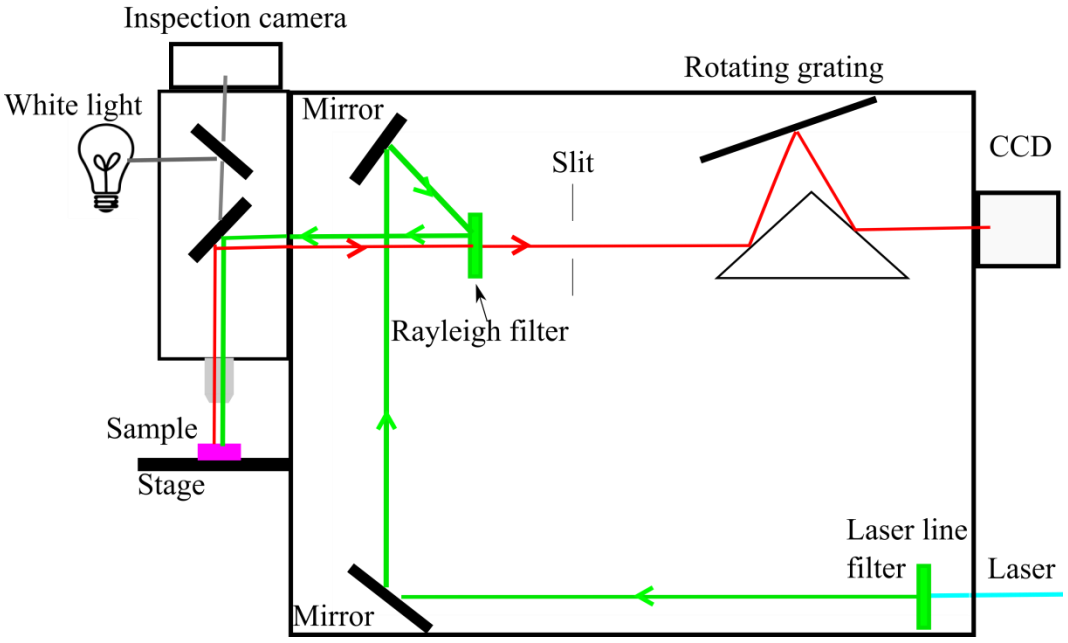

Figure 2-17 Schematic of Renishaw inVia optics.

The main laser used in this thesis is the Ar^+ 514 nm line which requires an hour to heat up and stabilise prior to use. It is important to check that the cooling fan is housed properly as misalignment of tubing and fan can cause the laser to overheat. The protective screen should be placed around the sample once it is on the stage to stop reflected light from potentially damaging eyes.

Once the laser has stabilised, the system must be calibrated and aligned to provide accurate results. Due to temperature and humidity changes the optics are able to shift positions slightly which can result in misalignment and therefore lower than usual efficiency. In order to obtain repeatable and comparable results on a day-to-day basis, the calibration must be checked, optical path optimised, and reference spectra obtained. A detailed guide to the calibration procedure can be found in the Appendix.

Fibre considerations

The fibres were analysed as soon as the thiophenol treatment was complete. This was in an effort to limit contaminants from the atmosphere, as well as general degradation of the sample. Therefore, all measurements for a fibre run (usually consisting of 10 fibres) were completed in one day. Spectra were collected from the tip of the fibre directly and remotely by coupling through the core. As the optical fibres are higher than most samples the stage was moved to the lowest point of its travel. Long working distance objective lens were used in order to protect the fibre tips from accidently being damaged. Due to ètendue considerations the microscope objectives chosen for fibre work were low magnification (5, 10, 20, 50×). This is contrary to conventional Raman work where a larger magnification high NA objective provides increased signal detection due to the large collection angle. The signal from the fibre material is many orders of magnitude larger than the analyte SERS signal so it is easy to swamp the detector. Therefore, low power (1-10% of 13 mW) was used.

Fibre storage

The fibres were stored on the mounting block in a nitrogen cabinet to prevent degradation. Once measurements on the fibres were complete, and the mounting block was required for other experiments, the fibres were carefully removed and stored in the nitrogen cabinet in case of future need. They were removed using acetone on a lint free tissue to carefully remove the crystal bond. Tweezers were used to move fibres from the block to a case. The case consisted of a piece of cardboard, less wide than the fibre length, with a piece of carbon tape along the centre. This secured the fibres and kept the tips from touching any surface and becoming damaged.

2-11 Summary of techniques

A summary of how each of the techniques will be employed can be found in Table 2-3 below.

Table 2-3 Summary of how each technique will be employed in the project.

Technique	Task
Optical fibre preparation	Used in Chapter 3 and 4 to prepare fibres for use as an optrode sensor
Thin film deposition	Used in Chapter 3 to deposit silver-island films onto fibre tips and a glass slide for characterisation. Used in Chapter 4 to deposit films onto the fibre tips for use in a comparison study for fibre optimisation.
SEM: Zeiss	Chapter 3 to image silver-island films and determine repeatability. Chapter 5 to image bacteria impaled on black silicon.
SEM: Nova	Chapter 3 used to image black silicon for height and radius of curvature measurements
SEM: Quanta 200	Chapter 5 used to image bacteria without destroying samples
TEM	Chapter 3 to determine chemical composition of black silicon needle tips
EDS	Chapter 3 to determine dopants in the core and cladding of optical fibres and to identify contaminants on black silicon.
XPS	Chapter 3 to determine chemical species on black silicon and silver-island film substrates.
AFM	Chapter 3 to determine surface roughness and film thickness of silver-island films
Thiophenol	Chapter 3 and 4 used on silver-island films for characterisation and comparison studies.
R6G	Chapter 3 as a test analyte on gold nanoparticles to determine biocompatibility of a SERS substrate
E. coli	Chapter 5 for incubating *E.coli* on black silicon to test a SERS bacterial sensor.
Live/Dead staining and fluorescence microscopy	Chapter 5 to check the live/dead state of bacteria after incubation on black silicon
Raman spectroscopy	Chapter 3, 4, 5 to collect Raman spectra of analytes in either the remote or direct configuration

Chapter 3

Substrate Characterisation

This chapter investigates three potential methods for creating SERS substrates, namely laser-ablated nanoparticles, OAD and black silicon. A range of characterisation techniques were used to analyse the characteristics and performance of each substrate including SEM, XPS, EDS, TEM, AFM and Raman spectroscopy. OAD was found to provide the best combination of enhancement, ease of fabrication and reliability in the context of SERS fibre probe development. The OAD procedure was analysed to determine if it was accurate and reproducible when producing films on fibres mounted on the custom block. The results provided confidence to complete further studies focused on comparing different optical fibre platforms. Black silicon was found to have a complicated chemical composition at the surface. It was also found to have very sharp tips which make this substrate useful for bacterial sensing. Some of the results from this chapter have appeared in *International Journal of Nanomedicine* [28] (Section 3-1), *Annalen der Physik* [29] (Section 3-3) and *Proceedings of SPIE* [35] (Section 3-4).

3-1 Laser-ablated nanoparticles

Gold nanoparticles with a size of 15 ± 10 nm were created using laser ablation by colleagues in Pessac, France [28]. Ultra-pure laser-ablated nanoparticles were considered for use as a SERS substrate as they are biocompatible (produced using ultra-pure water) and do not require a citrate layer to stabilise each particle. Citrate is cytotoxic and could produce its own Raman signal [27].

Initially a piece of silicon wafer, with dimensions of 1 × 1 cm, was cleaned using some ethanol on a lint free tissue. Once the ethanol had evaporated, a drop of gold nanoparticle aqueous solution was placed on the wafer and left to dry. Then a drop of 4.3 μM solution of Rhodamine 6G (R6G) in water was placed on the wafer and left to dry. R6G was chosen as it is a common SERS active dye and as it is water soluble it was used to mimic a biochemical analyte.

Viewing the sample under the microscope revealed a ring of gold around the circumference of where the drop was placed on the wafer (Figure 3-1, Figure 3-2). SERS was attempted on the gold band and other areas across the surface using 633 nm and an 1800 l/mm grating; however no signal was obtained. SERS was attempted again with the gold nanoparticles and R6G in aqueous form; however this also did not produce any signal. Therefore, it was determined that a cross-linker would be required to attach the nanoparticles to the silicon wafer and uniformly cover the surface.

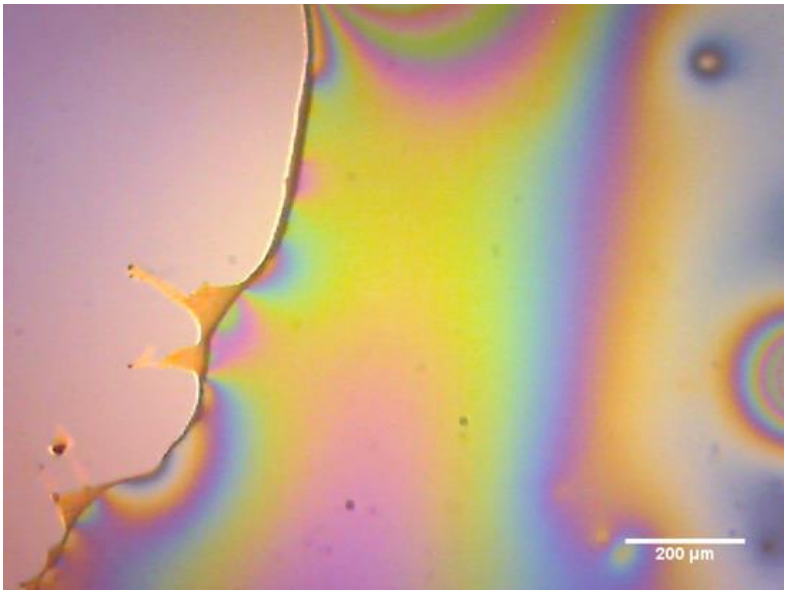

Figure 3-1 Optical microscope image of dried drop which was placed on surface.

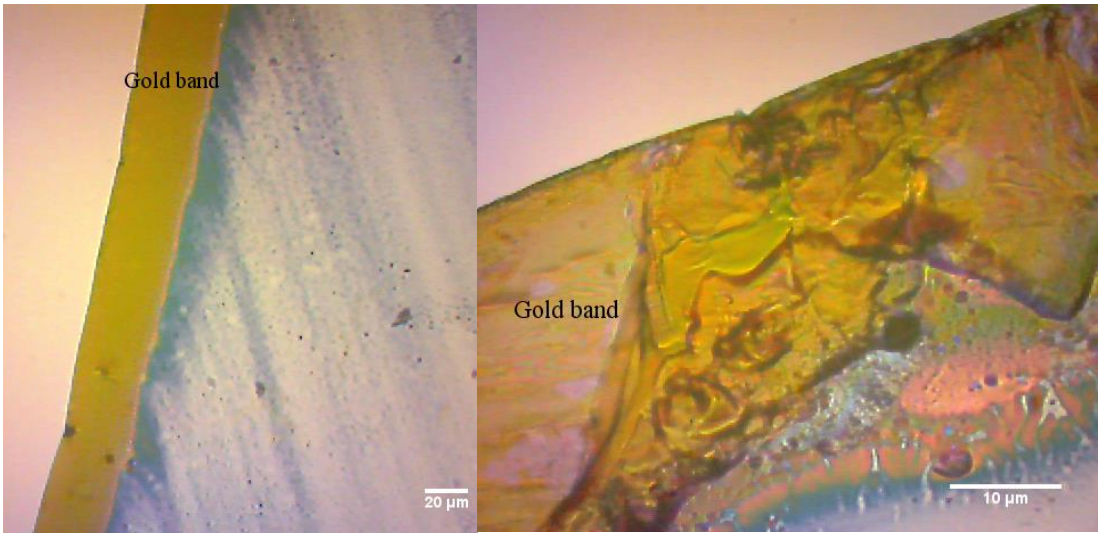

Figure 3-2 Optical microscope image with increasing magnification of gold band formed when a drop of gold nanoparticles dried on the silicon wafer surface

SERS samples were prepared using a mercaptosilane cross linker to attach the gold nanoparticles to the oxidized surface of a silicon wafer. This was used to form an even layer of nanoparticles on the surface and prevent highly concentrated groupings, thus allowing reproducible measurements [72]. The silicon wafer was sonicated for 10 minutes in detergent Decon 90 (Bacto Laboratories Pty. Ltd.), rinsed with deionized water and dried with pure nitrogen to ensure a clean surface prior to treatment. An oxide

layer was then deposited onto the surface using an ozone machine. The wafer was immersed in a 10 mM solution of 3-mercaptopropyl trimethoxysilane (95%, Sigma-Aldrich) in ethanol (99.5%, Sigma-Aldrich) and allowed to functionalize overnight. The wafer was rinsed thoroughly with ethanol and dried with pure nitrogen prior to immersion in a solution of Au nanoparticles for 24 hours. The nanoparticles were sonicated for an hour before immersion to resuspend them. The sample was then soaked in a 4.3 μM solution of R6G in water for 15 minutes, after which it was rinsed with deionized water.

SERS spectra were collected using an inVia Raman microscope (Section 2-10) with an excitation wavelength of 632.8 nm and a holographic grating with 1800 lines/mm. The power exciting the sample was approximately 0.4 mW. A 50× long working distance lens (NA 0.5) was used for excitation and collection of spectra. The spectra were collected with three acquisitions of 10 seconds each. Multiple spectra were taken over the sample to assess reproducibility.

No agglomeration of colloidal nanoparticles was observed with an optical microscope at a resolution of ~1 μm; if surface anchoring was not used, clustering of Au nanoparticles occurred and was discernible under optical observation. Spectra were analysed with Matlab (Math Works, Natick, MA, USA). The multiple reference and R6G spectra were averaged. The averaged reference was subtracted from the averaged R6G spectrum. However, due to a sample-induced change in the Raman background, the reference spectrum was shifted and warped slightly to provide a close fit for the subtraction. The background-corrected R6G data were smoothed with a Savitzky-Golay filter using a window size of 15 and a third-order polynomial. This method of smoothing is suitable as it minimally affects the shape and height of the peaks, yet significantly improves the signal-to-noise ratio.

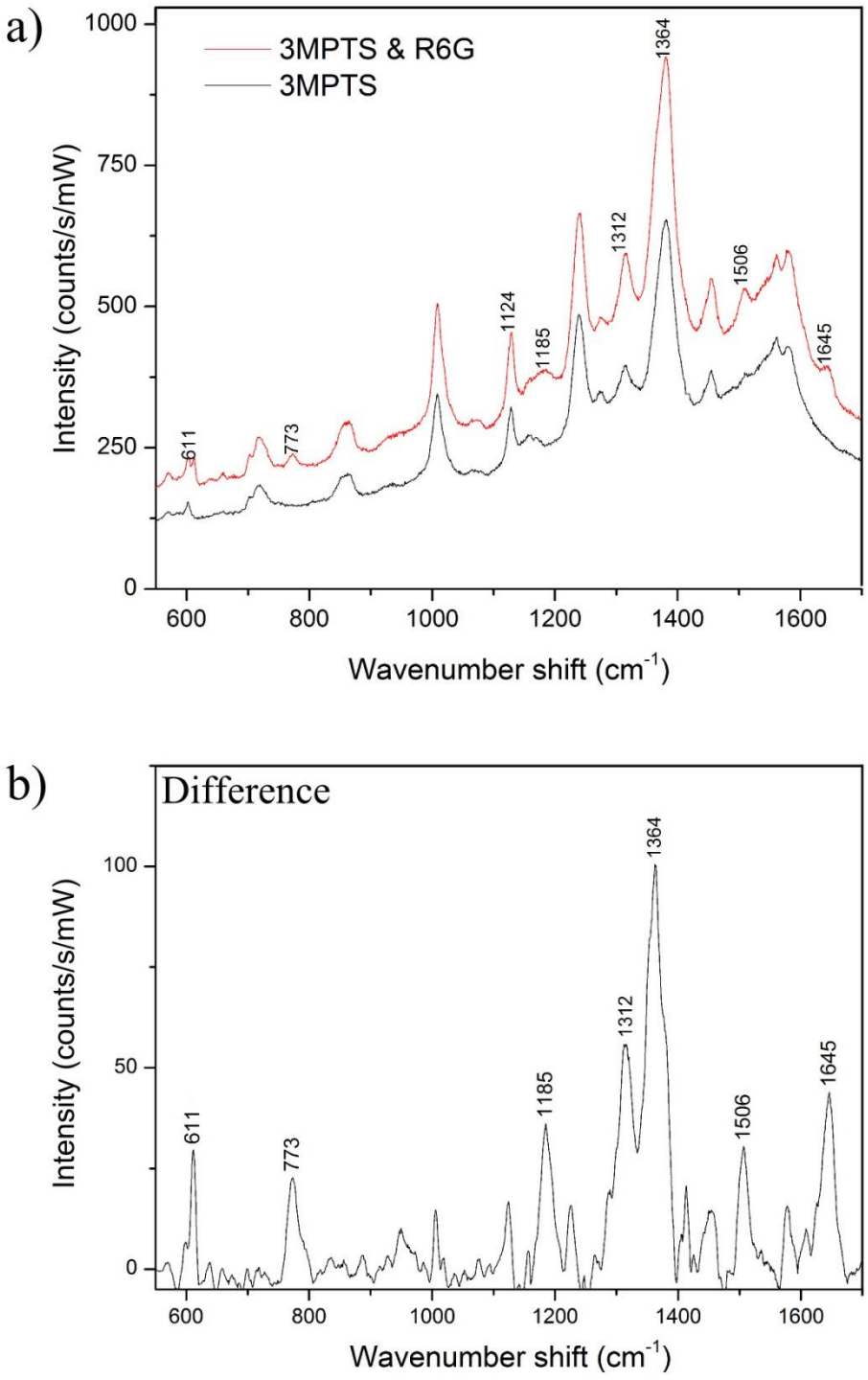

Figure 3-3 (a) Comparison of SERS spectra obtained from gold nanoparticles treated with mercaptosilane cross linker with mercaptosilane and R6G. (b) The same sample showing peaks for 4.3 μM R6G after subtracting the mercaptosilane background.

The immobilized Au nanoparticles were expected to act as a SERS substrate [73]. When the nanoparticles were exposed to the R6G solution, the SERS spectrum clearly showed the R6G signature peaks with a small shift from those in solution [74] at: 611 cm^{-1} (614 cm^{-1} in solution), 773 cm^{-1} (774 cm^{-1}), 1124 cm^{-1} (1129 cm^{-1}), 1185 cm^{-1} (1183 cm^{-1}), 1312 cm^{-1}(1310 cm^{-1}), 1364 cm^{-1} (1363 cm^{-1}), 1506 cm^{-1} (1509 cm^{-1}), and 1645 cm^{-1} (1650 cm^{-1}) as shown in Figure 3-3a. Change of spectral positions of the peaks by ±(7–10) cm^{-1} corresponds to 1.24 meV or 0.12 kJ/mol and is expected for adsorbed molecules. The spectrum (Figure 3-3b) clearly reveals R6G and demonstrates the feasibility of using laser-ablated Au nanoparticles for SERS sensing.

Unfortunately, even though it is feasible to use gold nanoparticles for SERS sensing in general, it is not feasible to use them for weakly scattering biological molecules. The cross-linker produces a strong Raman background signal which covers most of the commonly used wavenumber shift range. This would swamp the signal from weakly scattering biological materials. Combined with an optical fibre probe, where the signal can be swamped from the silica core, it would be difficult to detect a signal from the analyte. Also, the cross-linker could cause issues with biocompatibility. Therefore, laser ablated gold nanoparticles are not considered suitable for optical fibre biochemical sensing.

3-2 Oblique angle deposition

Oblique angle deposition has been used in conjunction with optical fibres to produce optrode sensors [19]. This well-established technique promises to be reasonably enhancing, reproducible and suitable for an optrode configuration. The repeatability of the fabrication procedure was analysed and the surface characterised using a range of techniques. The SERS repeatability was also examined in an effort to assure the comparability of different samples. This provides necessary information for optical fibre probe applications which appear in Chapter 4.

3-2-1 SEM analysis of repeatability

The fibres were prepared according to the procedure of Section 2-1. The films were created using the Emitech evaporator to deposit 100 nm of metal at an angle of 86°

(Section 2-2). The films were imaged in the Supra SEM to check film structure and repeatability (Section 2-3-1). Figure 3-4 shows several examples of the 100 nm silver films deposited using the OAD procedure on a batch of optical fibres. Each image is from a different fibre in the batch and the similarity in microstructure demonstrates the repeatability of the procedure. Unfortunately low magnifications were used due to charging of the sample. As the silver film was not continuous on the glass fibre, charge was not able to dissipate and consequently the charge built up on the surface and made imaging problematic at higher magnifications.

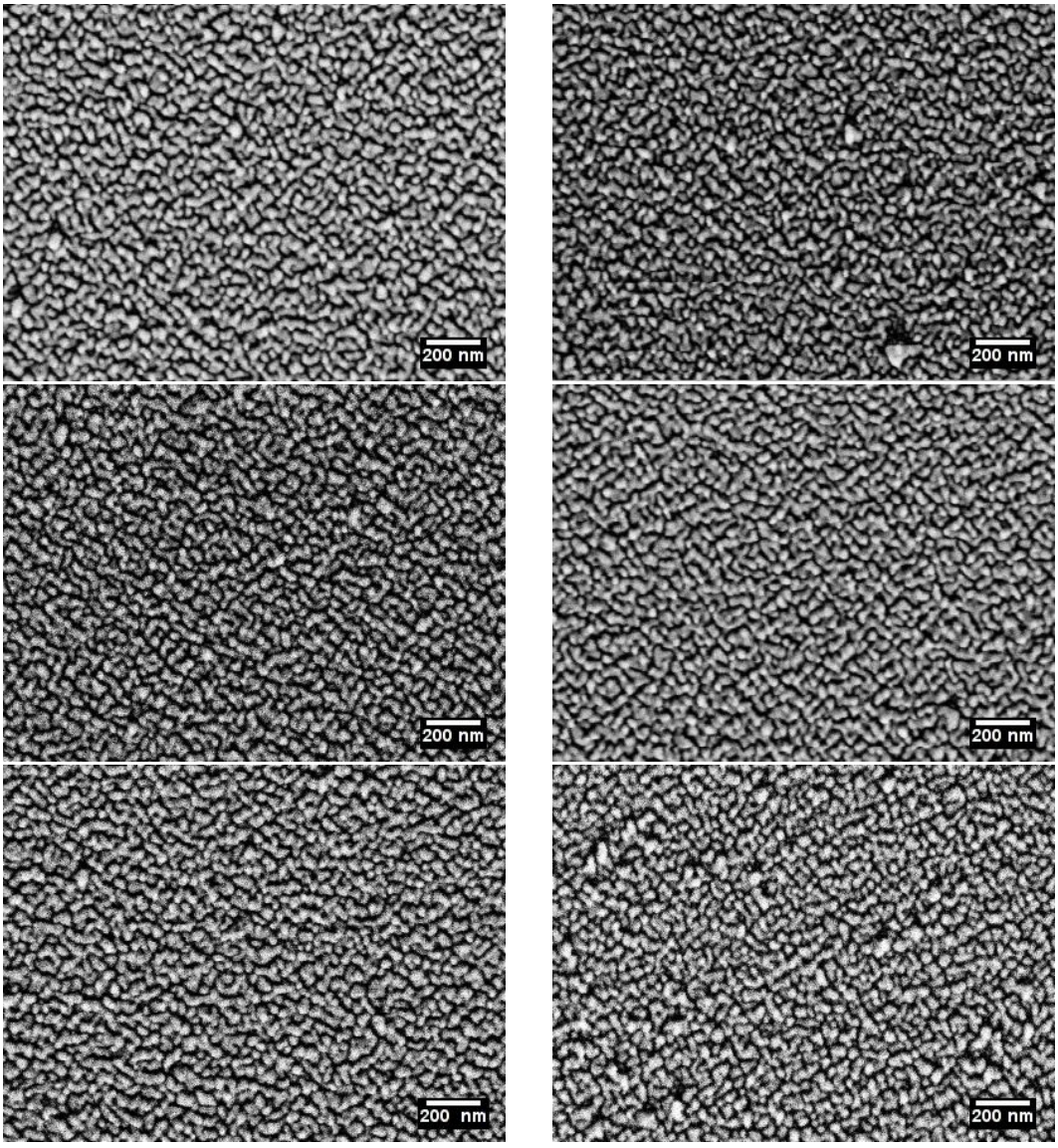

Figure 3-4 SEM images of 100 nm silver films deposited on multiple fibres

The islands in Figure 3-4 can be described as randomly sized particles with an average diameter of 40 ±5 nm (12% RSD across the batch of fibres). The diameter was determined using MATLAB to plot intensity values as a function of distance across each image. The RSD between fibres is small, compared to other reported values (Driskell *et al.* [75] obtained a RSD of 30% for similar structures using OAD), and this shows the islands are reasonably repeatable.

3-2-2 Nominal and actual film thickness

The nominal film thickness as determined by the quartz crystal balance was 100 nm. However, as the substrate was created with an 86° angle between source and sample, it is well known [19] that the island thickness is much smaller. For the purposes of characterisation of the silver-island film a more convenient substrate is required. Glass, due to its similarity to the silica based optical fibres, is considered to be a suitable substitute and is expected to produce a film of very similar microstructure and as such was used in place of the optical fibre for some of the characterisation of the silver-island thin films.

For an independent measure of film thickness, the silver film was deposited onto a glass slide. The slide was sonicated in ethanol for 2 minutes. Three permanent marker dots were placed along the slide. A 2 nm chromium adhesion layer was sputtered directly onto a glass slide and then 100 nm of silver was evaporated at an angle of 86°. The dots were removed with ethanol and then an AFM (Section 2-7) was used to determine step height. The step height was determined by positioning the AFM tip near the edge of the removed area. A line scan was used to measure from the film side to the dot void (Figure 3-5). This provides a measure of the height difference between the film and glass slide. It was determined that the height of the film, including Cr layer, was 17 ± 3 nm. This thickness is suitable to allow for excitation in the remote configuration [76].

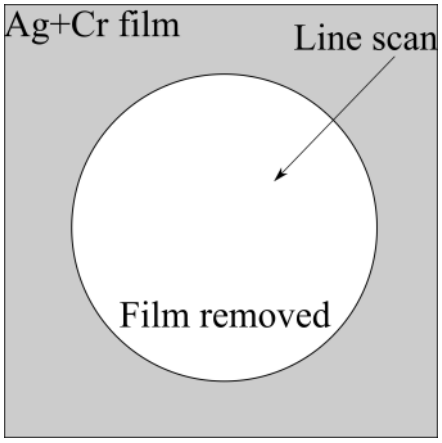

Figure 3-5 Diagram of AFM step height scan across film and void.

3-2-3 Surface roughness

To measure the surface roughness, the silver island films deposited on a glass slide substrate were used. AFM, as described in Section 2-7, was not able to be performed on a fibre tip as there is limited space under the probe to position a fibre accurately and due to lateral fibre movement. Therefore the film deposited on the glass slide substrate was used to determine surface roughness (Figure 3-6).

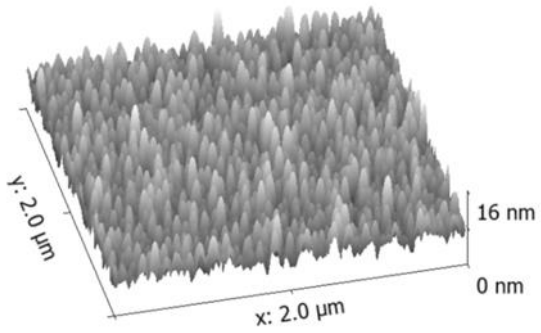

Figure 3-6 AFM images of glass slide with silver island film and a chromium adhesion layer.

AFM was performed in a 2 µm × 2 µm grid to show the surface roughness of silver island films. The AFM tip used is not able to recreate the exact topography due to its size relative to the structures. However, a general representation of the roughness can be visualised. Roughness values were obtained in Gwyddion analysis software where the film has an average roughness of 1 nm and a peak to trough height of 5.5 nm. The

difference in film thickness determined by step height (17 nm) and peak to trough height (5.5 nm) is due to AFM probe tip limitations (size of probe tip compared to nanostructure gaps).

3-2-4 Surface chemistry

The XPS system has a large collection area (400 μm spot) and a low magnification camera which makes it unrealistic to attempt to collect spectra from a fibre. Therefore, the OAD films on the glass slide were used instead. The flood gun was turned on for this study as charging otherwise prevented useful signal from being obtained. This is due to the very thin films that are not continuous and therefore not conductive. XPS was performed as described in Section 2-6 and the results can be seen in the subplots of Figure 3-7.

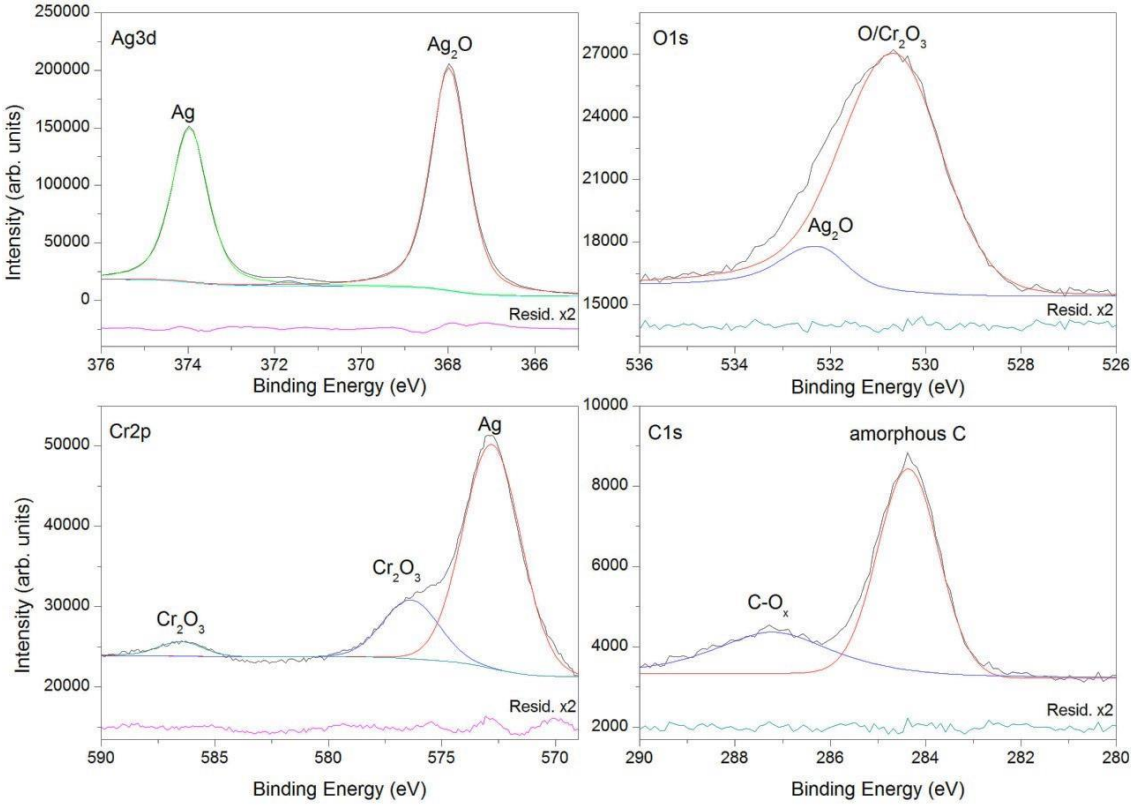

Figure 3-7 XPS elemental plots for silver-island films with a chromium adhesion layer.

The XPS analysis of the silver island films (peaks fitted with Avantage data systems, Thermo Scientific software) shows the presence of silver in its elemental form at

374 eV and 573 eV [77]. There is a strong formation of Ag_2O (368 eV and 532.3 eV [78]) and Cr_2O_3 (530.7 eV [79], 586.6 eV and 576.4 eV [77]). The large presence of Ag_2O does not necessarily mean that there is less metallic silver present. Metallic silver is more likely to be buried under a layer of Ag_2O where XPS is less sensitive. This is also the case for Cr and Cr_2O_3. The main O1s peak (530.7 eV) is normally attributed to oxygen [78] but can also be attributed to Cr_2O_3 [79]. The samples were stored in nitrogen when not in use in an effort to limit oxidation.

Amorphous carbon (284.4 eV [80]) is also present with a contribution from C-O_x (287.2 eV [81]). This indicates contamination of the surface. Carbon contamination is unavoidable on any sample or surface. There are a few factors which can increase the amount of carbon contamination and will be discussed in relation to the OAD procedure (Section 2-2). The deposition system is kept vented which allows for contamination of the chamber. The system must also be vented to change from sputtering to evaporation mode which allows carbon to attach to the sputtered chromium before silver is evaporated. There can be impurities evaporated off the silver when it begins to heat. Therefore, the shutter was placed underneath the source for 1 minute to boil off any contaminates prior to deposition. Samples were kept as clean as possible but adventitious carbon contamination is unavoidable.

Raman spectroscopy was performed (Section 2-10) to determine if the surface chemistry will produce background signals that could interfere with measurements. A wavelength of 514 nm with a 2400 l/mm grating was utilised and the signal was collected with a 20× objective (NA 0.4). Spectra collected on the surface of a fibre before and after modification with thiophenol (Section 2-8-1) are shown in Figure 3-8 (normalised for acquisition time, all other parameters were consistent). It should be noted that silver is not polarisable and should therefore have no Raman spectra. The fact that a spectrum was obtained from the surface, as seen in Figure 3-8, indicates that the surface has been contaminated. This is due to atmospheric carbon, which is consistent with XPS results [82, 83]. Fortunately, after modification with thiophenol there is no indication of the contamination. This is probably due to thiophenol bonding strongly with silver and displacing carbon contamination. Silver contamination could be

problematic with weaker bonding molecules or biological materials. Other substrates should be investigated for use with these analytes.

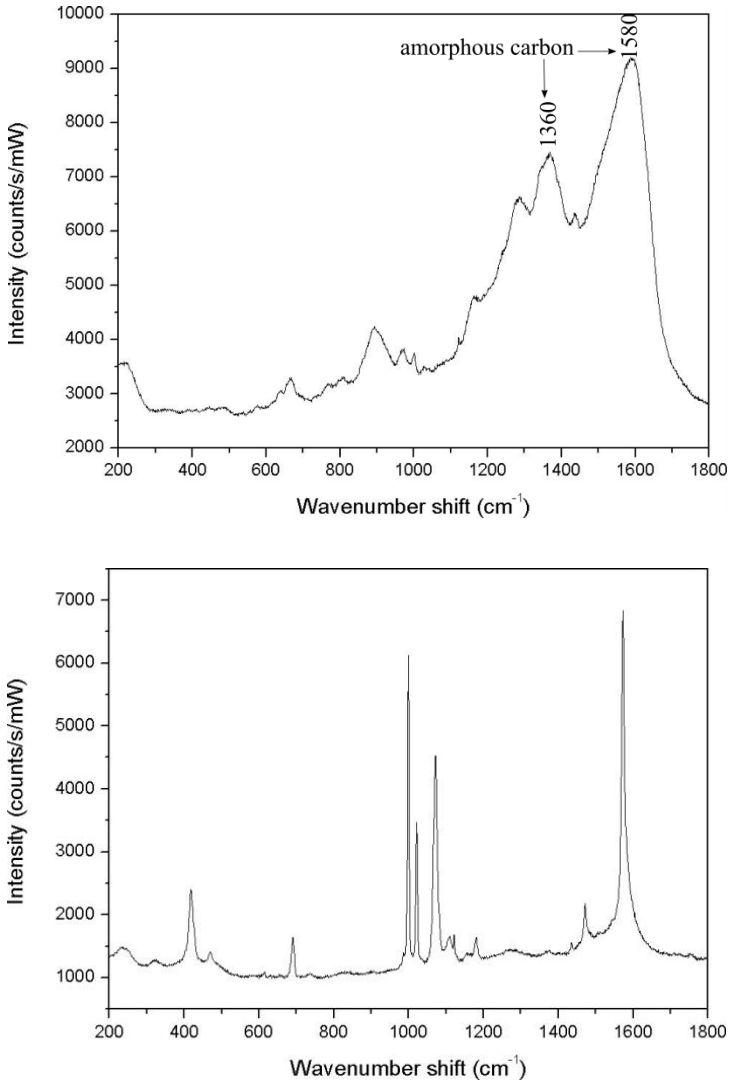

Figure 3-8 Top: Raman spectrum of as-produced silver thin-island film. Bottom: SERS spectrum after functionalization with thiophenol.

3-2-5 SERS repeatability

The Renishaw inVia Raman spectrometer was used to determine the relative standard deviation (RSD) between fibres. The fibres from Section 3-2-1 were prepared with thiophenol as in Section 2-8-1 and were investigated using the Raman spectrometer as described in Section 2-10. A wavelength of 514 nm was chosen as thiophenol and silver may have a resonance near this wavelength [84]. A high resolution grating with

2400 l/mm was used. A 20× long working distance lens (NA 0.4) was used for excitation/collection. The exposure time was 10 s and three acquisitions were normally acquired. The laser power at the sample was 0.1 mW. All data were normalised for the laser power, exposure and acquisition time used during collection.

Ten measurements were obtained across the face of each fibre. The SERS signal was quantified by taking the average intensity of the four major thiophenol peaks at 998, 1022, 1070 and 1572 cm^{-1}. The average was used in calculating the relative standard deviation of a fibre. The relative standard deviation between different fibres was also calculated (Table 3-1). These results indicate that the signal collected across a fibre face is repeatable (among the best reported for random island films [76]) and comparable to other fibres in the same batch.

Table 3-1 Relative standard deviation across single fibres and over the batch of fibres.

Fibre #	**Peak height (counts/s/mW)**	**RSD %**
1	3272	11.0
2	3374	15.3
3	4055	5.6
4	3333	10.4
5	3685	4.1
6	3546	4.6
Batch of fibres	3544	8.2

3-2-6 Substrate SERS aging test

The lifetime of a probe is important as the longer a probe can work efficiently, the less often probes are required to be replaced. The degradation of signal with age is also an important factor in quantitative analysis. The fibres prepared and analysed in Sections 3-2-1 and 3-2-5 were stored for one month in a nitrogen cabinet. They were analysed using the Renishaw inVia Raman microscope under the same parameters as well as under a high confocal setting. The results can be seen in Table 3-2.

Table 3-2 Silver island film analysis after one month of storage. The RSD and average peak height is compared for standard and high confocal settings.

Fibre #	Peak height (counts/s/mW) standard	RSD (%) standard	Peak height (counts/s/mW) confocal	RSD (%) confocal
1	309	56	79	44
2	300	61	97	48
3	355	49	102	38
4	353	68	97	36
5	343	48	-	-
6	256	50	-	-
Batch of fibres	319	12	94	10

The relative standard deviation between fibres is larger after one month of storage than when the fibres were freshly prepared (Table 3-1). The RSD is slightly larger in the standard confocal mode compared to the high confocal setting. The overall intensity is reduced to 10% after one month of aging. The intensity of the peaks is lower in the high confocal setting compared to standard confocality. Using high confocal mode reduces the number of out-of-focus rays reaching the CCD. The intensity of signal from the analyte is also heavily reduced, which is detrimental to remote sensing probes, especially if the analyte is a weak scatterer. The standard confocal mode benefits large core projections, allowing more of the core area to reach the CCD. Therefore, standard confocality is the preferable choice for optrode analyte detection. Storing fibres significantly reduces signal intensity so it is preferable to use fresh fibres.

3-2-7 Summary of silver-island films as a sensing platform

The silver-island films were characterised for structure, surface roughness, surface chemistry, SERS repeatability and aging. It was shown that the structures formed are repeatable enough for the project's purpose (RSD of 12% across a batch of fibres) and that the SERS performance is also repeatable (RSD of 8.2% across a batch of fibres) but deteriorates to 10% of originally intensity over time. The atmospheric carbon on the surface is displaced when functionalising with thiophenol. Therefore, these films appear

to be ideal for applications where SERS performance is to be compared across different samples.

As mentioned in Section 1-6-3, access to the internal constituents of bacteria is necessary for differential identification of bacterial species. Silver-island films are not able to pierce bacteria and so the SERS interaction volume is limited to the cell wall. Also, due to the strong carbon bands overshadowing weak analyte signal (common to biological materials), biological applications are not advised with silver-island films and so alternative substrates have been investigated for these applications (black silicon needles and pyramids).

3-3 Black silicon needles

Black silicon with a needle-like surface structure was created using a dry reactive ion etching technique (RIE) (Table 3-3) by colleagues in the Melbourne Centre for Nanofabrication (MCN) [29]. It was desirable to characterise the needles in depth for their structure and chemical composition prior to implementation as a SERS platform. This was in an effort to understand the different structures that could be fabricated (see also Section 3-4) and how the fabrication process affected the samples. SERS applications using black silicon can be found in Chapter 5.

Table 3-3 Parameters for fabrication of black silicon needles.

Parameter	**Needles (MCN)**
Instrument	Oxford PlasmaLab 100 ICP380
SF_6 gas flow rate	65 sscm
O_2 gas flow rate	44 sscm
Process pressure	0.047 mbar
Power	100 W
Etching time	25 minutes

3-3-1 Needle structure

The Nova NanoSEM (Section 2-3-2) was used to collect SEM images of the needle sample. The substrate shows promise as a highly enhancing SERS substrate due to the

needle like protrusions from the surface (Figure 3-9). Unfortunately, the needles have random tips being pointed, forked or multi-pronged. Also, it can clearly be seen that the structures have different sizes and spacing in the micron scale and so positioning of the focus can have a substantial influence on the excitation area. A typical microscope spot size is approximately 1 μm in diameter. This area, depending on position, could include mostly empty space, lots of prongs or a part of a prong and part empty area. This could cause a large variation in signal for SERS measurements if signal strength is to be compared. However, this should not have a large impact on bacteria as signal strength comparisons are not as important as identification. Low signal to noise may be an issue for biological samples.

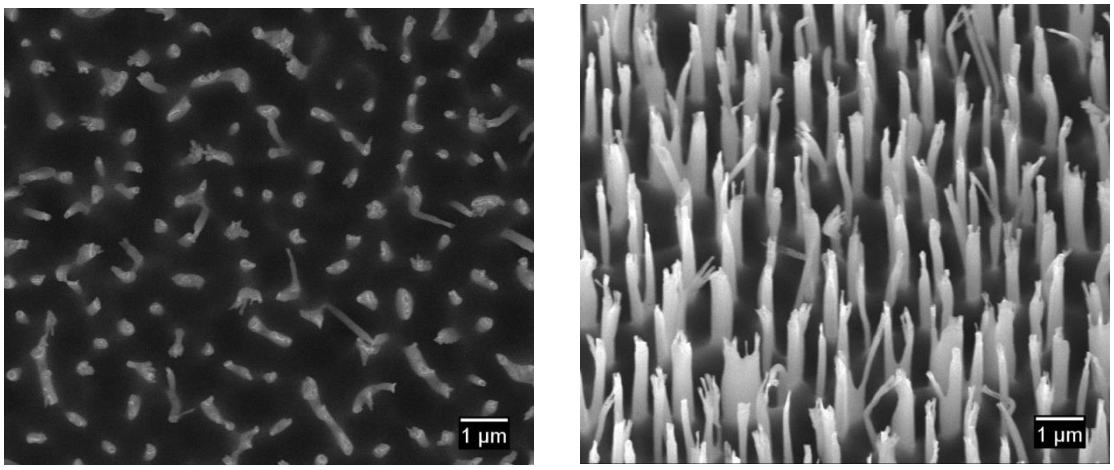

Figure 3-9 SEM images of black silicon nanoneedles with top-down view (left) and with 20° angle (right).

The radius of curvature of the tips of the needles was determined to be 5.4 ± 1.6 nm. This value was determined by measuring the sharpest point on a needle using ImageJ (National Institute of Health, USA). This was completed for approximately 40 needles. The height and width of the needles was also determined using ImageJ by measuring approximately 45 needles. The height of the needles is 4.1 ± 0.3 μm and the width is 239 ± 75 nm. This height is significantly larger than the diameter of *E. coli* and the tips are reasonably sharp. Theoretically these structures should be able to pierce the bacteria, although the bacteria are smaller than the gaps between the needles.

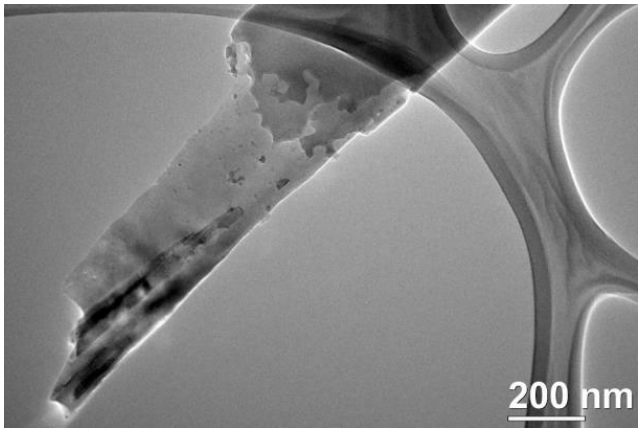

Figure 3-10 TEM image of a black silicon nanoneedle.

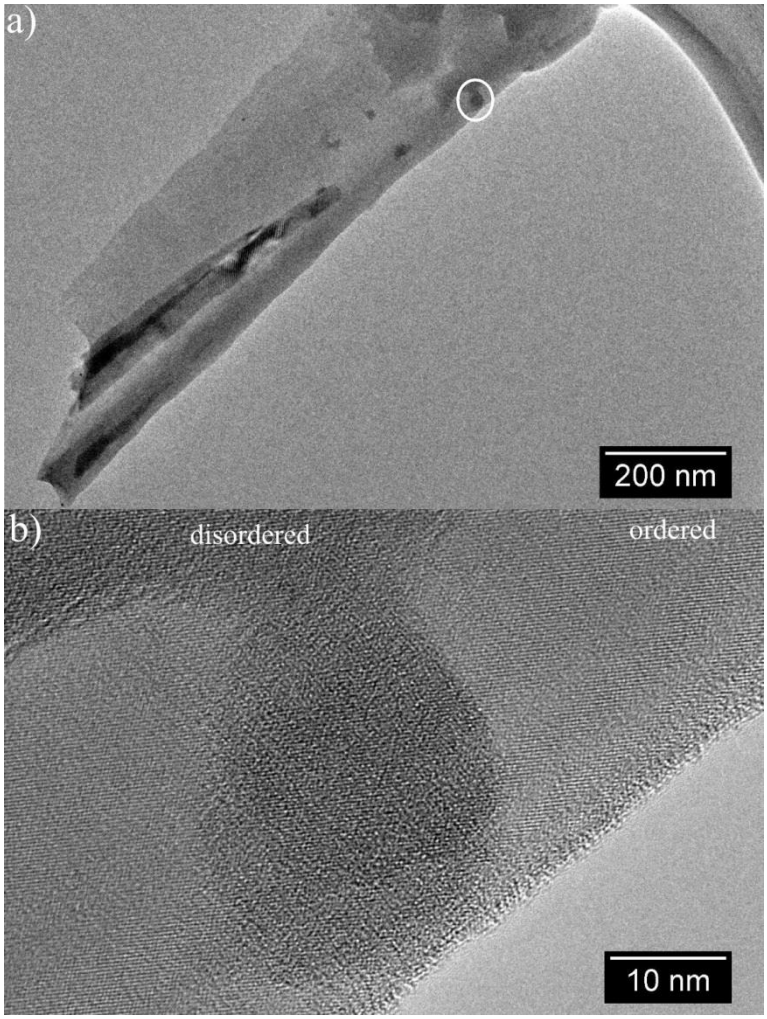

Figure 3-11 a) HRTEM image of a needle highlighting the section to be used for increased magnification. b) increased magnification of a) showing ordered and disordered crystal structures.

TEM was used to further investigate the structures (Section 2-4). TEM shows that there is a coating which thins towards the tip (Figure 3-10). The HRTEM image (Figure 3-11) shows ordered and disordered crystal structures for an area that encompasses the exposed needle and the coating. The ordered section is indicated by the presence of lattice fringes whereas the disordered section appears as random structures. Further analysis with EDS mapping can identify the elemental composition of these areas.

3-3-2 Chemical analysis

Elemental mapping was conducted using STEM mode and an EDS detector inserted in the Jeol 2100F (Section 2-4). The elemental map can be seen in Figure 3-12 with a STEM image of the needle and scans for Si, O and F (no other elements were detected).

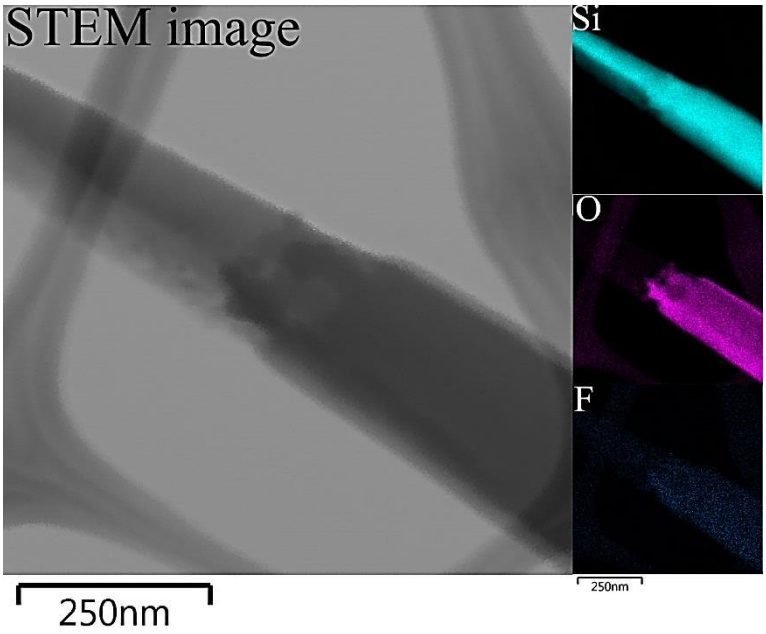

Figure 3-12 STEM EDS map of needle tip.

EDS revealed that the needle has an oxide and fluoride coating on the base which thins to reveal a silicon tip (Figure 3-12). Some oxygen is still present on the tip as it is unlikely that silicon will remain pure when exposed to atmosphere. This is supported by the HRTEM image (Figure 3-11) which showed lattice fringes on the thinned section of needle indicating an ordered crystal structure (Si) and a disordered crystal structure for the coating section (most likely SiO_2). It is possible that etching with HF could remove

the oxide layer from the main body of needle though this could add more fluorine in the process. This could also alter the tip geometry and may not be beneficial to sensing.

Surface contamination was investigated using XPS as this technique is sensitive to a wide range of elements and is able to determine chemical species. The samples were mounted following the procedure in Section 2-6. The flood gun was turned on as charging was deemed to be problematic during a test scan. A survey scan was used to determine all elements present on the surface. Then high resolution scans for Si, C, S, O and F were obtained as these elements were found to be present on the surface.

The presence of Si, S, C, O and F were all expected as these elements were accounted for during the fabrication process. The high resolution scans of note can be seen in the subplots (Figure 3-13). Sulphur is excluded as the intensity is relatively low and no useful information was obtained from a high resolution scan.

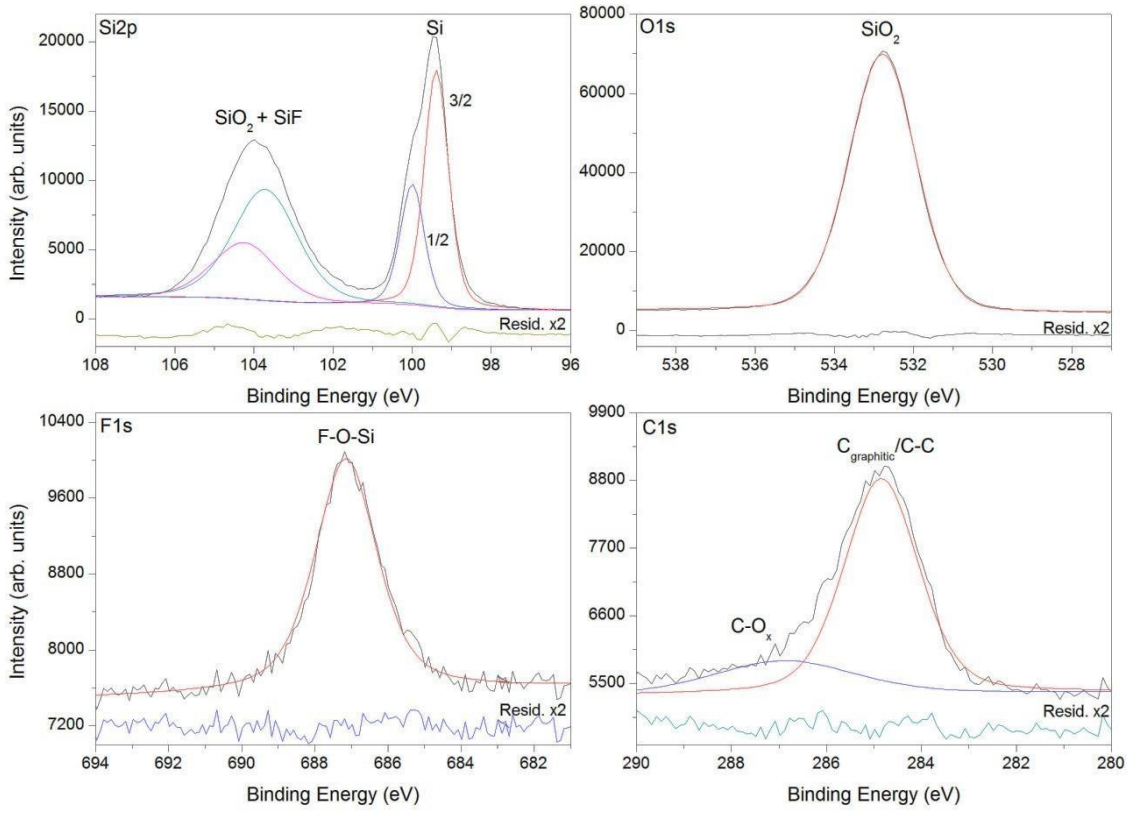

Figure 3-13 Subplots of elemental species analysis for black silicon needles using XPS.

Each high resolution scan was fitted using Avantage to determine the locations of all peaks contributing to the spectra. It is interesting to see the structure of silicon in high resolution. The main peak positions indicate the presence of Si (99.4 eV) and a probable overlap between SiO_2 [85] and SiF at 104 eV [86]. The sub peaks under silicon at 99.3 eV and 100 eV correspond to the 3/2 and 1/2 spin states respectively. The spins under the SiO_2 + SiF peak are not able to be accurately discerned due to broadening of the peak and the superimposed contributions of the oxide and fluoride species.

The largest contribution from the sample was found from the O1s scan where the peak position (532.7) can be attributed to SiO_2 [77]. The atomic percentage (At. %) of SiO_2 is 30 At. % from the O1s scan and 33 At. % from the joint SiO_2/SiF peak, whereas the atomic percentage of silicon in its elemental form is 28 At. % and the combined F-O-Si peak is 2 At. %. This shows that the majority of the silicon is forming SiO_2 which is consistent with the EDS mapping results in Figure 3-12 where only the very tip of each needle was close to pure Si.

The fluorine scan revealed a F-O-Si peak centred at 687.1 eV which is comparable with a similar silicon etching experiment conducted by Tomita *et al.* [87]. The carbon scan revealed a graphitic/amorphous carbon peak (284.8 eV) with a small C-O_x (287 eV) contribution. These carbon peaks have previously been reported in the literature for fluorinated carbon species generated by use of plasma [81].

The XPS elemental species analysis has confirmed that the pure silicon needle (28 At. %) is mostly covered in a SiO_2 layer (approximately 47 At. %). There is also some contribution from SiF (approximately 17 At. %), F-O-Si (2 At. %), graphitic/adventitious carbon (4.5 At. %) and C-O_x (1.5 At. %). It is interesting to note that for this fabrication process graphitic carbon or adventitious carbon could form. To ensure that this carbon is not problematic, the sample was investigated under Raman spectroscopy.

Raman spectroscopy (Section 2-10) was used to check if the surface contamination would affect the Raman background during sensing. A wavelength of 633 nm with an excitation power of 9 mW at the sample was focused with a 0.4 NA objective. Three

accumulations were collected and the data were then normalised for laser intensity, accumulations and exposure time. As shown in Figure 3-14 the only background generated by black silicon needles is silicon. Silicon is widely used as a reference to calibrate Raman spectra due to its high intensity, narrow peak at 520 cm^{-1}. Usually, this is the only peak that is visible due to its relatively large intensity compared to its second order peaks. The second order optical [88] and second order acoustic peaks [89] can become visible depending on the excitation wavelength used and the area of collection. Black silicon has quite visible second order peaks as the needles create a larger surface volume to be collected from.

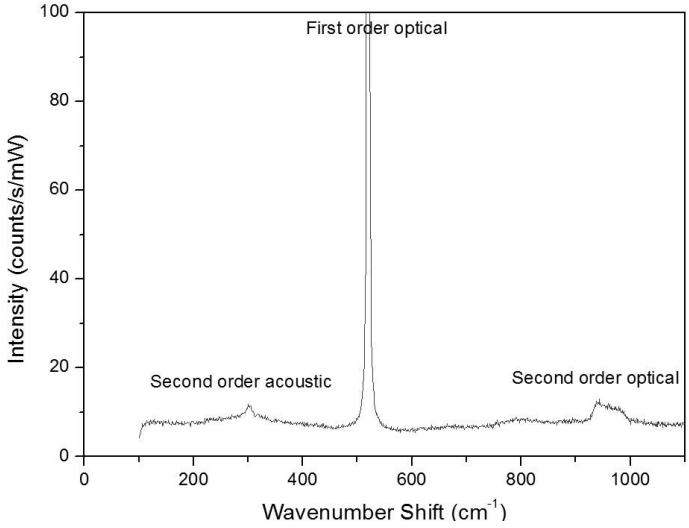

Figure 3-14 Black silicon reference showing sharp peak at 520 cm^{-1} attributed to silicon. A restricted Y range has been implemented to show second order peaks clearly.

The needles were also tested to determine if the surface was hydrophilic or hydrophobic. The surface had a contact angle of 91° (droplet shown in Figure 3-15) which is classed as a hydrophobic surface (hydrophobic is a contact angle > 90°). This could be due to the high-aspect ratio needles or perhaps the surface chemistry of the sample.

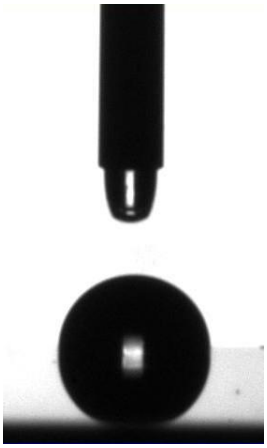

Figure 3-15 Contact angle measure for black silicon needles.

3-3-3 Summary of black silicon needles

The black silicon needle sample has been characterised for structure and chemical composition. It has been shown there is a SiO_2 layer covering the majority of the needle along with an F-O-Si and SiF contribution. The very tip of the needle is mostly Si with a very thin oxide layer on the outside. Regardless of the complex surface chemistry, the Raman background is dominated only by silicon. This should result in background-free measurements for the majority of the fingerprint region though care should be taken around 520 cm^{-1} to avoid saturating the detector. The needle surface had a contact angle of 91° which is classed as a hydrophobic surface. It is uncertain whether if this large contact angle is due to the high-aspect ratio or the surface chemistry. This could pose problems in sensing due to attachment of bacteria which prefer a hydrophilic surface [90].

As mentioned in Section 1-7-2, bacterial impalement is critically important in SERS for differential identification of bacterial species. The high aspect-ratio of the black silicon needles should be able to [71] completely pierce the bacteria and allow access to the internal constituents. However, the hydrophobicity of the surface may inhibit attachment. The effect this will have in biological sensing will be tested (see Chapter 5).

3-4 Black silicon pyramids

Black silicon pyramids [35] were created by colleagues in the NanoLab at Swinburne as an alternative to the needle structures created in MCN. Table 3-4 shows the parameters used for the pyramid structures and the needle structures for comparison. As chamber geometries varied between instruments, different flow rates and pressures were experimented with when fabricating the black silicon pyramids. RIE was assisted by inductively coupled plasma (ICP) for fabrication of pyramidal black silicon. The pyramid structure was determined to have potential as a SERS platform and thus was characterised for comparison with the MCN sample. It was desirable to characterise the pyramids in detail for their structure and chemical composition prior to implementation as a SERS platform. This was in an effort to understand the different structures that could be fabricated and how the fabrication process affected the samples. SERS applications using pyramidal black silicon can be found in Chapter 5.

Table 3-4 Parameters used in fabrication of black silicon pyramids and needle structures for comparison.

Parameter	Pyramids (NanoLab)	Needles (MCN)
Instrument	RIE-101iPH (SAMCO Inc.)	Oxford PlasmaLab 100 ICP380
SF_6 gas flow rate	35 sscm	65 sscm
O_2 gas flow rate	45 sscm	44 sscm
Process pressure	0.01 mbar	0.047 mbar
Power	15 W RIE 150 W ICP	100 W RIE
Etching time	15 minutes	25 minutes

3-4-1 Pyramid structure

The Nova NanoSEM (Section 2-3-2) was used to view the structure of the black silicon pyramids top-down and at an angle of 20 degrees. The top-down view (Figure 3-16) shows “cloud-like” structures sitting on top of the pyramids. The pyramids appear to be more closely packed than the needle structures, though there are still areas where two peaks join so it appears that there are multiple tips on some pyramids.

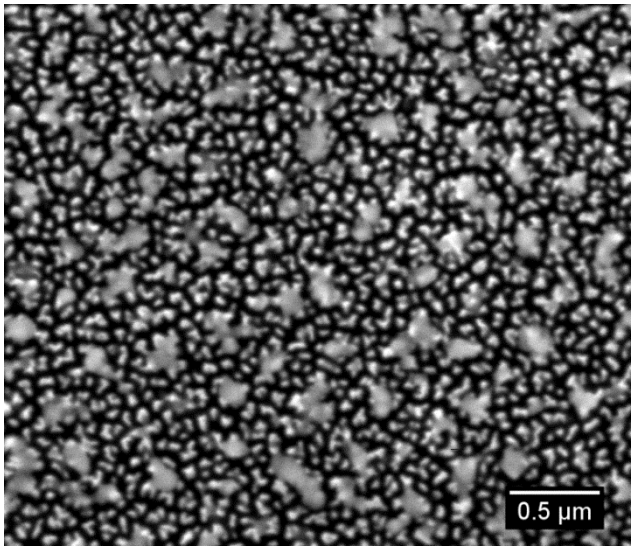

Figure 3-16 Top down view of black silicon the NanoLab sample. Cloud-like structure can be seen on the tips of pyramids.

Tilting the sample to 20 degrees provides a clearer view of the pyramid structure and the "cloud" structures (Figure 3-17). It is clear from these images that the NanoLab black silicon has a pyramid structure which is closely packed and in some cases two pyramids are not completely separated. Unfortunately the "cloud-like" structures contaminating the surface are widespread and would be problematic for SERS sensing. Measurements obtained may not be reproducible as the nanoscale roughness contributing to the SERS effect would be significantly different if the objective was aligned and focused on a cloud structure, on bare pyramids or in between. Sample cleaning was attempted using sonication in ethanol but this was ineffective. Sample cleaning was also attempted with oxygen/hydrogen plasma but this did not remove the "cloud-like" structures either.

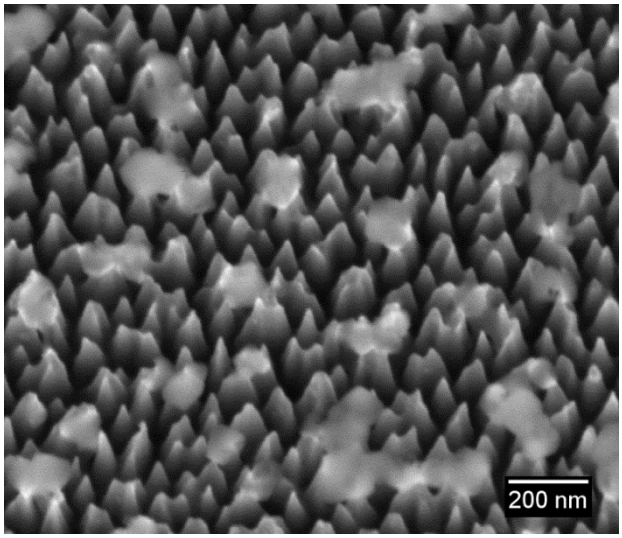

Figure 3-17 Black silicon pyramids at a 20 degree angle to better visualise the "cloud-like" structures.

The radius of curvature of the tips of the pyramids was determined to be 10 ± 2.4 nm. This value was determined by measuring the tip of the pyramid using ImageJ. This was completed for approximately 40 pyramids in a contaminant-free zone. The height and width of the pyramids was also determined using ImageJ by measuring approximately 30 pyramids. The height of the pyramids is 185 ± 30 nm and the full width half maximum is 54 ± 10 nm. This height is significantly smaller than the diameter of an *E. coli* cell (500 – 800 nm). Gold coating the sample with 200 nm of gold increased the height to approximately 300 nm but this still smaller than *E. coli*. Thicker gold coatings produced a continuous film which is not suitable for SERS [35].

The pyramid structure is quite different to the needles created at MCN. However, it is possible that there is also an oxide layer on the outside and inside is a sharp silicon needle. This could be easily proven with TEM if the samples were suitable. However the samples were not suitable for TEM analysis as the pyramids tended to agglomerate and TEM is only viable for thicknesses less than 100 nm. Milling them to a suitable thickness would result in damage due to their small size. Unfortunately the internal structure of the pyramids could not be determined in this study.

3-4-2 Chemical analysis

The Nova NanoSEM (Section 2-3-2) was used to create an elemental map of the pyramid sample in an effort to identify the distribution of elements across a section which was populated with clear tips and cloud-covered tips. The map can be seen in Figure 3-18. The elements detected included silicon, oxygen, fluorine and aluminium. The cloud-like contamination in the SEM image appears lighter in colour than the bare pyramids. Fluorine is mostly concentrated on the contaminated areas. There is a slight increase in the concentration of aluminium on the clouded area as well. Silicon and oxygen do not exhibit a discernible difference across the area. In order to determine the species fluorine and aluminium are forming, XPS analysis was performed.

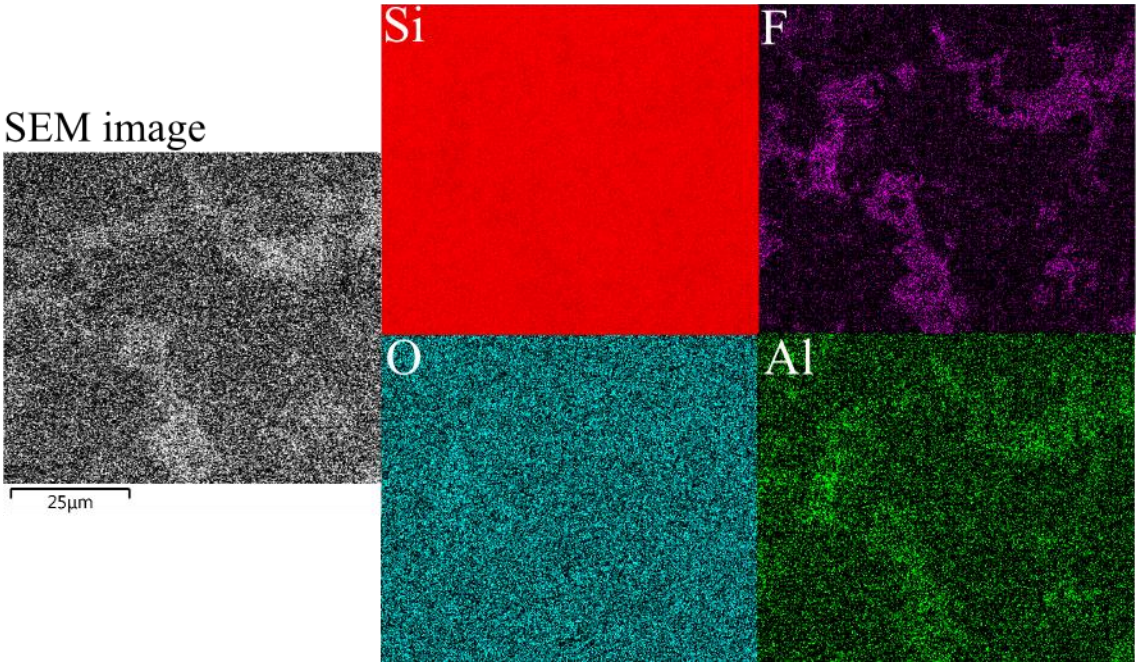

Figure 3-18 Elemental mapping of black silicon pyramids.

XPS (Section 2-6) was used to determine the chemical species present on the black silicon pyramids. A survey scan was undertaken to determine which elements were present. Higher resolution scans were then completed for Si, F, O, Al and C (Figure 3-19). The oxygen scan was omitted in the subplot as it had the same position and shape compared to the oxygen peak of the needles (Figure 3-13) as well as almost identical atomic percentages (29 At. % for pyramids compared to 30 At. % for needles). There is

aluminium present on the pyramids which was absent on the needles. The presence of aluminium can be explained by the use of two holders inside the etching chamber made of Al_2O_3. It is possible that Al molecules were etched and settled on the surface of the silicon during the etching process.

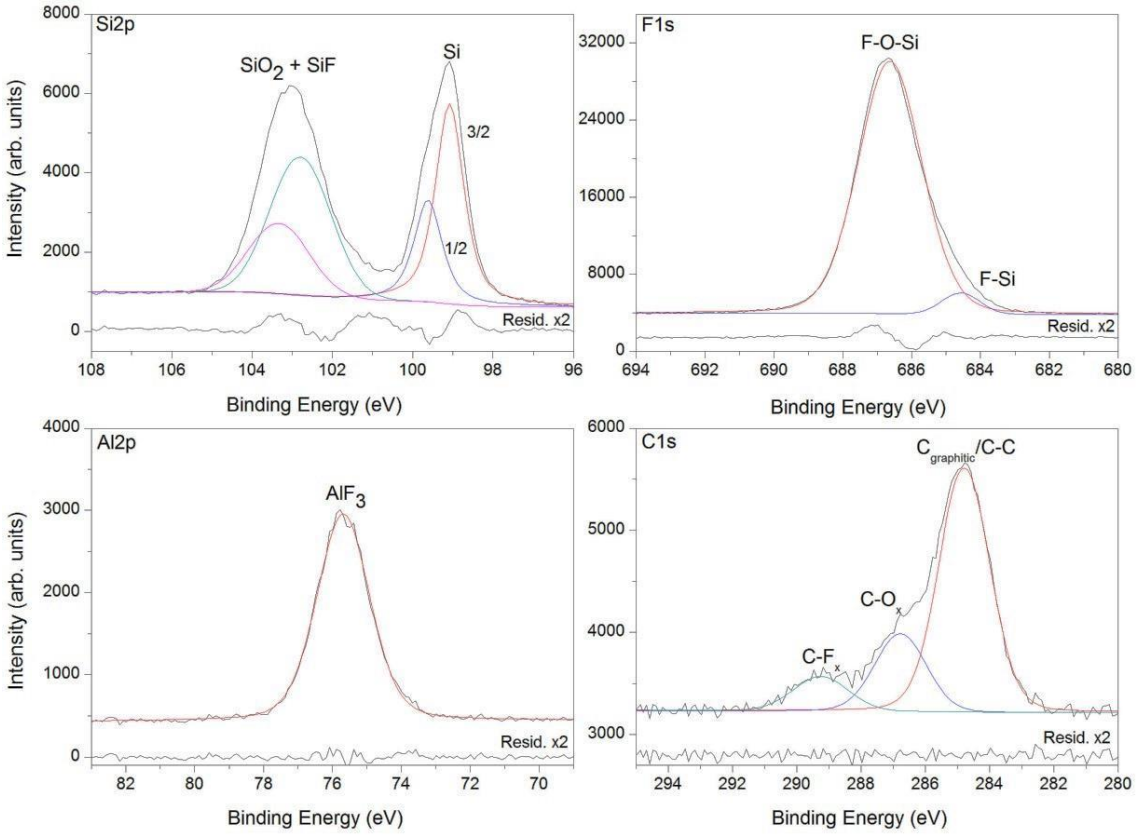

Figure 3-19 Subplots of potential chemical species identification of black silicon pyramids using XPS.

The silicon high resolution scan has the same peak positions as for the needle sample; however, the pyramid sample has a different Si:SiO_2 +SiF peak ratio. This could indicate a higher percentage of SiF formation which shares the same peak position as SiO_2 [86]. Also, the atomic percentages of Si (17.2 At. %) and SiO_2 +SiF (20 At. %) are significantly lower (approximately 10 At. % less) in the pyramid sample compared to the needle sample. Any difference in signal intensity between the two samples needs to be considered in terms of microstructure differences. The high-aspect ratio needles will have less sample volume available for XPS compared to the small-aspect ratio pyramids which are also closely packed. Considering the needles are 4 µm

tall, it is clear that photoelectrons from the base of the needle would be blocked by the tips. Therefore it is difficult to make accurate comparisons between the two samples due to sample volumes available for collection. Nonetheless, due to the greater volume of silicon exposed to the beam in the pyramid sample it was expected that the silicon signal would be higher. However, due to the widespread surface contaminants, it is possible that the signal is being skewed towards the composition of the contaminants.

The atomic percentage of the F-O-Si peak (16.3 At. %) is significantly larger than that of the needle sample (2 At. %). There is also a contribution (0.8 At. %) from F-Si (684.5 eV) which was absent on the needle sample but is common for this sort of fabrication process [87]. Again, it is difficult to accurately compare signals from the two samples due to the sampling volume. However, the significant presence of F-O-Si can be partially explained by the prevalence of the surface contaminants which fill a large portion of the available sampling volume on the pyramids.

Fluorine was also found forming AlF_3 (75.7 eV [77]) which can be explained by the etching gas interacting with an unused aluminium holder and forming AlF_3 which has bonded to the surface. AlF_3 is contributing 8 At. % of the surface chemistry in the pyramid sample but is missing from the needle sample due to a different chamber set up which does not require the second holder to remain inside the chamber.

The carbon scan revealed identical peaks for graphitic carbon/amorphous carbon and C-O_x (4.4 and 1.4 At. % respectively) with a small (0.7 At. %) addition of a C-F_x species (289.4 eV) [81]. This suggests that increased levels of fluorine may allow the formation of this carbon species from adventitious carbon in the chamber.

The XPS analysis has determined that the “cloud-like” structures are most likely due to the formation of AlF_3, F-O-Si, F-Si and C-F_x. This contamination is widespread and contributes to the majority of the signal, swamping signal from the silicon structures. Raman spectroscopy was performed to check if the contaminants produced any background signal. The same parameters were used as in Section 3-3-2 and as can be seen (Figure 3-20) the only contribution is from silicon.

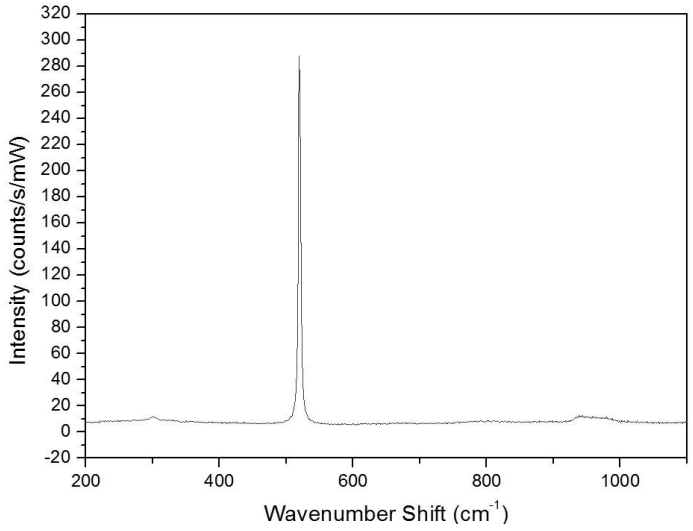

Figure 3-20 Black silicon pyramids tested under Raman showing a sharp peak at 520 cm^{-1} that was attributed to silicon and two second order silicon peaks.

The contact angle for the pyramid structures could not be measured as the drop immediately dispersed once it touched the surface. Therefore it was determined that the contact angle was zero and that the pyramid sample is hydrophilic (0-90° contact angle) which may prove beneficial for biological sensing.

3-4-3 Summary of black silicon pyramids

The black silicon pyramids were randomly covered in large areas of "cloud-like" contamination. The contaminants were not able to be removed using standard sonication or plasma cleaning methods. They were however identified using a combination of EDS mapping and XPS. The contaminants formed are AlF_3, F-O-Si, F-Si and C-F_x. The sample exhibited strong hydrophilic behaviour which may be beneficial for biological sensing. The tips of the pyramids are not as sharp as the needles and they have a small aspect-ratio. The hydrophilic surface should be favourable for bacterial attachment [90]; however the small aspect-ratio pyramids may not be able to completely impale the bacteria. This will affect the depth of penetration of the SERS active hot-spots inside bacterial cells and may not allow for differential identification of bacterial species. The effect this will have in biological sensing will be tested (see Chapter 5).

3-5 Conclusion

This chapter has investigated three different substrates and their suitability for application based SERS. A summary of the substrates and properties has been provided in Table 3-5 below.

Table 3-5 Summary of SERS substrates favourable properties and limitations.

Substrate	Favourable Property	Limitations
Laser-ablated nanoparticles	-	• Require cross-linker to attach to substrate harming biocompatibility; and • Strong cross-linker bands in fingerprint region.
Silver-island films	• Reproducible structures; • Low RSD; • Allows remote excitation; • Can be deposited directly onto a fibre tip; • Suitable for optrode devices; and • Suitable for comparison studies.	• Strong carbon background would swamp biological analyte signals; and • Thin films not able to penetrate bacteria so SERS would only originate from cell wall.
Black silicon needles	• High aspect ratio and sharp radius of curvature should pierce bacteria; • Only silicon background Raman;	• Hydrophobic surface may not be amenable for bacterial attachment; • Opaque so not suitable for remote excitation; • Requires imprinting into a curable layer on a fibre tip to create probe.
Black silicon pyramids	• Hydrophilic; • Only silicon background Raman.	• Small aspect ratio may not pierce bacteria completely; • Pyramids covered in contamination; • Opaque so not suitable for remote excitation; • Requires imprinting into a curable layer on a fibre tip to create probe.

Laser-ablated nanoparticles appear unsuitable for most real world applications due to the strong cross-linker bands covering most of the fingerprint region. The cross-linker

also harms the bio-compatibility of this substrate and therefore the nanoparticle substrate was not investigated further.

The silver-island films created by OAD were successfully fabricated on the tips of optical fibres. A strong signal from atmospheric carbon was observed though it was displaced when functionalising the tips with thiophenol. This substrate would not be suitable for use with biological samples because of the strong atmospheric carbon signal and it is not able to pierce bacteria. However, the films were shown to be reproducible and the SERS signal has a relatively low RSD between samples. Therefore, the OAD technique is suitable for a study which compares signal strength between different fibres. The low RSD imbues confidence in the comparability of results obtained from different samples. The silver island films will be used as they are sufficiently thin to ensure that sufficient laser power will excite the sample in the remote configuration. Standard confocality is preferable as the slit does not limit the core projection onto the CCD. Standard confocal is also beneficial as more signal from the analyte is able to reach the CCD. These findings will be useful for a study optimising signal collection from an optrode sensor. Therefore, silver-island films will be exclusively used in the comparison study (presented in Chapter 4) to determine which fibre parameters are required for an efficient remote sensor probe.

The two black silicon samples show promise as potential bacterial sensors due to their sharp tips and spikey structures. The surface chemistry did not contribute to any unwanted Raman bands; however, it is uncertain how the chemistry will affect bacterial attachment and growth on the surface. The contaminants were not able to be removed and so application based testing with bacteria will need to be performed to examine the effect these “cloud-like” structures have. The difficulties in fabricating an optrode sensor using black silicon as the SERS substrate precludes black silicon from being assessed as part of the optrode optimisation study (Chapter 4).

Chapter 4

Optimising Optical Fibres as Probes

A range of optical fibres with surface-enhanced Raman scattering functionalized tips have been evaluated for use as micro-scale sensing devices. In order to optimize the sensitivity of the optical fibre probe, the relationship between SERS intensity and different fibre parameters was investigated. Parameters of interest include numerical aperture, core size, mode structure and core material as well as the numerical aperture of the microscope objective. In order to provide a consistent SERS substrate to control for differences between fibres, silver-island films were utilised as they can be fabricated with ease and provide a repeatable and reproducible substrate (low RSD between fibres, see Chapter 3). Pure silicon is opaque to 514.5 nm excitation wavelength which prevents the use of black silicon as a remote SERS substrate. Some of the material from this chapter has appeared in Applied Optics [91].

4-1 Test parameters

Ten different commercial fibres were compared as they are easily available and relatively low cost. The fibres had a range of different core sizes, NAs and V-numbers as shown in Table 4-1 which are based on the manufacturer's specifications where available, or data on the spool. The V-numbers at 514 nm were calculated from the NA and core diameter [36].

Table 4-1 List of fibres tested where (m) is a measured value.

Fibre ID	NA	Solid Angle (sr)	Core Diameter (µm)	V-Number (at 514 nm)
S405	0.12	0.04	3.3	2.4
Hi 1060 Flex	0.14	0.06	3.4	2.9
780HP	0.13	0.05	4.4	3.5
Hi 980	0.21	0.14	3.5	4.5
Pure Silica Core	0.10 (m)	0.03	7.6 (m)	4.6
F-SBC	0.16	0.08	6.6 (m)	6.4
SMF28	0.14	0.06	8.2	7.0
SM1500	0.30	0.29	4.2	7.7
MMF	0.195	0.121	50	60
MMF	0.272	0.237	62.5	103

The dopants were determined by performing EDS (Section 2-5) on each fibre as this information was not in the specifications provided by the manufacturer. Each fibre listed in Table 4-1 was investigated with EDS using the Philips XL30 to determine the composition of the core and the cladding. Unfortunately, the instrument has a boron window and so if the cladding was doped with boron (a common cladding dopant) it would not appear on the spectrum. Two fibres were found to have a pure silica core but there was no detectable cladding dopant. There is a possibility that boron, or perhaps fluorine, is present. A fluorine peak would be very close to the strong oxygen peak and if the percentage is small in comparison it may not have been detected. Two fibres had a visible trench surrounding the core. The detected elements for all fibres are shown in Table 4-2 where the percentages are quoted as atomic percent.

Table 4-2 Composition of core for each fibre measured in atomic % with the Philips XL30 SEM in EDS mode.

Fibre ID	**Core Composition**
S405	Pure SiO_2
Hi 1060 Flex	SiO_2-GeO_2 Ge: 4.3% Ge in trench: 2.2%
780HP	SiO_2-GeO_2 Ge: 2.1%
Hi 980	SiO_2-GeO_2 Ge: 4.6%
Pure Silica Core	Pure SiO_2
F-SBC	SiO_2-GeO_2 Ge: 4.2% Ge in trench: 0.7%
SMF28	SiO_2-GeO_2 Ge: 1.8%
SM1500	SiO_2-GeO_2 Ge: 7.9%
MMF50	SiO_2-GeO_2 Ge: 6.9%
MMF62.5	SiO_2-GeO_2 Ge: 13.1%

Four different NA and magnification microscope objectives were used in order to test the dependence of solid angle on collection efficiency for each fibre. The objectives are listed in Table 4-3.

Table 4-3 Microscope Objective Specifications.

Magnification	NA	Solid Angle (sr)
5	0.12	0.04
10	0.25	0.20
20L	0.40	0.52
50L	0.50	0.84

4-2 Procedure

4-2-1 Fibre probe design

The single-ended optrode approach does not allow the fibre Raman background to be filtered out [37]. Therefore short fibre lengths of about 25 mm were used in this study to minimize the background. These short lengths are of interest for transcutaneous biosensing [92]. Each of the test fibres shown in Table 4-1 were prepared and glued to the test block as described in Section 2-1 (Figure 4-1 shows mounting and sensing geometries).

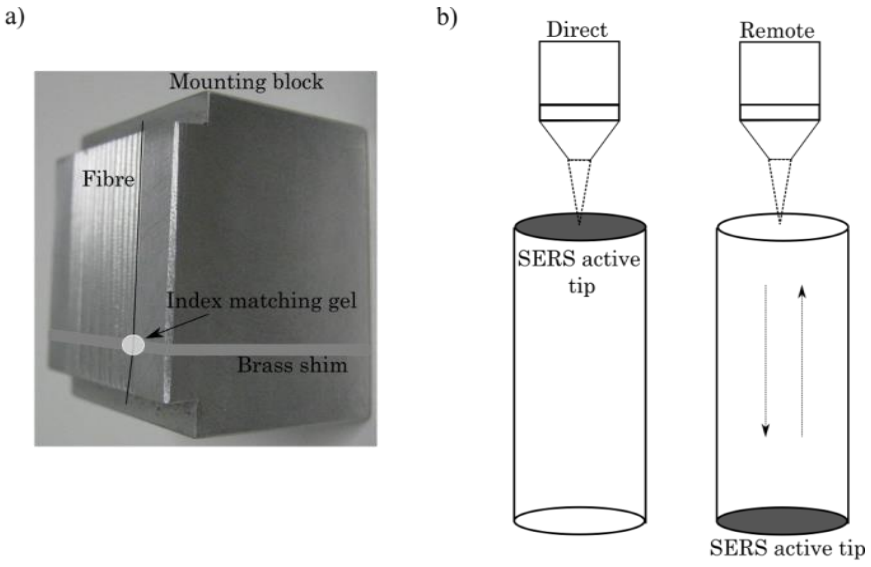

Figure 4-1 (a) Samples and mounting block, showing the brass shim used to bend the fibres. (b) Direct and remote sensing configurations.

Modes can propagate in the core and cladding of a fibre; however cladding modes are normally undesirable as they are difficult to control. The polymer jacket surrounding

the cladding is designed to attenuate any modes that start to propagate in the cladding. Unfortunately, as the jacket is stripped from the fibres used in this work, cladding modes are not adequately suppressed and can cause significant uncertainty in terms of coupling efficiency [93]. Therefore index matching gel (Thorlabs, G608N, n_D = 1.4646 at 25 °C) was placed along the length of each fibre to remove the cladding modes. However, this was not successful in stripping all of the cladding modes, as the index matching gel does not exactly match the refractive index at the SERS excitation wavelength (514 nm). A thin sheet of metal (brass shim, 0.2 mm thickness) was slipped underneath the coated end of the fibres, providing an angle larger than the critical angle in order to suppress total internal reflection in the cladding. The required bend angle was determined by inspection of the transmitted light patterns. These efforts ensured that the substrate was uniformly excited and allowed reliable comparison of different fibre types.

4-2-2 SERS substrate fabrication

Silver-island films produced by OAD were utilised for the SERS-active tip of the test fibres. The films were fabricated as described in Section 2-2. Note that this substrate fabrication process was chosen to ensure good repeatability between samples (Section 3-2-5), rather than to achieve the highest possible SERS signal. Increased signal levels can be obtained in thicker nanorod films [19], but at the cost of reduced transmission in the remote geometry [76]. A number of more highly enhancing substrates are available for future development of the probes [15, 94-96]. The tips were functionalised with thiophenol (Section 2-8-1) as it is known to form stable and reproducible self-assembled monolayers on silver [19, 51].

4-2-3 Experimental setup

A Renishaw inVia Raman microscope was used for coupling, NA testing and collecting SERS spectra of the test analyte (Section 2-10). The stage has a hollow section where a microscope slide can be mounted. The block (Figure 4-1a) was carefully placed on the slide, allowing the fibres to protrude off the edge. When the laser light was coupled, the transmitted light pattern could be observed underneath the stage. Visual inspection of the transmitted light assisted in achieving reproducible coupling to each fibre.

The spectrometer was operated with an excitation wavelength of 514.5 nm, a holographic notch filter and a 2400 l/mm grating. The slit width was set to 65 µm, which is a relatively relaxed setting compared to the confocal setting of 20 µm. A range of microscope objectives were used to couple light into the fibre (see Table 4-3). Spectra were acquired for three accumulations of 10 s. All spectral data have been normalized for excitation power at the SERS substrate and exposure time. For the remote measurements, the excitation power was inferred from measurements of the power transmitted through uncoated fibres. Laser powers in the range 1-5 mW were used, depending on the particular objective and fibre background signal levels.

4-3 Cladding mode elimination

The transmitted mode pattern for each fibre was investigated before and after applying index matching gel and introducing a bend greater than the critical angle. Some examples of the results are shown in Figure 4-2. The mode structure was similar for all objectives; the size of the pattern changed with different magnifications, but otherwise the pattern was very similar. The examples shown here were chosen as they produced the clearest images when photographed. It was challenging to photograph the cladding modes as there is limited space beneath the stage. A tripod was used so the camera was always in the same position. Identical camera settings were used to photograph the modes. Settings had to be chosen so the majority of images were able to be seen without oversaturating the camera. The clearest images which portray the general mode structure for each fibre investigated are shown in Figure 4-2.

In general there was a significant improvement in mode pattern after mode stripping and in most cases the cladding modes completely disappear, as demonstrated by the lack of circumferential interference fringes after mode stripping. The improvement was particularly significant for the small core fibres but there was no noticeable difference in the coupling pattern for multimode fibres. Therefore, it is prudent to remove the cladding modes in single mode fibres if reproducibility is desired.

The mode intensity profile simulation of SMF28 shown in Figure 1-9 is the same as that observed after stripping the fibre of cladding modes. This confirms that the stripped

mode pattern is the correct modal structure for SMF28 under normal operating conditions (lengths of greater than 1 m) when using a short wavelength such as 514 nm. As the fibres were used when the cladding modes were stripped, it is unnecessary to delve into a complex modelling of cladding modes.

Fibre /NA **Obj/NA**	**Before stripping**	**After stripping**
SM1500 /0.3 10/0.25	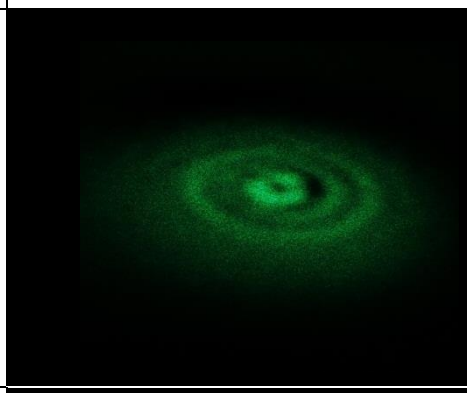	
SiO_2 /0.1 20/0.40	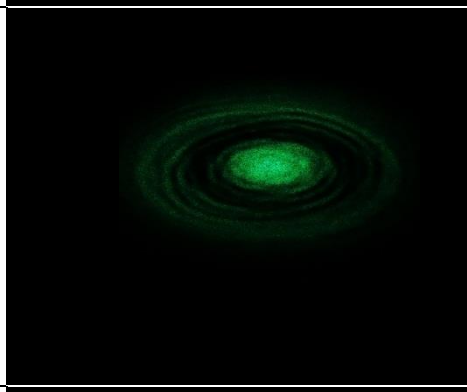	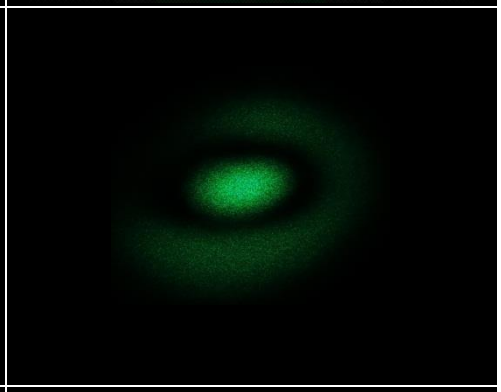
S405 /0.12 10/0.25	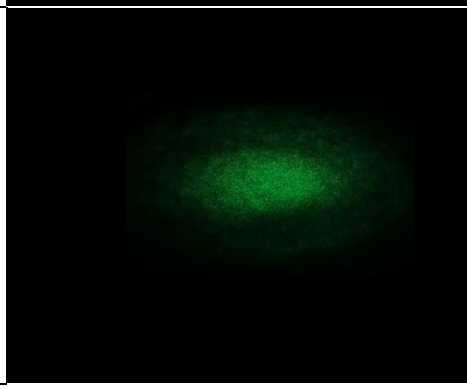	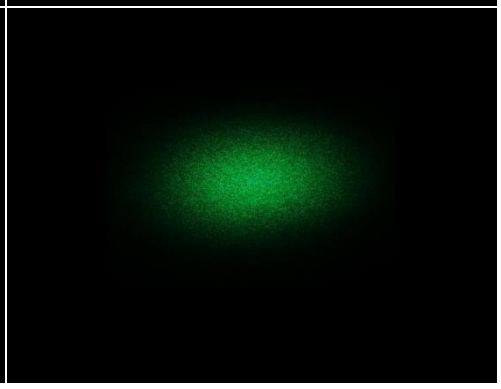

HI1060 Flex /0.14 10/0.25	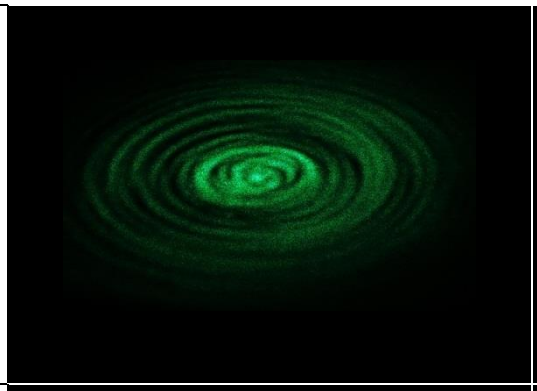	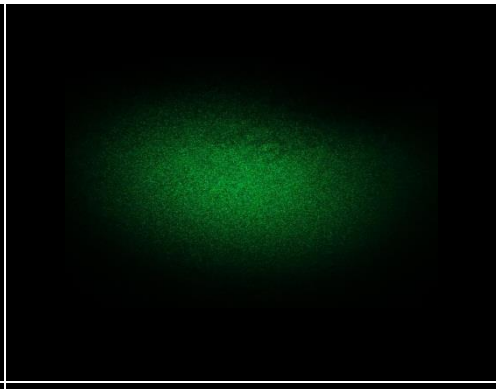
F-SBC /0.16 10/0.25	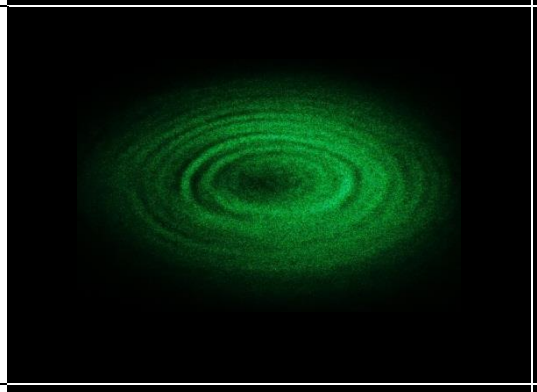	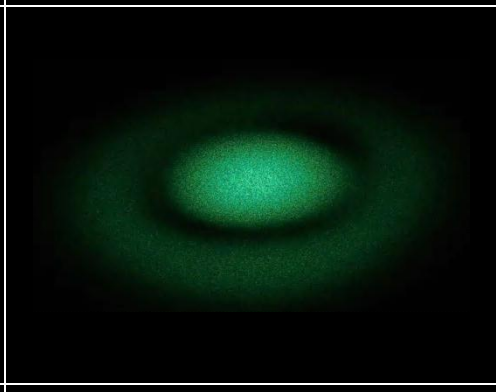
MMF_{50} /0.20 50/0.5	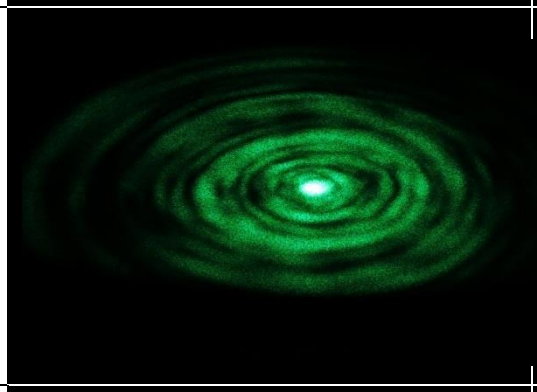	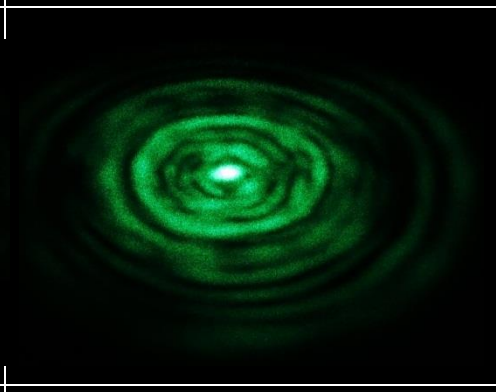
780HP /0.13 10/0.25	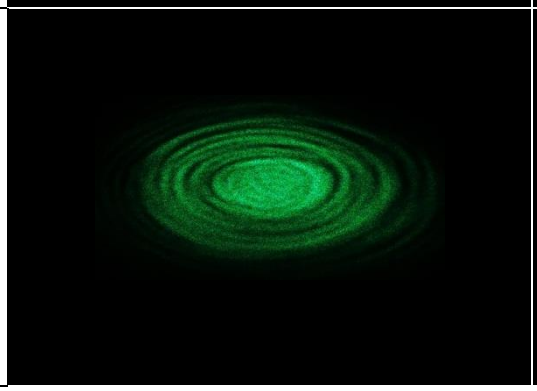	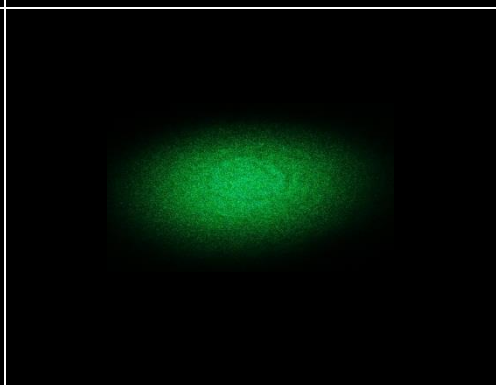

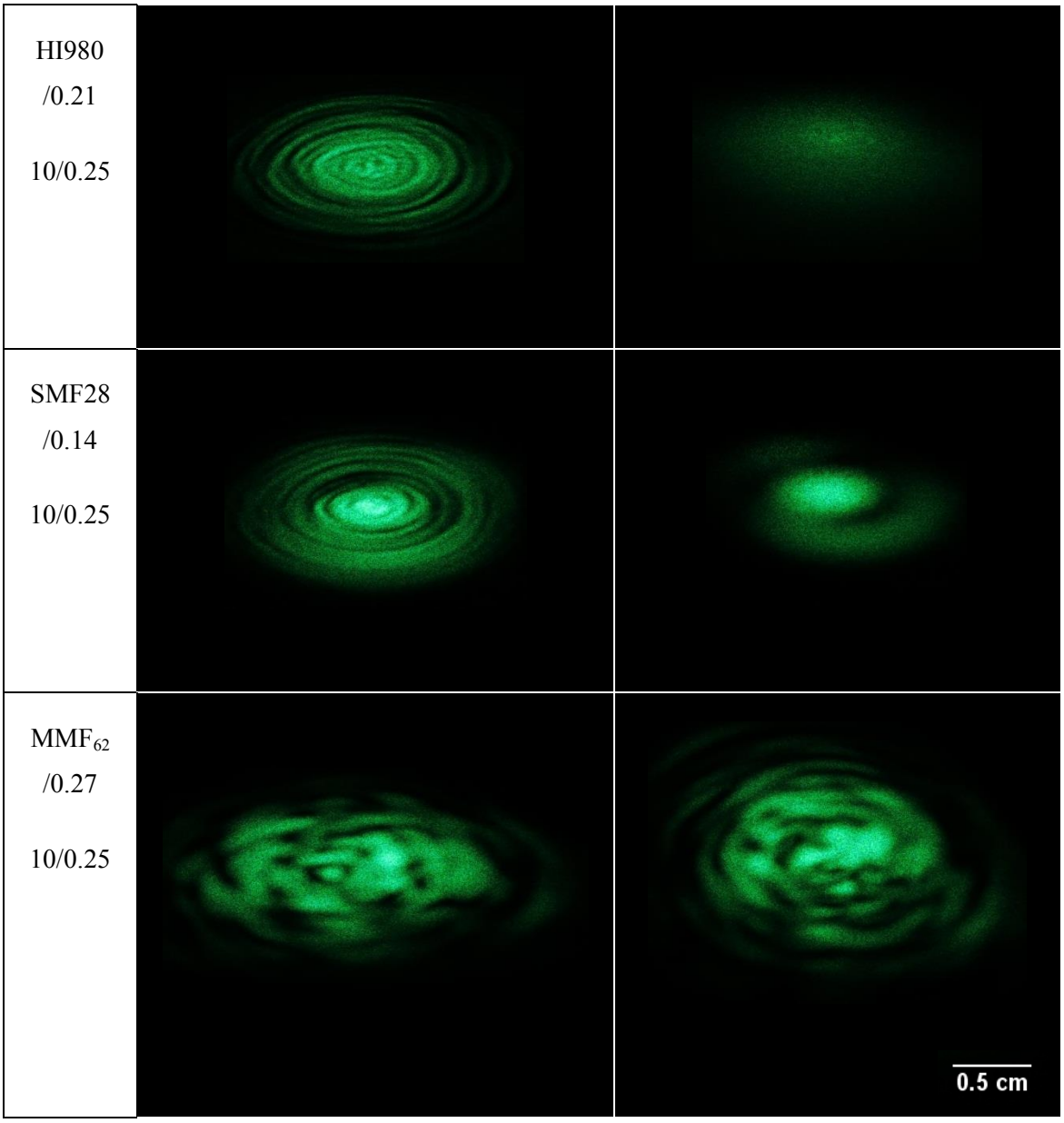

Figure 4-2 Examples of projected mode patterns before and after stripping the cladding modes for different fibre/NA, objective/NA combinations. The patterns appear oval as the camera was positioned obliquely due to space constraints. Also note the angle and size difference in before and after images which is due to the bend in the fibre needed for mode stripping. A scale bar is shown in the final image.

4-4 Fibre probe performance

4-4-1 Direct SERS signal

Prior to remote probe analysis, the direct intensity obtained from the end of the fibre tip as a function of solid angle should be checked to ensure that it follows the linear progression as expected for these silver-island films [97]. As shown in Figure 4-3 the direct intensity does indeed follow a linear relationship with increasing solid angle. The linear fit (R^2 value of 0.98 indicates that a linear relationship is a reasonable assumption) demonstrates isotropic scattering. This provides confidence that any non-linearity or variation in NA dependence observed in the remote geometry is influenced by the NA and core size of the fibre in question, rather than any anisotropy in the SERS signal.

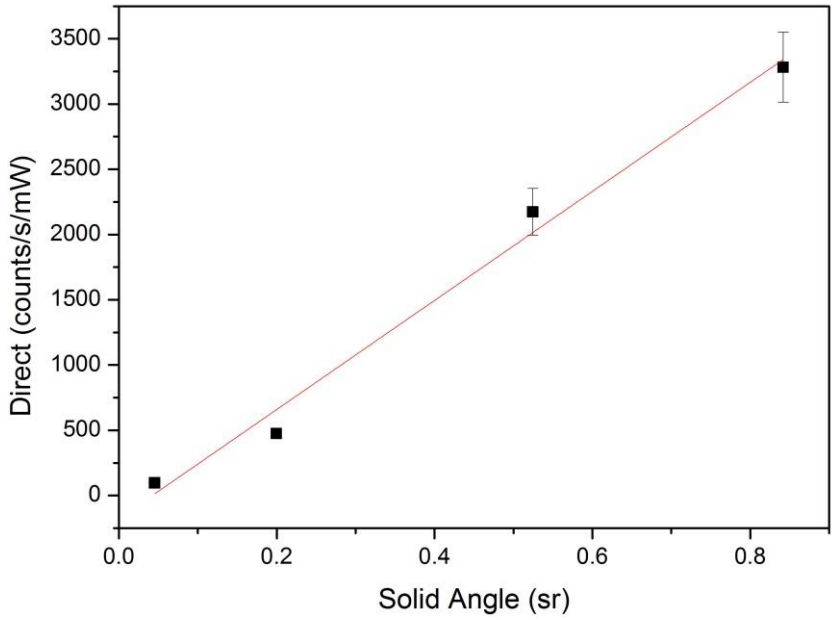

Figure 4-3 Direct SERS trend with linear fit (error bars are smaller than data symbol when not visible).

4-4-2 Subset of four fibres analysis

Initially four fibres were compared for simplicity. SM1500, S405, SMF28 and MMF62.5 were chosen as they provided an example of each type of fibre. SM1500 is single mode with large NA, S405 is single mode with pure silica core and small NA,

SMF28 is single mode, Ge doped with small NA and MMF62.5 is multimode with large core and large NA.

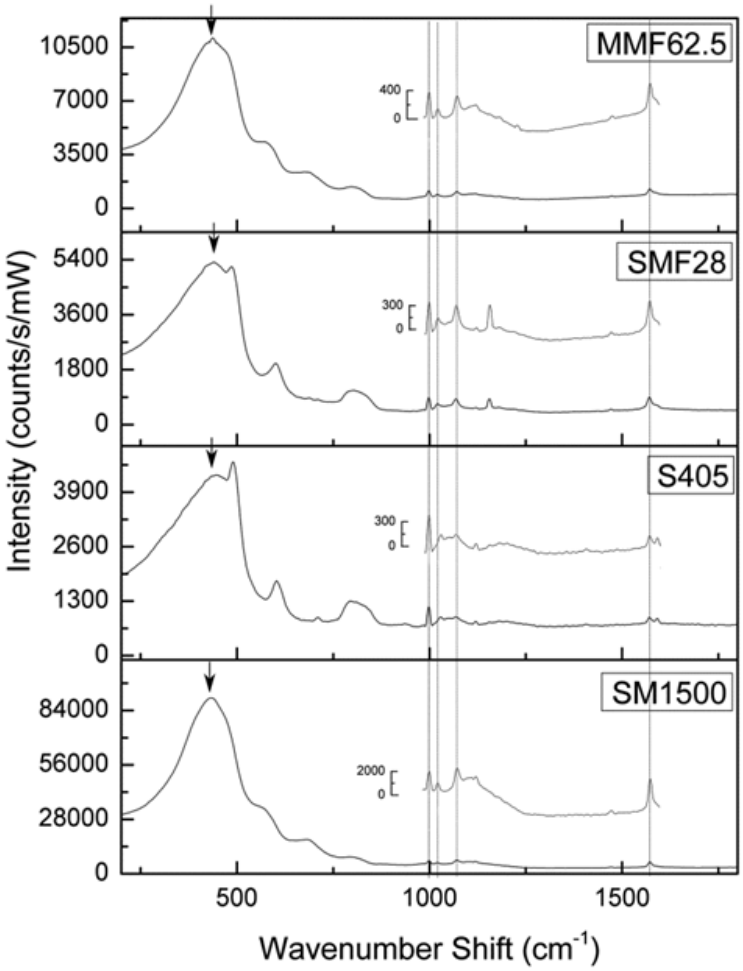

Figure 4-4 Comparison of remote measurements for a sub-set of four fibres. The lines show the main thiophenol SERS peaks and the arrows show the most intense silica band. These peaks were used to quantify probe performance.

The spectra which exhibited the largest SERS signal are shown for each fibre in Figure 4-4. The SERS signal was quantified by taking the average intensity of the four major thiophenol peaks at 998, 1022, 1070 and 1572 cm^{-1} (indicated by the dashed lines in Figure 4-4). Although different SERS peaks may in general be subject to different levels of enhancement, no significant changes were observed in the relative peak heights under the conditions of these experiments. This observation is in keeping with previously reported SERS studies of metal-bound thiophenol [96]. Thus the average

intensity value is regarded as a satisfactory measure of the overall substrate performance. The fibre Raman background was quantified by taking the peak intensity of the broad silica peak at about 430 cm^{-1} (arrows in Figure 4-4). Insets with a magnified intensity scale have been used to highlight the main thiophenol peaks for each fibre. The magnified scale also highlights the fibre background in this range, including some additional peaks (e.g. 1156 cm^{-1} in SMF28 and 1590 cm^{-1} in S405) that have been attributed to the glass dopants.

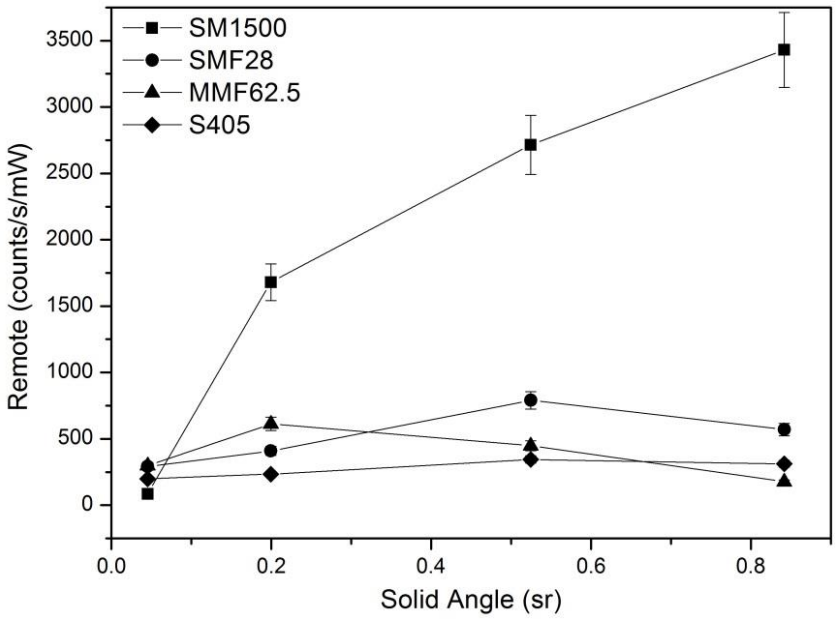

Figure 4-5 Average intensity of the thiophenol SERS signal measured in the remote configuration where error bars are generally smaller than the data symbols.

In order to compare the basic performance of each fibre as a probe, the average intensity of the remote SERS signal is plotted as a function of solid angle in Figure 4-5. SM1500 delivers the largest SERS signal and shows that the intensity increases as a function of solid angle. According to Equation (1-15), the signal would generally be expected to become constant once the objective collection angle is larger than that of the fibre. However, it is known that the mode structure can take up to 50 m to stabilize [22], so it appears likely that the effective NA of these short sections of SM1500 fibre is higher than suggested by the specifications in Table 4-1.

The other fibres exhibit a more complex relationship, with the SERS signal peaking at intermediate collection apertures before dropping slightly for the largest collection angle studied here. MMF62.5 provides the lowest signal level for the largest collection angle. This can be understood in terms of the area factor in Equation (1-15), $(\alpha/\rho)^2$ since MMF62.5 has the largest core size of all of the fibres considered here. The size of the entrance slit projected onto the fibre core is smallest for the highest magnitude microscope objective, which corresponds to the largest solid angle. In contrast, the small core fibres are mainly influenced by NA matching.

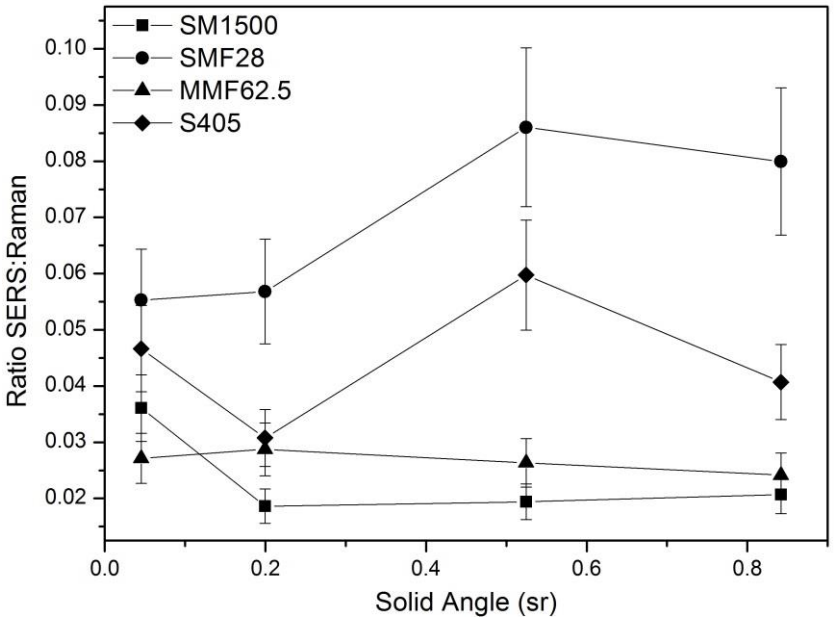

Figure 4-6 Ratio of SERS signal to fibre Raman background.

Perhaps the most important feature of a probe is to have a high ratio of SERS signal to fibre Raman background. This is indicative of the background noise level that the fibre introduces to the SERS signal. According to this measure, SMF28, as seen in Figure 4-6, has the highest ratio and therefore the best overall performance of the four fibres. This good performance of SMF28 is largely due to the relatively low intensity of the glass Raman spectrum, while the intensity of the SERS signal is comparatively constant with solid angle (Figure 4-5). It has previously been reported that high NA fibres capture more of the Raman scattering generated within the core [54]. However, the high NA fibres should also capture more SERS signal from the tip, leading to no net

disadvantage. Therefore the increased background of the high NA fibres may be due to increased levels of Raman scattering from the more highly doped cores. This explanation is indirectly supported by the fact that the glass spectra of the high NA fibres (MMF62.5 and SM1500) are quite different to SMF28 and S405 (Figure 4-4), which are themselves very similar to pure SiO_2 [98]. It should be noted that the fibre background is highly fibre dependent. Motz *et al.* [50] reported that some low NA fibres exhibited high fibre background due to the doping in the cladding.

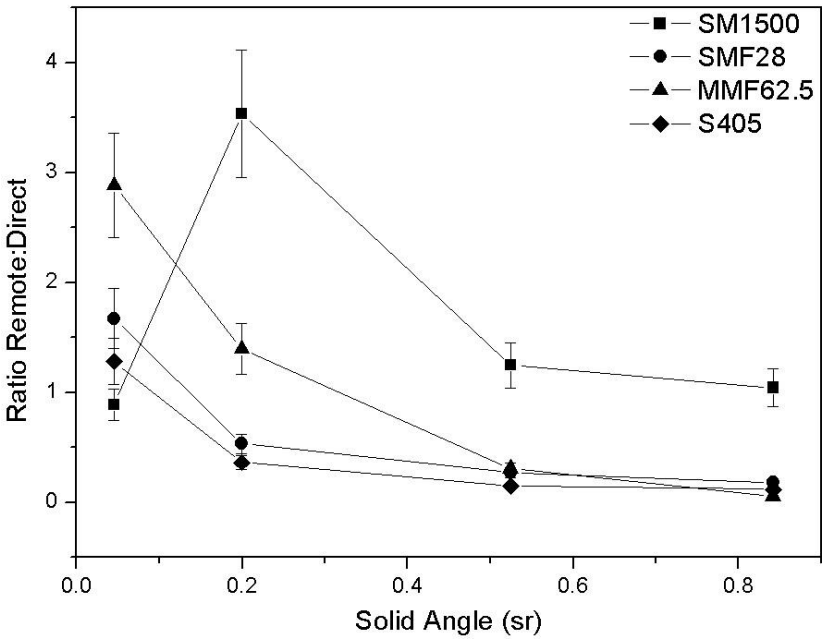

Figure 4-7 Ratio of remote to direct SERS intensities where error bars are generally smaller than the data symbols.

The ratio of remote to direct SERS (Figure 4-7) gives an indication of how much signal is lost or gained when performing a remote measurement through the fibre, as opposed to a direct measurement from the SERS substrate. With close NA matching, each fibre delivers a higher signal in the remote situation than in the direct geometry. This phenomenon has recently been explained in terms of an additional enhancement for the near field amplitudes that occurs due to Fresnel reflection and transmission at the interface [53]. SMF28 (low NA fibre) has the highest intensity when NA matching and the intensity drops at high objective NA where there is poor NA matching. However, with SM1500 the ratio remains around 1 (or higher) due to a smaller mismatch with the

high NA objectives. SM1500 has the highest capture efficiency and encouragingly SMF28 (highest signal to background ratio) has an efficiency of approximately 1.5 at the lowest collection angle. S405 follows the same trend as SMF28, although it has slightly lower remote intensities (Figure 4-5). Once again, MMF62.5 performs poorly at high collection angles due to a poor matching of the source and slit areas, in keeping with Equation (1-15) and previous results [51].

4-4-3 Selective comparison of similar fibre types

Now a selective comparison will be presented of similar fibre types to the four discussed so far.

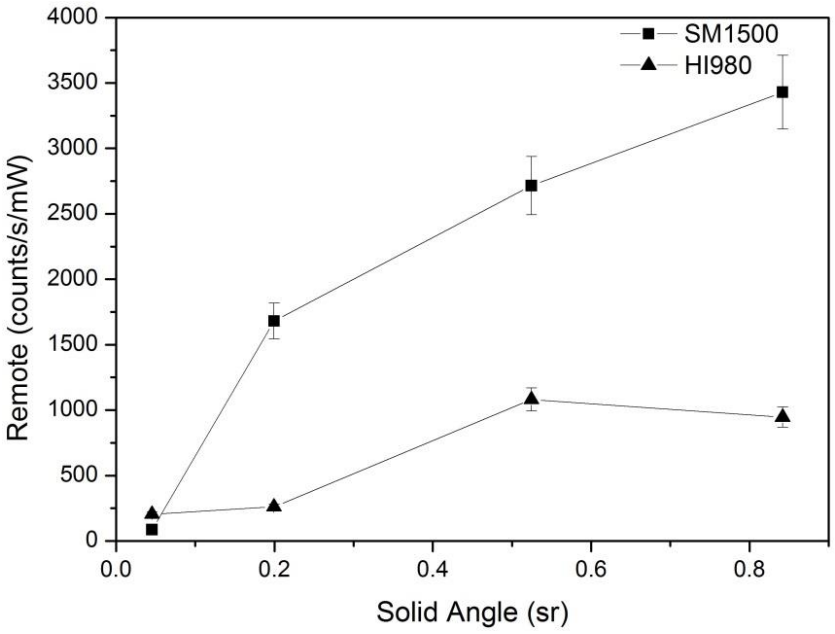

Figure 4-8 Selective comparison for single mode, large NA fibres SM1500and HI980 where error bars are smaller than the data symbol when not visible.

In Figure 4-8 two single mode large NA fibres are compared, SM1500 (0.3 NA/0.29 sr) and HI980 (0.21 NA/ 0.14 sr). Due to the short lengths of fibre it can be speculated that the fibres are able to support higher order modes than their specifications suggest. It appears that the higher NA fibre (SM1500) does this to a greater extent, leading to an overall increase in intensity as the collection aperture is increased. The smaller NA fibre (HI980) peaks in intensity at 0.52 sr, which indicates

that this fibre is also supporting higher order modes, but to a lesser extent. If the fibres were performing to specification, it would be expected that the peak in intensity would occur when the collection aperture and fibre NA matched.

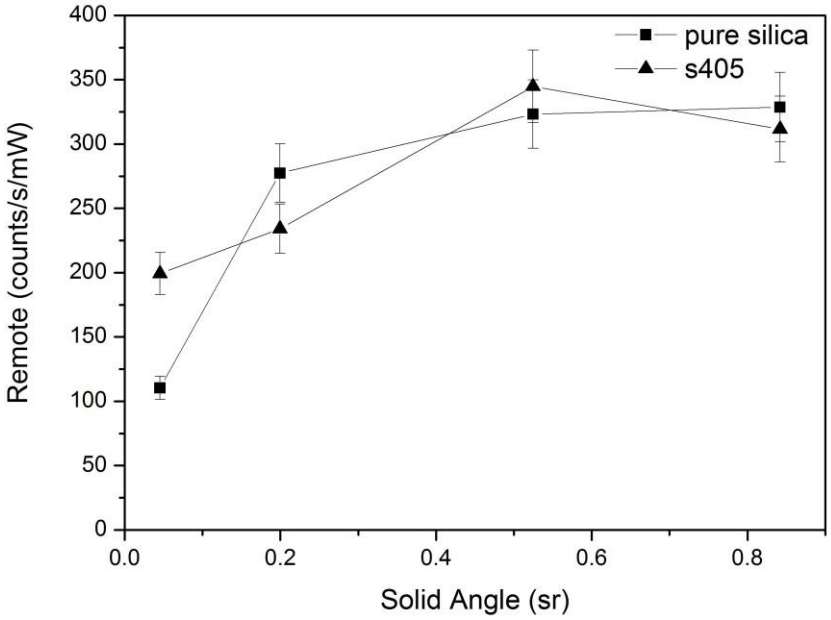

Figure 4-9 Selective comparison for pure silica core fibres s405 and pure silica.

A selective comparison for pure silica core fibres was undertaken for S405 (0.12 NA/0.045 sr) and for the fibre designated as pure silica core (0.10 NA/0.031 sr). The comparison (Figure 4-9) shows a peak in intensity at 0.52 sr, indicating the presence of higher order modes. The behaviour of the two fibres is similar due to similar characteristics such as core material and NA. The core of the pure silica fibre is larger; however, due to the larger slit opening the signal is not restricted and so performance differences are not drastic. Slight differences in performance could be due to slightly different levels of higher order modes being supported.

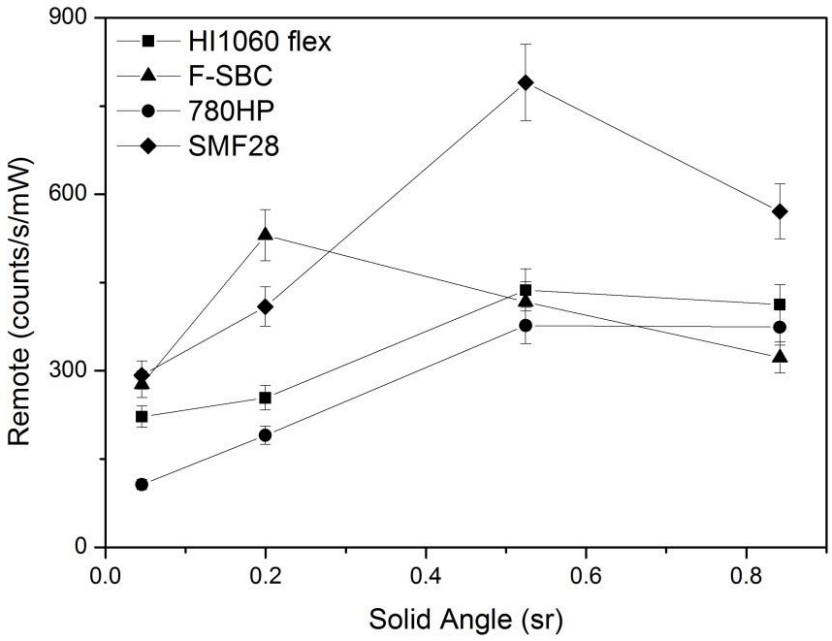

Figure 4-10 Selective comparison for single mode low NA fibres HI1060flex, F-SBC, 780HP and SMF28.

A selective comparison for single mode low NA fibres was undertaken for HI 1060 flex (0.14 NA/0.06 sr), F-SBC (0.16 NA/0.08 sr), 780HP (0.13 NA/0.05 sr) and SMF28 (0.14 NA/0.06 sr). The results (Figure 4-10) show that all of the small NA fibres have a peak in intensity at 0.52 sr, except for F-SBC which peaks at 0.2 sr. F-SBC could be exhibiting different behaviour due to different cladding dopants. It was not possible to check the cladding dopants with EDS so it is conceivable that F-SBC differs in this regard. It should also be noted that while conducting EDS a trench cladding surrounding the core was visible. There was a low Ge content in this region indicating other dopants. Whereas HI 1060 flex, which also has a visible trench, has a high Ge content in the trench so it is unlikely this area has been doped. These differences could account for the lower saturation point for F-SBC. It is unclear why SMF28 out performs other fibres in its class.

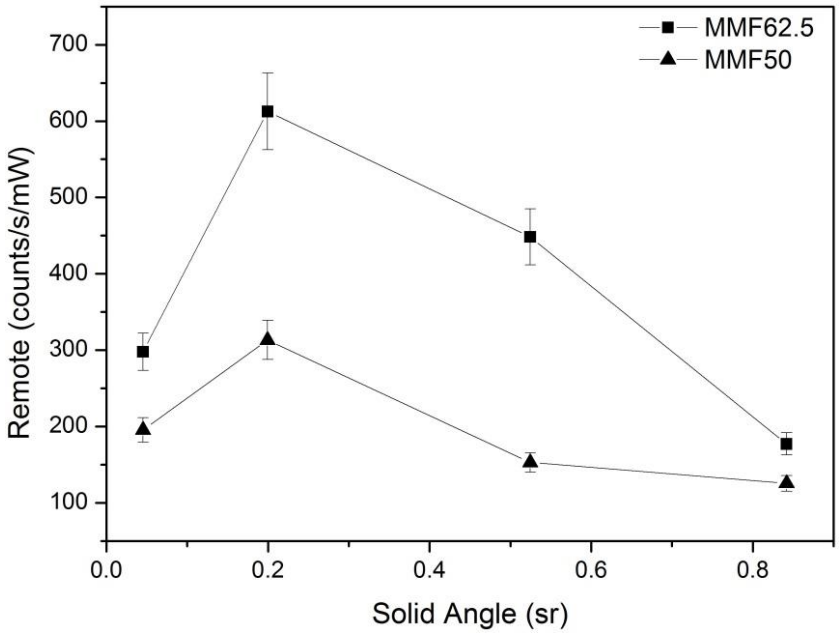

Figure 4-11 Selective comparison for multi-mode, large core and NA fibres MMF62.5 and MMF50.

A selective comparison for multi-mode fibres 50 (0.195 NA/0.121 sr) and 62.5 (0.272 NA/0.237 sr), which both have large cores and NAs, was undertaken. The results (Figure 4-11) show a peak in intensity at 0.2 sr, then a dramatic drop of intensity for both fibres. These low intensity counts at larger apertures could be due to under-sampling of the core. Even though MMF62.5 has a larger core, the distribution of intensity is not uniform with the concentration of intensity being in the centre. Coupled with its larger NA, MMF62.5 is able to outperform MMF50.

4-5 Renishaw set-up considerations

The Renishaw inVia Raman spectrometer is purpose-built for high spatial resolution spectral mapping. Therefore, it is important to note that the system is optimised for the 50× microscope objective. It was advised that the machine can also function with the 20 and 100× objectives. However, the 5 and 10× objectives are not normally used and the system is not necessarily optimised for these low magnifications. This could be causing the deviation from theory (max intensity at an objective NA larger than fibre NA) observed in the results and requires further investigation.

The collection area was determined for each objective by using a depth profile of silicon. The results are shown in Figure 4-12. The 20 and 50× objectives follow the expected trend for confocal optics, where intensity peaks when the surface coincides with the focal plane and then decreases with depth in a Gaussian fashion. The 5× objective has the same intensity regardless of depth and the 10× objective intensity increases steadily where the highest measured intensity was at 40 μm above the Si wafer surface. These results show that the system exhibits good confocality when using the 20 and 50× objectives whereas the spectrometer has not been optimised for confocality when using the 5 and 10× objectives. This design adds uncertainty to interpretation of fibre performance. A full understanding of the fibre-Raman setup would be needed for optimising the system.

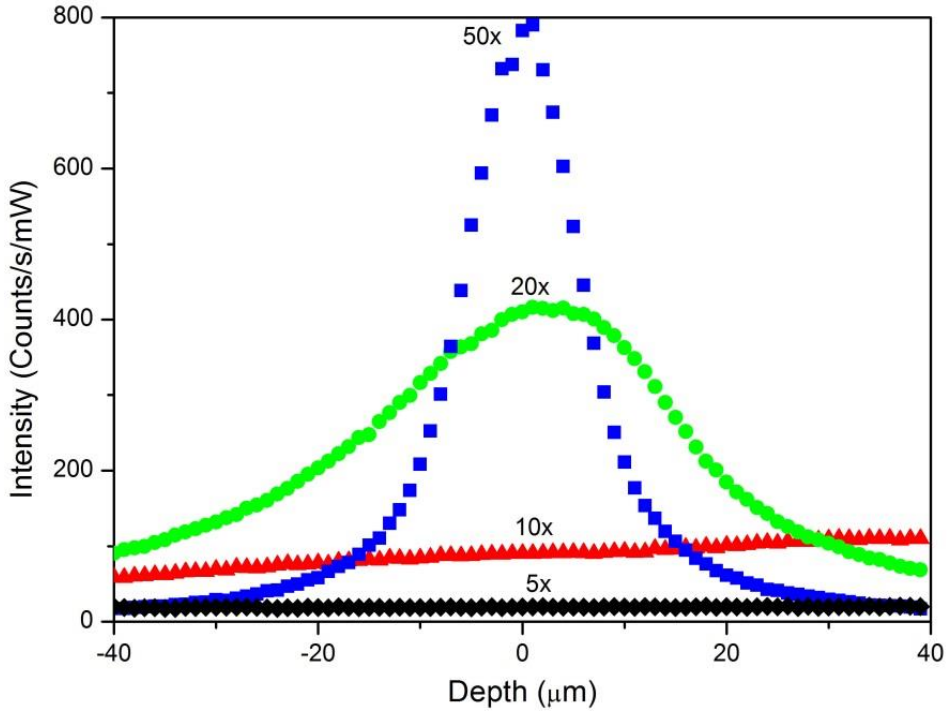

Figure 4-12 Comparison of depth profiles for 5, 10, 20, 50 × microscope objectives

There is also uncertainty caused in quantifying NA as the rear apertures (see Figure 4-13) of the microscope objectives are not always entirely filled by the laser beam, which will alter the way the light is focused into the fibre core. The laser beam diameter was measured without an objective in the system and then the objective rear apertures were measured. The results in Table 4-4 show that only for the 50× objective does the

laser completely fill the aperture. The 20× objective is slightly under-filled which accounts for its reasonable profile in Figure 4-12. However, the 5 and 10× objectives are significantly under-filled and this could be contributing to the unexpected profiles.

Figure 4-13 Diagram of microscope objective showing rear aperture. Reproduced from Murphy and Davidson [99].

Table 4-4 Diameters of objective apertures and laser spot size.

Objective rear aperture/ laser beam	**Diameter (cm)**
5×	1.0
10×	1.1
20×L	0.82
50×L	0.45
Laser beam	0.63

4-6 Conclusions

These results suggest that lower dopant levels produce a higher signal to fibre background ratio in the remote probe geometry. This implies that pure silica core fibres may be attractive for use as SERS probes. Also, it has been shown that matching the nominal NA of the optical fibre with the NA of the microscope objective is generally not a critical requirement to produce the highest level of SERS signal. This is believed to be due to the presence of leaky modes in these short lengths of fibre. Further analysis of the fibre-length dependence of the NA should be considered in terms of the beam propagation formalism in future work [100]. Note that a strong dependence on NA would still be expected for longer fibres where the mode structure has stabilized,

although the dependence would be expected to match the predictions of Equation (1-15) more closely. However, there is still uncertainty as to whether this deviation in theory is entirely due to higher order modes in these short lengths of fibre or if the optics in the spectrometer are also contributing. It could be that the small NA fibres are not really peaking for the 20× objective, but just appear to do so due to the spectrometer arrangement. Future work would be needed for clarification of the trends in the smaller NA fibres.

The highest overall intensities were obtained in the fibre with the highest NA. However the large NA also has the largest levels of Raman signal from the fibre core materials. A high signal to noise ratio is of more importance for applications than highest overall intensity. Taking all of these factors into consideration, the ideal optical fibre for use in miniaturised SERS probes should offer the following features:

- low dopant concentration in the core;
- high NA; and
- small core size.

There is no fibre design with all of these ideal characteristics currently available on the market. Of the fibres studied here, SMF28 appears to offer the best combination of properties. Note that the development of customized fibres for SERS probes would allow further miniaturisation by reducing the fibre cladding diameter from the 125 μm fibres used in this work. Silica fibres can also be tapered by acid etching in order to reduce the probe tip diameter down to the size of the core [101].

In terms of core size, single-mode fibres should provide more reproducible performance than few-mode designs, because of the stability of the fundamental mode. If a single mode fibre is selected, it should be single mode at both the excitation and scattering wavelengths to ensure good coupling between the two intensity distributions. While it is generally harder to couple light into small cores than large cores, high-precision connectors have allowed widespread use of single-mode fibres (primarily SMF28) in the telecommunications industry. Smaller core sizes are also beneficial in allowing the entire signal to pass the entrance slit and enter the detector.

Previous work has shown that fibre Raman background can be minimised using hollow core fibres [44]. Although this provides an obvious means to reduce fibre Raman background, the distal end of the fibre would have to be sealed for in vivo and in vitro studies, adding to the complexity of the construction. Therefore further work appears justified to identify improved SERS probe designs based on conventional fused silica fibres.

Chapter 5

Bacterial Detection Using SERS

This chapter builds upon the characterisation work completed in earlier chapters in order to test a significant bioanalytical target, *E. coli*. A recent Nature Communications publication [71] showed that spore forming bacteria are impaled on black silicon needles when incubated on the surface. They used the same black silicon as characterised in Section 3-3 so it is conceivable that the same procedure could be used to impale *E. coli* for SERS sensing. When using SERS to study bacteria, normally only the outer surface of the cell is excited and so it is relatively difficult to differentiate bacterial species. It was hypothesised that impaling the bacteria on a SERS active substrate would allow measurements of their inner constituents to be performed. If successful, SERS could then become a differential identification technique. This chapter investigates the potential to use SERS as a bacterial identification technique. Prior to fabricating a black silicon based optical fibre optrode sensor, proof of concept was demonstrated with the as-grown black silicon substrates in the direct configuration.

5-1 Optimising incubation procedure for use with E. coli

5-1-1 Experimental outline for procedure optimisation

The procedure to impale spore forming bacteria on black silicon needles [71] was used as a starting point to create a black silicon SERS platform for *E. coli*. The bacterial preparation was outlined in Section 2-8-3. Initially 1 hour and 18 hour incubation times were tested on the needles and the pyramids which had been sputter coated with 50 nm of gold. These samples were investigated under an environmental SEM and a high resolution SEM.

5-1-2 ESEM images of needle and pyramid samples

The Quanta 200 operating in low vacuum mode was utilised to non-destructively test all four samples (Section 2-3-3). This was important in case further testing or staining was to be performed later. Images were taken both at 0 and 30 degrees stage tilt (Figure 5-1).

As can be seen in Figure 5-1, the needle samples had no bacterial attachment. It should be noted that this sample is hydrophobic and this could be the cause of the lack of bacterial attachment. It is uncertain as to how Ivanova *et al.* were able to have attachment with this sample. Even though the same procedure was followed, no attachment was observed with *E. coli*. This could be due to the strain of *E. coli* used here and perhaps the bacteria Ivanova *et al.* tested were more amenable to the hydrophobic surface.

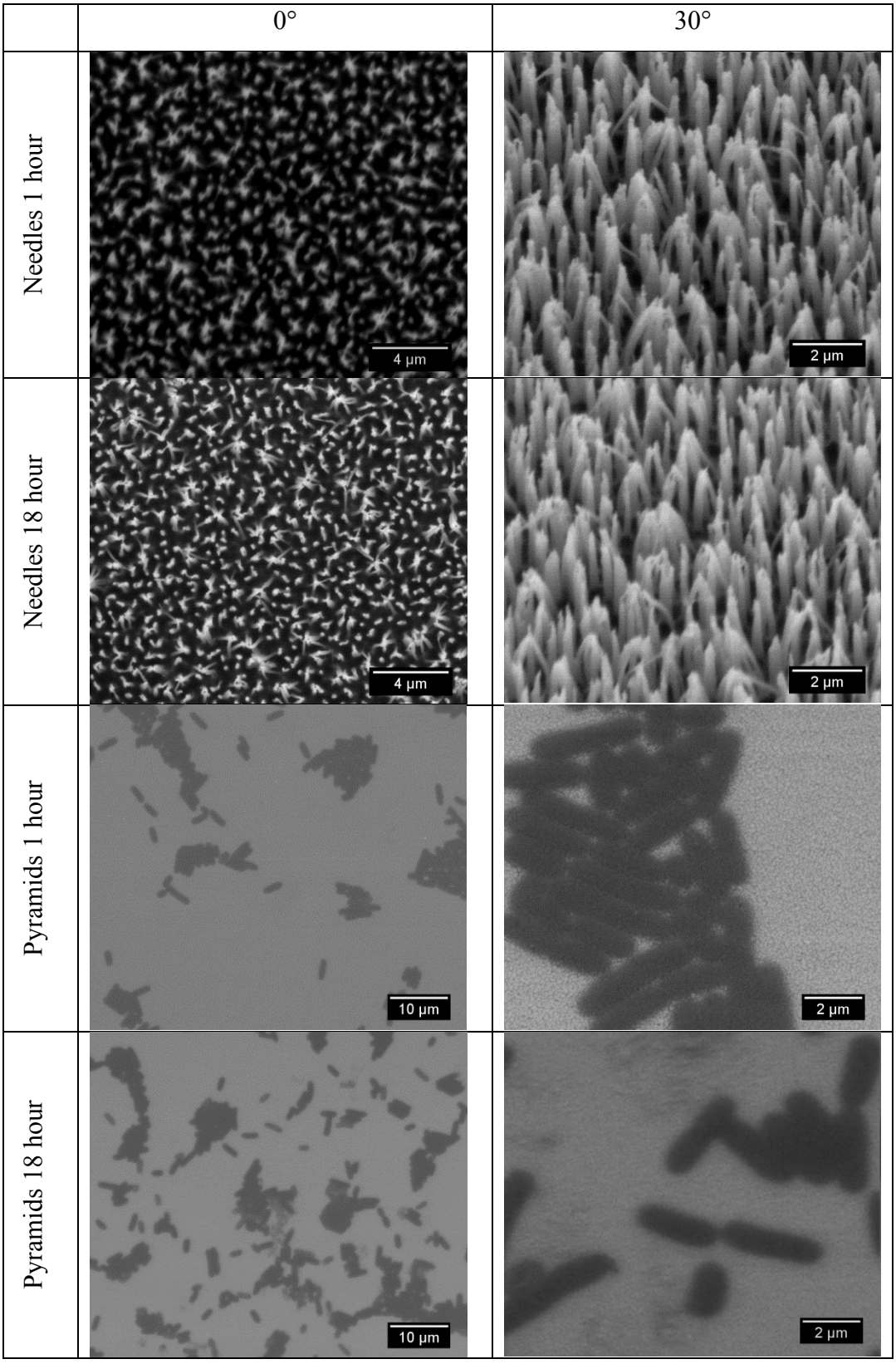

Figure 5-1 Quanta 200 images of the needles and the pyramid samples when incubated with E. coli for 1 and 18 hours.

The pyramid samples were covered in bacteria, more so for the longer incubation time. The pyramid sample exhibits a hydrophilic nature and this appears to encourage the bacteria to attach and potentially divide on the surface. In the pyramid 1 hour sample the spiky structure of the surface was visible on screen, yet was not seen in the 18 hour sample. In the 18 hour sample the bacteria were not able to be clearly resolved indicating that perhaps there is a larger concentration of biofilm waste on the surface making imaging difficult. The presence of a biofilm and cell groupings indicate that the cells are dividing and are in fact thriving on the surface. The pyramid sample appears to encourage cell growth which is the exact opposite of the needle sample which repels attachment.

It is well understood that light elements will have a significantly deeper interaction volume when considering secondary electrons in the SEM [102]. As such, a low accelerating voltage is required to image light element samples such as bacteria. In Figure 5-1 (Pyramids 1 hour imaged at 30°) the black silicon spikes are visible through the bacteria. In order to ascertain how effectively the bacteria have been penetrated, a low kV beam energy is required. However, a relatively high accelerating voltage of 10 kV had to be used due to poor contrast which is exacerbated by the low pressure environment required to image these potentially volatile samples. This voltage is too high, resulting in an interaction volume that extends through the bacteria thus revealing spikes underneath. It must be determined if the spikes are really penetrating this far or if it is an artefact of the high accelerating voltage. This can only be accomplished with higher pressure which requires gold coating. The 1 hour pyramid sample was sacrificed for this purpose.

5-1-3 Supra SEM images of 1 hour pyramid sample

The Zeiss Supra SEM (Section 2-3-1) was used as it has high resolution and magnification in high vacuum mode. Prior to imaging, the pyramid 1 hour sample was sputter coated with gold (see Section 2-8-3). The sample was then loaded into the SEM and an accelerating voltage of 3 kV was used.

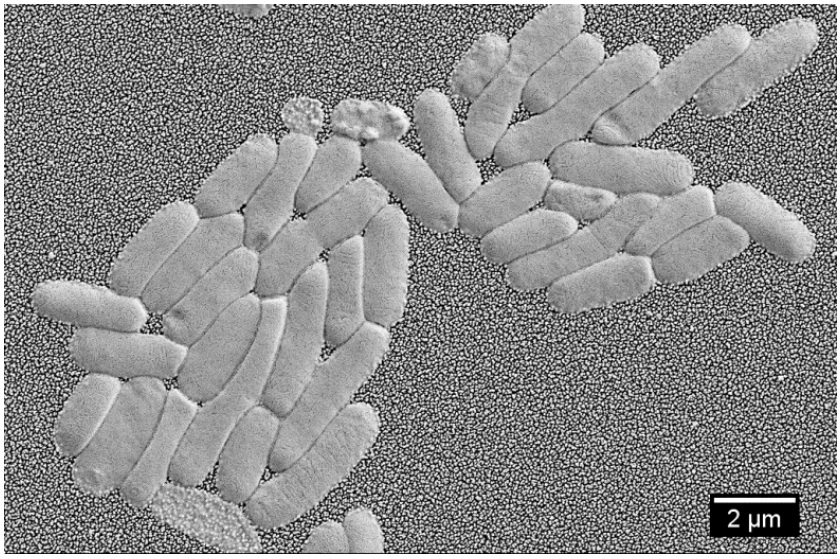

Figure 5-2 Low magnification image of E. coli incubated for 1 hour on the pyramid structures.

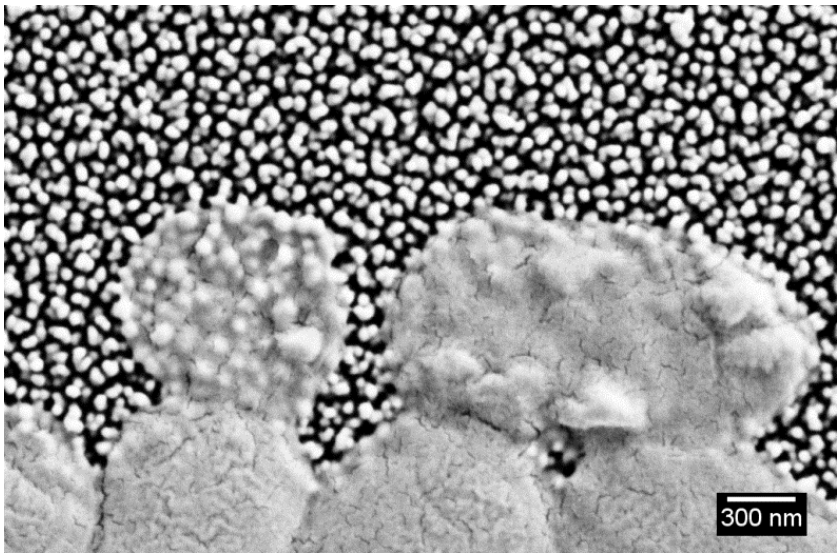

Figure 5-3 High magnification image of two E. coli cells that show piercing from 1 hour incubation on pyramid structures.

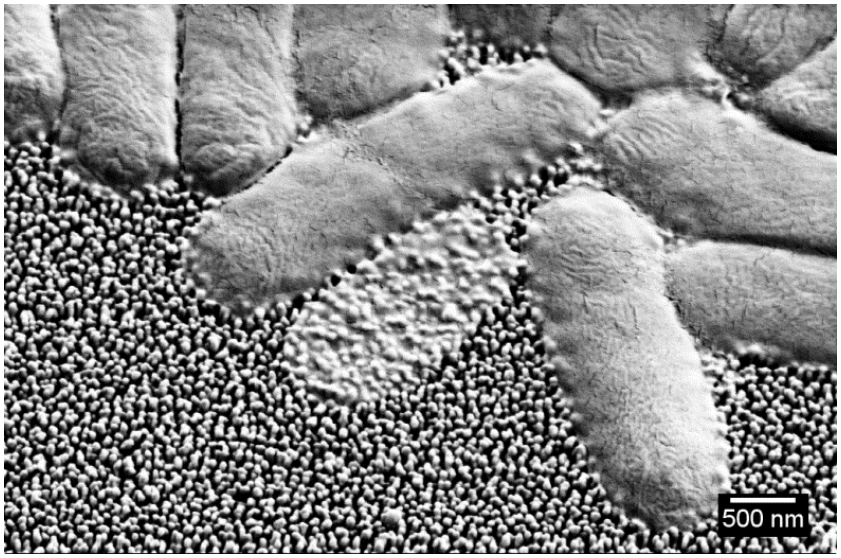

Figure 5-4 High magnification image with a 30 degree stage tilt showing 1 cell that has collapsed onto the pyramids and the other cells being pierced around the perimeter. Cells were incubated on pyramid structures for 1 hour.

As can be seen from the image in Figure 5-2, most of the bacteria appear to be intact. Some have collapsed and the spikes are clearly visible under the collapsed cell (Figure 5-3). Upon closer examination (Figure 5-4) it can be seen that the spikes are penetrating around the edges of the cell. The cells edges would normally be more rounded so this indicates that the underneath of the cells have been pierced and the top is holding together as the spikes are not large enough to fully penetrate the cell. This could provide SERS of the interior structure if the gold coated tips are in fact inside the cell.

5-1-4 Incubation procedure conclusion

It has been determined that the needle samples are unsuitable for *E. coli* attachment. The pyramid sample showed suitable attachment and piercing of the cells and therefore this sample will be optimised for SERS sensing. There were a large number of cells present after 1 hour of incubation and less biofilm was produced at this time. The presence of biofilm may produce conflicting SERS signals which are not desirable. Therefore, an incubation time of 1 hour will be used for future experiments.

5-2 SERS optimisation

5-2-1 Experimental outline for optimising the SERS platform

The next factor to optimise for *E. coli* sensing is the thickness of the gold coating. It would also be ideal to understand how the cell piercing occurs as the samples exhibit growth and yet they also appear to be pierced. Therefore, live/dead staining (Section 2-9) was implemented along with more high resolution SEM images for gold coating thicknesses of 50 and 200 nm. Finally, SERS from the inside of *E. coli* cells was attempted.

E. coli culture, incubation, SEM and SERS preparation was completed following the procedures described in Section 2-8-3. The cells were incubated for 1 hour on the NanoLab pyramid samples which had been coated with 50 nm or 200 nm of gold. Three replicates of each were created to assess the repeatability.

5-2-2 SEM confirmation of impalement

The Supra SEM was used to collect images across the samples at both 0 and 40° stage tilt (Figure 5-5). There was some evidence of cells which have become hollow which is a common problem when using high vacuum under SEM [103]. Unfortunately, due to compromised cell membranes, the cells could not be fixed prior to gold coating. ESEM would be ideal in this situation; however the resolution was not capable of distinguishing the spikes. Therefore, the high vacuum Supra was used with the risk of bursting cells.

The replicates had similar numbers of intact and pierced bacteria present. The 50 nm and 200 nm thick gold coatings both showed pierced bacteria. The 200 nm gold coating appears to have pierced the cells more effectively than the 50 nm thick coating even though the spikes are no longer sharp. The collapsed cells really do appear to have been pierced, as there are different levels present, with some cells remaining mostly intact and others partially pierced, and only a few burst cells over the sample. Therefore, 200 nm thick gold coating can be used for internal SERS of the cells and this will

hopefully eliminate most of the spectral background from cultural conditions and increase SERS signal levels.

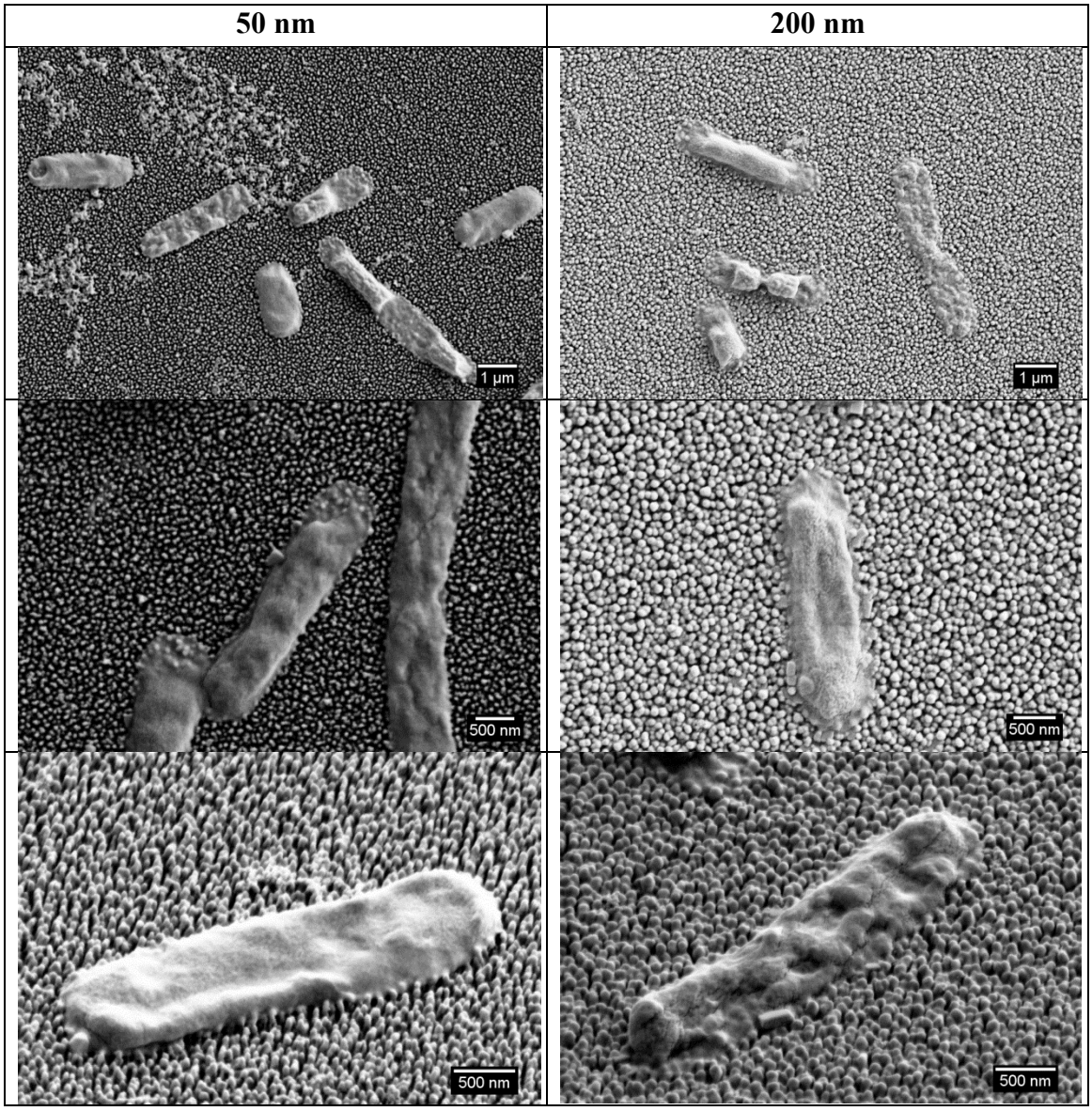

Figure 5-5 Comparison of impalement for 50 and 200 nm gold coatings as viewed under the SEM. Cells were incubated for 1 hour on the pyramid structures. The last row was taken at 40 degree stage tilt.

5-2-3 Live/dead confirmation

Duplicates of the samples prepared in Section 5-2-2 were stained for live/dead imaging using the epifluorescent microscope (procedure described in Section 2-9). It appears that for the 50 nm gold coated substrates there was an even amount of live/dead cells on

each substrate. However, for the 200 nm gold thickness there were more cells which were alive (Figure 5-6). This does not seem to correlate with the SEM images obtained. It is possible that as the substrates are still wet the cells have not been fully impaled and are still healthy. This is reinforced by the groupings and dividing cells which were seen under SEM. If the cells were pierced immediately it is unlikely that so many cell divisions and groupings would be present. The drying process could be responsible for impaling the bacteria. The cells dry and then settle on the surface. The drying makes the cell wall weaker and capillary forces in between the spikes draw the cells onto the spikes to be pierced. Therefore, it can be concluded that the drying process aids in piercing the cells and 200 nm gold thickness therefore may be suitable for use in SERS of the interior of the cell.

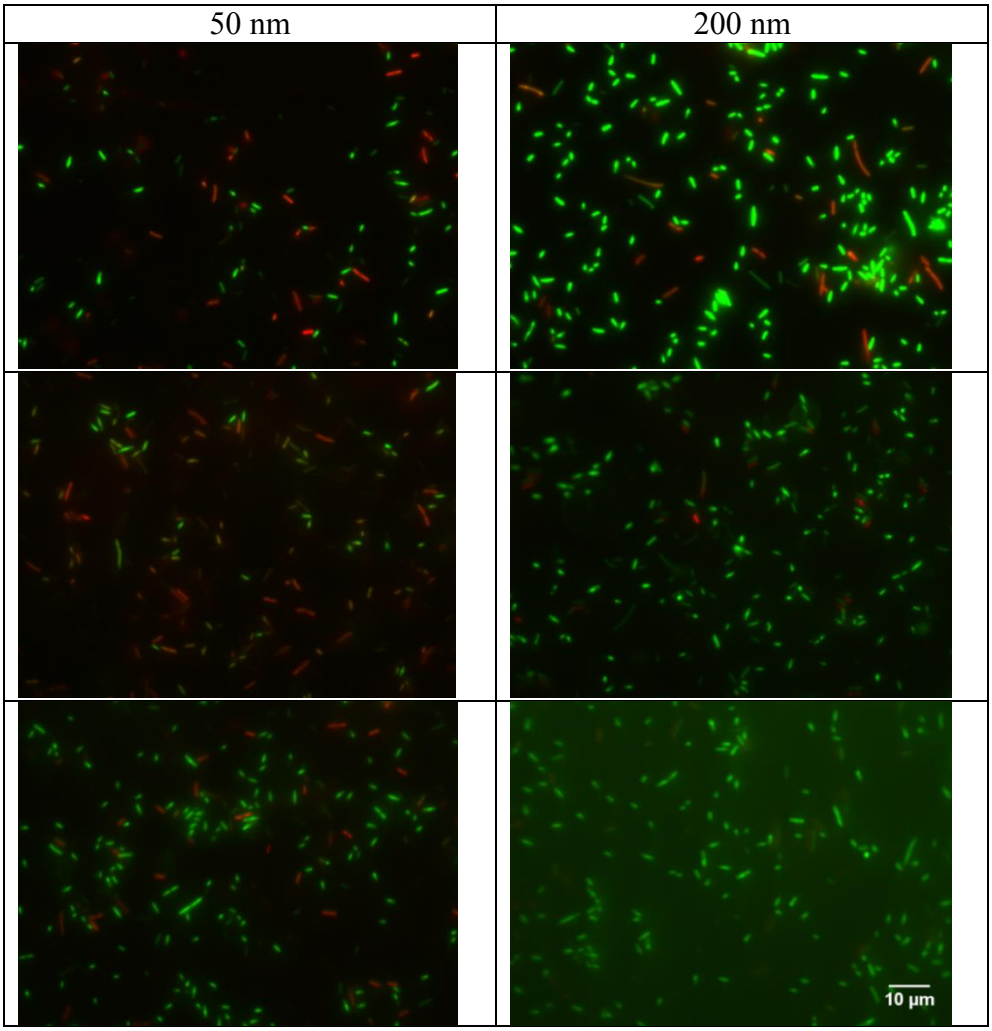

Figure 5-6 Live/dead state of 50 and 200 nm gold coatings as viewed under epifluorescence.

5-2-4 SERS of E. coli

SERS spectra were obtained from the 200 nm gold coated pyramid sample as this should provide the largest SERS enhancement while still impaling the cells. An excitation wavelength of 785 nm with a 1200 l/mm grating was used to limit fluorescent background. The laser was focused with a 100×/0.85 NA objective. Power at the sample was 150 mW and 10 seconds exposure was used for 3 accumulations. Data were normalised for plotting as shown in Figure 5-7.

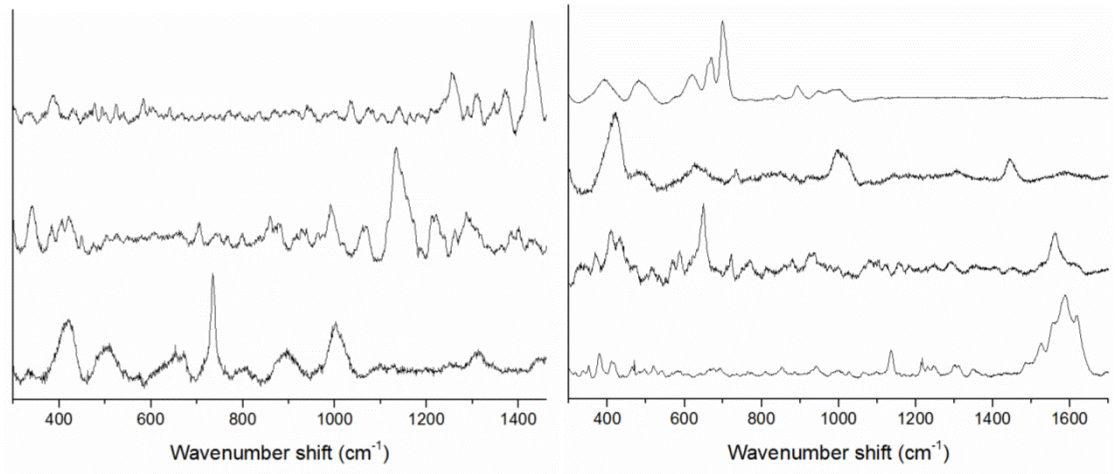

Figure 5-7 Examples of SERS spectra obtained from 1 hour incubation of *E. coli* on 200 nm gold-coated pyramid samples. Each spectrum represents a different cell on the sample. Collected under 785 nm, 150 mW, 10 second exposure time and 3 accumulations.

The data shown in Figure 5-7 represents a different cell for each spectrum. The wavenumber range was altered in an attempt to find the fingerprint region for this sample. Unfortunately all of the spectra obtained differed between cells, though some peak positions are similar between multiple spectra. After a review of the relevant literature it became apparent that SERS spectra of *E. coli* vary depending on the SERS conditions/substrate and experimental setup [104]. Therefore, it is not surprising that none of the obtained spectra perfectly match those published in the literature. However, it was found that some of the peak positions of the obtained spectra corresponded to peak positions published in various papers. The data have been re-plotted and lines have been used to indicate the peaks which match with published work (Figure 5-8).

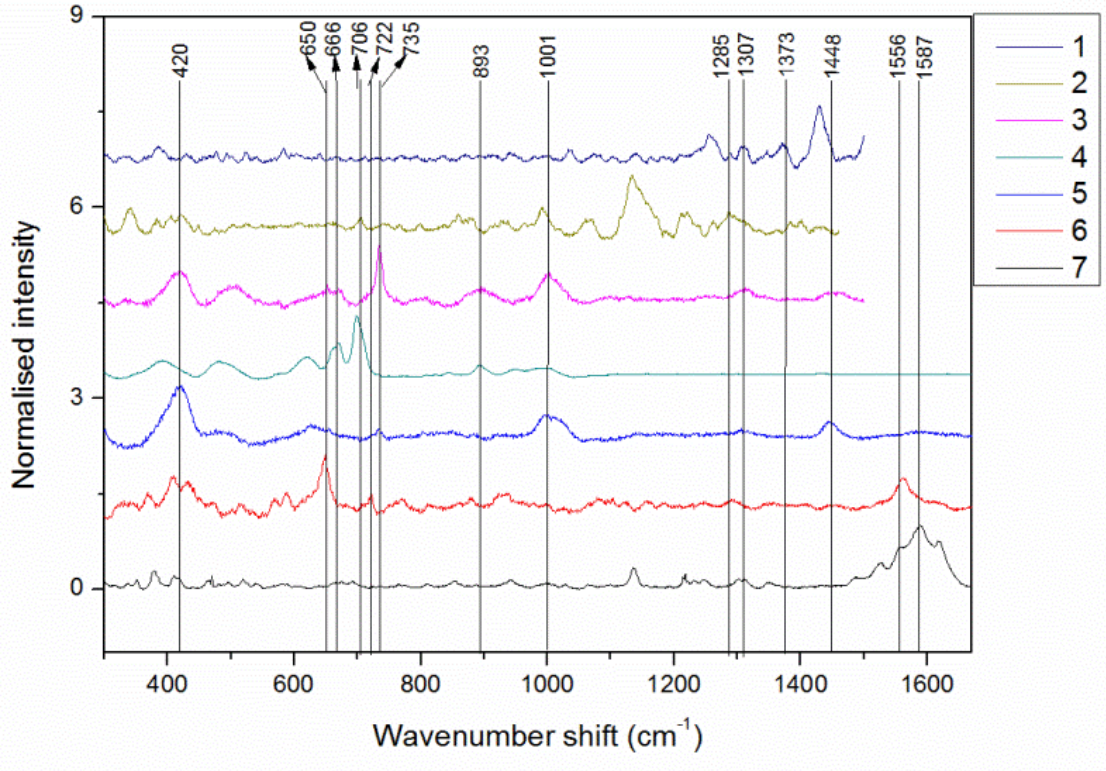

Figure 5-8 Stacked plot of *E. coli* SERS spectra with lines indicating the position of peaks which match with published results.

As can be seen in Figure 5-8 some of the peak positions clearly appear in multiple spectra (peak positions 420, 893, 1001, 1285 and 1307 cm^{-1}). Spectrum 3 has a high proportion of peaks matching published values. This is also the case for spectrum 5 which shares a few peak positions with spectrum 3. The peak locations and the value they match from published results are shown in Table 5-1. It should be noted that there are many small peaks which do not appear in the literature. This could be due to molecules which would normally have a strong signal but have not been detected here. These strong peaks would swamp any smaller peaks from being detected. It is conceivable this is why many of the small peaks have not been seen in published spectra. It is also possible that the unidentified peaks are due to how the metal particles are being introduced into the cells. The spikes could be exciting specific molecules and as such new peaks are detected that are normally swamped when all molecules in the cell are excited.

Table 5-1 Comparison of peak position between obtained data and published literature.

Obtained peak positions	Sengupta [105]	Kahraman [106]	Tamer [107]	Cui [108]	Wang [109]
420			420		
650			650	652	
666		666			
706	703				
722				724	
735			732		
893					890
1001		1004 [110]		1002	
1285	1283				
1307		1310			
1373				1370	
1448				1451	
1556					1558
1587	1587			1589	

Cui *et al.* [108] conducted an antibacterial activity study with increasing concentrations of silver nanoparticles inside *E. coli*. They observed that at increased concentrations a peak at 736 cm^{-1} appeared, indicating potential damage to the cells. They noted that hypoxanthine, adenosine, adenine and guanosine are metabolic footprints of bacteria. The intensities of these peaks decreased with increasing nanoparticle concentration. At a large nanoparticle concentration all bands significantly decreased or disappeared. Although gold nanoparticles may not have the same anti-bacterial activity, this shows a strong relationship between the concentration of nanoparticles and the bands present in a SERS spectrum.

The results and peak allocations of Cui *et al.* (Table 5-2) highlight that the majority of the obtained peaks from this study are related to metabolic activity. Therefore the strength of these peaks may also indicate how active the cells are. Therefore, the lack of peaks in some spectra (spectrum 1 and 7) can be attributed to cells with limited metabolic activity due to a large presence of metal particles residing in the cell. This

finding is supported by the SEM images where it appeared that some cells were still mostly intact where others were completely collapsed. Therefore, the variation in spectra could potentially be partially attributed to some cells still showing strong metabolic activity while other cells have died and ceased metabolic activity.

The differences between the spectra and the relatively few peaks per spectrum could also be explained by the different impalement locations for the cells. SEM showed that the cells are not impaled equally. Also, the pyramid height is smaller than the diameter of *E. coli*. As SERS occurs within approximately 2 nm from an active metal particle, the location of the metal particles could cause different macro molecules to be excited in each cell and hence a different spectrum is obtained. To test this theory new substrates would need to be fabricated which provide spikes which are higher than the cell diameter. Such fabrication is beyond the scope of this thesis.

Table 5-2 Peak positions and preliminary allocations.

Peak position	Preliminary allocation	Reference
420	Carbohydrates	[107]
650	Guanine, tyrosine nucleic acid	[107]
706	Adenine from flavin	[105]
722	Hypoxanthine	[108]
735	Adenine	[107]
1001	C-C aromatic ring stretching (phenylalanine)	[110]
1285	=CH in plane (lipid) or amide III (protein)	[105]
1373	Hypoxanthine or C-H bend protein	[108] or [110]
1556	CH_2 deformation	[109]
1587	C=C (lipid)	[105]

5-3 Conclusion

The preliminary results in this chapter show the potential for bacterial identification with SERS on black silicon. It was clearly shown that the pyramid structures allowed a substantial number of *E. coli* to attach and divide on the surface. All cells showed some level of impalement, which could be further enhanced by using structures which are similar to the cell diameter. Even though the MCN needles appear to be an ideal choice,

the surface was too hydrophobic to allow attachment. Therefore, the structures must be taller than the cell diameter but not so tall as to increase the hydrophobicity to a point of discouraging attachment.

The SERS results support the hypothesis that the cells need to be uniformly impaled in order to obtain reproducible results. A large dataset could be obtained and principal component analysis performed. This would aid in explaining the peaks' origins; however, it would not aid in differential identification as many of the peaks would not be unique between bacteria. Ideally the substrate should pierce all bacteria completely so as to excite all the macro molecules present inside the cell and this should result in reproducible spectra to differentiate between different species. This approach could also be useful in studying the biochemical response of bacteria to their environment.

It has been shown, that with further work, the procedures used in this chapter could result in a SERS platform capable of detecting and identifying bacteria. It should be remembered that only one bacterial species was tested and once reproducible results are obtained for *E. coli*, other species should be tested to ensure differential results. As *E. coli* is gram negative and has a thick cell wall, theoretically the spikes should also be able to pierce the weaker gram positive cells without difficulty. However some bacteria, especially spore forming bacteria, may be much larger in diameter and so the substrate chosen should be suitable for all sizes. This would require a lot of research and fabrication to optimise the ideal structures needed to allow for differential identification.

Chapter 6

Conclusions and Further Work

Chapter 6 concludes all the work presented in this thesis and proposes further work which would extend what was presented here. This involves other methods for sensing bacteria, fibre tip alteration, design of a portable spectrometer and more complicated simulations which could explain the fibre mode propagation.

6-1 Conclusions

The purpose of this work was to investigate various substrates for different SERS applications. Firstly the substrates were characterised for surface chemistry and structure. Then they were implemented in application-based scenarios. Silver-island films were incorporated onto the tip of an optical fibre to characterise the suitability of different fibres for remote biochemical sensors. Black silicon was used to impale bacterial cells which introduced metal particles inside the cell. SERS was evaluated to see if this could produce a differential identification technique.

6-1-1 Optical fibre biochemical sensors

Oblique angle deposition was successfully used to deposit a repeatable metal island film across multiple fibres simultaneously. Depositing 10 fibres in one run cycle reduces the amount of time preparing and handling samples. More importantly, it reduces material costs. Every time the deposition system is run it depletes the silver in the evaporation basket or uses more of the chromium target. Coating multiple fibres in one run reduces the amount of material used and thus makes the OAD technique an efficient and affordable method while still reasonably enhancing.

The surface was characterised and determined to be reasonably repeatable. The size of islands was determined and the SERS performance was analysed across a fibre and between fibres. The surface chemistry showed large levels of carbon which was also present under Raman microscopy prior to functionalization. This result highlights the importance of finding a SERS substrate with lower levels of carbon background as any biological material would be swamped by the large bands. However, the substrate was shown to be ideal for use with thiophenol as the chemical quenched the carbon signal. Thiophenol is known to form monolayers on silver. Therefore the number of molecules attached to the silver in a given area will be the same for all fibres and thus a comparison of enhancement can be made with confidence. A range of standard telecom fibres were compared using OAD and thiophenol.

The comparison study indicated that the ideal fibre is single mode at the excitation wavelength, has a small core and a large NA, and is doped in the cladding. For a more

expensive yet lower background probe, a hollow core fibre could be used. This would result in the ability to use longer lengths without swamping the signal or to keep to short lengths with a much higher signal to noise ratio. It appears that it cannot be assumed that matching the NA of the fibre to the NA of the microscope objective will automatically optimise collection efficiency. However, lower NAs (0.25 and 0.4) did produce, on average, more signal collection across all fibres. This could be due to the fibres having a larger effective NA that matches well with these objectives. NA is normally measured with long lengths of fibre (20 m) that have stable mode structures. The short fibres still have non-equilibrium modes present and could potentially have a larger effective NA. It should also be kept in mind potential issues with the confocality of the optics setup which could be altering NA trends.

The fibres were compared to investigate the effect of different optical parameters on the remote signal collection. Insight into how optical fibres function as an intrinsic sensor when coupled with a spectrometer provides necessary information required to optimise a biological probe. This information will assist in the design and implementation of optical fibres as miniaturised SERS probes in the biomedical industry.

6-1-2 Black silicon bacterial impalement

Two different black silicon structures were characterised for surface chemistry, structure and SERS performance. It was determined that the surface of both samples had significant levels of fluorine present. On the pyramid structure this was one of the causes of the “cloud like” structures sitting atop the spikes. Unfortunately this contamination could not be removed by rinsing, sonication, plasma cleaning or etching.

The high-aspect ratio needles were not able to impale bacteria. It is believed that the surface was not hydrophilic enough to encourage *E. coli* to attach. Fortunately, the pyramid structures were extremely hydrophilic and showed strong bacterial attachment and growth. It was shown that the pyramids were impaling the cells to differing degrees. This was confirmed in the SERS results as all the spectra obtained showed different

peaks. This is believed to be due to the impalement locations exciting different macro-molecules inside the bacteria.

Black silicon was shown to have potential to be used to impale bacteria for SERS sensing. Unfortunately, no conclusive results were able to be obtained with the present samples. Once a black silicon sample has been fabricated that provides accurate and repeatable SERS spectra of bacteria, then it can be incorporated into an optrode sensor probe by replication in a polymer coating [59, 94].

6-2 Recommendations for further work

6-2-1 Beam propagation method

The beam propagation method (BPM) [100] is a powerful technique which is able to calculate the mode structure under varying conditions. The input beam profile can be simulated to accurately reflect the source. Points can be sampled along the length of the fibre in order to view the change in mode structure as the wave propagates. Leaky modes can be introduced to accurately reflect modes that leak into the cladding and propagate for a distance before they decay. The mode structure is determined for the core of the fibre. If the mode structure outside the core is required, it is a simple matter of taking the Fourier transform of the core structure. It is recommended that the BPM be implemented to more accurately simulate the mode structure inside/outside the fibre and determine the effective NA. The BPM can be simulated in 3D for further accuracy.

6-2-2 SERS substrate

A highly enhancing yet reproducible substrate should be implemented to allow the fibre probe to sense low concentrations of scattering molecules. The substrate needs to be cheap to manufacture so silver is an appropriate option. However, the substrate must not be easily contaminated with atmospheric carbon as this will swamp low scattering signals.

A promising technique could be photochemical modification [58] where a silver nanoparticle film is deposited directly onto the core of an optical fibre. An aqueous solution of tri-sodium citrate and silver nitrate is prepared and the fibre tips are placed

inside the solution. A 514 nm laser is coupled into the core of the fibre which induces a chemical reaction that creates the nanoparticles which are then drawn to the tip of the fibre. The particle size and shape is determined by the exposure time and power of the laser. The particles form on the tip in a pattern representing the mode profile. Modifying short lengths of fibre where there is a ring pattern formed by cladding modes will result in the particles forming a ring pattern. This could be problematic as there will be nulls where no analyte can attach and this will result in lower signal than if the whole core was covered in particles/analyte.

This technique should be characterised and optimised for use with short lengths of fibres. Care must be taken to eliminate cladding modes prior to modification. A possible technique to eliminate cladding modes could be to create a mirror surface on the cladding area [111]. This would stop any cladding modes from exiting the fibre and interfering with core modes to create the ring pattern. The approach outlined in [111] utilises a photolithography technique. The fibre is dipped in negative photoresist and the core is exposed with an ultraviolet (UV) light source. The exposed section is masked and the unexposed cladding area is removed with acetone. The cladding is then coated with metal and the core mask is removed leaving the core exposed and the cladding mirrored. This method of removing cladding modes has the benefit of a consistent nanoparticle layer on the core using the photochemical modification technique. There is the added benefit of removing the cladding modes without having to bend the fibre or coat it in gel. This will aid in the miniaturisation and ease of use of a biomedical probe.

6-2-3 Fibre Raman background

Hollow core fibres could be an alternative to the conventional solid silica telecommunication fibres. As the core is hollow there is less glass to generate Raman background. This could result in longer probes that are easier to handle but still have a manageable Raman background signal or, in the case of standard short fibres, significantly reduced background resulting in stronger analyte signal collection. Unfortunately, as the core is hollow there is the possibility of analyte entering the core of the fibre. There is also a strong chance of contamination. Therefore it is advisable to seal the ends of the fibre. Sealed ends also allows for mirrored cladding and

photochemical modification to produce the SERS substrate. A method to seal the ends of the fibres could involve photolithography [59]. The fibre would be pressed against a mould of photoresist which would be exposed through the mould. The fibre could then be removed from the mould by snapping the photoresist at the mould interface, leaving the end sealed.

6-2-4 Bacterial identification

Further investigation is required to determine if SERS can be used to obtain reproducible spectra of bacteria and if they can be used for species level identification. A potential method to combat variability and test the theory of SERS due to different piercing locations would be to use spikes which are larger than the cell diameter. This would ensure that the SERS active metal particles are exciting the same macro molecules for every cell and reproducible spectra should then be obtainable.

One other explanation of the variability could be due to some cells being dead and others alive or partially dead. This could alter the SERS spectrum due to live cells still showing metabolic activity. To test if this is the cause of the variability, a sample could be heated in an oven to uniformly kill all the cells. If the spectra are sensitive to changes in metabolic activity this method provides potential for studying bio-chemical changes in bacteria in response to environmental factors.

If the spectra are still not reproducible, a large dataset could be obtained to see if there are a number of spectra which are repeatable. Then principle component analysis could be untaken and this may aid in understanding the variability in the spectra.

6-2-5 Impaling fibre tip

The work completed in Chapter 4 has shown the optimal parameters for creating remote fibre probes. However the substrate used is not desirable for use as a biological sensor. This is due to its low enhancing performance, strong carbon background and bactericidal properties. Use as a bacterial probe also has the further complication of the islands only exciting the cell wall. Therefore, it may be of interest to develop a microbiologically-suited substrate on the fibre tip.

Incorporating the black silicon pyramids, that were used for impaling, with an optical fibre tip could produce a remote probe capable of using SERS to identify different bacteria. This could be problematic as you cannot directly imprint into a fibre except at temperatures above the glass transition (approximately 1475 K) or by using polymer fibres which have a lower transition temperature [112]. A polymer would need to be used between the fibre tip and a shim imprinted with black silicon pattern [35, 59]. The background produced by a polymer layer has been shown to be negligible [59]. However, it is uncertain what effect it would have on the refractive index matching (polymer to glass) when excited in the reverse geometry. While Kostovski *et al.* [59] have shown that imprinted fibre endfaces are feasible, additional characterization would be required to establish whether the performance would justify the additional technical challenge required to replicate the structures on a fibre endface.

If successful, incorporating the two platforms would have many potential application in the medical industry, such as testing for bacteria in an implant or wound site. There are also applications in environmental and food science. Water supplies could be tested onsite for contamination with no preparation or tagging required. This requires a suitable portable Raman spectrometer to be designed that would be compact, compatible with optical fibres and have enough throughput to detect low concentrations.

6-2-6 Portable Raman spectrometer

A portable Raman spectrometer made completely from optical fibre components could be built. Such a device would eliminate alignment errors, be compact and cheap to produce. After a fibre probe has successfully been optimised and is able to sense biological materials remotely, the next logical step is to incorporate it into a portable device. If the device is small enough it can be used in the field for diagnostics or worn as a continuous monitoring device on a person. In the case of a glucose sensor, the device could be in a closed loop feedback system with an insulin pump. When blood glucose levels rose above a certain value the pump could provide the necessary insulin.

A fibre-optic Raman spectrometer would benefit from the alignment free nature of the optics. The components would initially be coupled together and then no more

alignment is necessary. This eliminates moving parts and tedious realigning of components. A diode laser would provide a cost-effective and reasonably powerful excitation system that could be fibre-coupled into the system. A Bragg grating fibre could be used as a notch filter to remove Rayleigh scattered light. An affordable high-resolution spectrometer would be used to collect Raman spectra. A fibre probe would be attached to the system, preferably hollow core to allow for longer lengths.

6-3 Summary

This project provides much needed technical information regarding optical fibres and their suitability as a SERS probe. Optical fibres create a complex optical element when coupled with a Raman spectrometer. Physical parameters of fibres, such as core size and NA, impact the ètendue of the fibre-spectrometer system. The information presented in this thesis will allow for further work to progress the development of an optical fibre probe and a portable Raman spectrometer.

E. coli was successfully impaled on a black silicon sample. Unfortunately, SERS results are currently inconclusive. After the successful completion of the further work recommended, a high efficiency biological probe will have been created and analysed. Such a probe will benefit the medical diagnostic world greatly as well as providing a safe probing mechanism in volatile situations (explosives, biomedical hazards).

Appendix

Renishaw standard procedures and troubleshooting

1. Using the 50× microscope objective to focus on a silicon sample.

2. Check the alignment of the laser spot to cross hairs on sample.

3. Alter position by using Tools>manual beamsteerer (left motors only). It takes a little while for the laser to settle when altering position.

4. Tools>Calibration>Quick calibration.

5. Set up a static spectral acquisition using the following parameters:

- Standard: 1s exposure time, 100% power
- High Confocal: 10s exposure time, 10% power

6. Expand measurement in navigation pane>Right click on measurement child tab>advanced setup.

7. Right click on instrument>properties.

8. Microscope tab>pick 99%silicon>ok.

9. File>return to application.

10. Run acquisition.

11. Right click spectrum>tools>curve fit.

12. Click on the peak.

13. Right click spectrum>start fit.

14. Check tolerances (Table A-)- allow 10% variation.

Table A-1 Tolerances for Renishaw inVia 514 nm laser laser.

Mode	Location	Width	Height
Standard	520	4.15	45,000
confocal	520	3.4	25,000

15. If the intensity is too low it may be prudent to perform an auto slit align and CCD auto align. Only perform these alignments if no logical reason for low intensity can be found (i.e. laser power is lower).

16. If the intensity and width are within tolerances then experiments can be performed.

Width of peak is too large in confocal mode

It is possible that the slit is not properly closing from 65 μm to 20 μm. In order to check the size of the slit, enter Tools>System Configuration. NOTE: Do not alter values unless you write a record of previous values as there is no undo. If the slit is still at 65 μm manually change it to 20 μm in both instances.

Intensity is low in confocal mode

Perform a slit and CCD alignment.

References

1. Nafie, L.A., *Theory of Raman Scattering*, in *Handbook of Raman Spectroscopy*. 2001. p. 1-10.

2. Raman, C.V. and K.S. Krishnan, *A new type of secondary radiation.* Nature, 1928. **121**(3048): p. 501-502.

3. Hof, M., *Basics of optical spectroscopy*, in *Handbook of Spectroscopy*, G. Gauglitz and T. Vo-Dinh, Editors. 2003.

4. Lyandres, O., et al., *Progress toward an in vivo surface-enhanced Raman spectroscopy glucose sensor.* Diabetes. Technol. The., 2008. **10**(4).

5. Adar, F., M. Delhaye, and E. DaSilva, *Evolution of instrumentation for detection of the Raman effect as driven by available technologies and by developing applications.* J. Chem. Educ., 2007. **84**(1): p. 50-60.

6. Sheppard, N., *The historical development of experimental techniques in vibrational spectroscopy*, in *Handbook of Vibrational Spectroscopy*. 2002: Norwich.

7. Fleischmann, M., P.J. Hendra, and A.J. Mcquillan, *Raman spectra of pyridine adsorbed at a silver electrode.* Chem. Phys. Lett., 1974. **26**(2): p. 4.

8. Jeanmaire, D.L. and R.P. Van Duyne *Surface Raman spectroelectrochemistry Part 1: Heterocyclic, aromatic, and aliphatic amines adsorbed on the anodized silver electrode.* J. Electroanal. Chem., 1977. **84**.

9. Smith, W.E. and C. Rodger, *Surface-enhanced Raman scattering*, in *Handbook of Vibrational Spectroscopy*, J. Chalmers and P. Griffiths, Editors. 2001.

10. White, D.J., *Nanostructured optical fibre for use as miniature surface-enhanced Raman scattering sensors* in *CAOUS*2008, Swinburne: Melbourne.

11. Hicks, C.J., *Surface enhanced Raman spectroscopy.* 2001.

12. Schoen, C.L., et al., *Long fiber-optic remote Raman probe for detection and identification of weak scatterers.* Appl. Optics, 1992. **31**(36): p. 7707-7715.

13. Kneipp, K., et al., *Single molecule detection using surface-enhanced Raman scattering (SERS).* Phys. Rev. Lett., 1997. **78**(9): p. 1667-1670.

14. Fan, M., G.F.S. Andrade, and A.G. Brolo, *A review on the fabrication of substrates for surface enhanced Raman spectroscopy and their applications in analytical chemistry.* Anal. Chim. Acta, 2011. **693**: p. 7-25.

15. Buividas, R., P.R. Stoddart, and S. Juodkazis, *Laser fabricated ripple substrates for surface-enhanced Raman scattering.* Annalen der Physik, 2012. **524**(11): p. L5-L10.

16. Viets, C. and W. Hill, *Single-fibre surface-enhanced Raman sensors with angled tips.* J. Raman. Spectrosc., 2000. **31**: p. 625-631.

17. Lyandres, O., et al., *Surface-enhanced Raman sensors for metabolic analytes.* Biomedical Vibrational Spectroscopy, 2008.

18. Viets, C. and W. Hill, *Comparison of fibre-optic SERS sensors with differently prepared tips.* Sensor. Actuator. B., 1998. **51**: p. 92-99.

19. Jayawardhana, S., et al., *Optical fiber sensor based on oblique angle deposition.* Appl. Optics, 2011. **50**(2): p. 155-162.

20. Schatz, G.C. and R.P. van Duyne *Electromagnetic mechanism of surface-enhanced spectroscopy*, in *Handbook of Vibrational Spectroscopy*, J.M. Chalmers and P.R. Griffiths, Editors. 2002, John Wiley and Sons: Chichester.

21. Nie, S. and S.R. Emory, *Probing single molecules and single nanoparticles by surface-enhanced Raman scattering.* Science, 1997. **275**: p. 1102-1106.

22. Kneipp, K., *Surface-enhanced Raman scattering.* Phys. Today, 2007. **60**: p. 40-47.

23. White, I.M., S.H. Yazdi, and W.W. Yu, *Optofluidic SERS: synergizing photonics and microfluidics for chemical and biological analysis.* Microfluid. Nanofluid, 2012. **100**.

24. Qian, X.M., et al., *In vivo tumor targeting and spectroscopic detection with surface-enhanced Raman nanoparticle tags.* Nature. Biotech., 2008. **16**: p. 83-90.

25. Williams, C., et al., *Variable cytocompatibility of six cell lines with photoinitiators used for polymerizing hydrogels and cell encapsulation.* Biomaterials, 2005. **26**(11): p. 1211-1218.

26. Albrecht, A.M., C.W. Evans, and C.L. Raston, *Green chemistry and the health implications of nanoparticles.* Green Chem., 2006. **80**: p. 417-432.

27. Kerker, M., et al., *Surface enhanced Raman scattering (SERS) of citrate ion adsorbed on colloidal silver.* Appl. Optics, 1980. **19**(19): p. 3253-3255.

28. Kubiliute, R., et al., *Ultra-pure, water-dispersed Au nanoparticles produced by femtosecond laser ablation and fragmentation.* Int. J. Nanomedicine, 2013. **8**(1): p. 2601-2611.

29. Gervinskas, G., et al., *Surface-enhanced Raman scattering sensing on black silicon.* Ann. Phys. (Berlin), 2013. **525**(12): p. 1-8.

30. Hoyer, P., et al., *Terahertz emission from black silicon.* Appl. Phys. Lett., 2008. **93**(091106): p. 1-3.

31. Yoo, J.S., et al., *Black silicon layer formation for application in solar cells.* Sol. Energ. Mat. Sol. Cells, 2006. **90**: p. 3085-3093.

32. Yuan, H., et al., *Efficient black silicon solar cell with a density-graded nanoporous surface: Optical properties, performance limitations, and design rules.* Appl. Phys. Lett., 2009. **95**(123501): p. 1-3.

33. Xia, Y., et al., *X-ray photoelectron spectroscopic studies of black silicon for solar cell.* J. Electron. Spectrosc. Relat. Phenom., 2012. **184**: p. 589-592.

34. Halbwax, M., et al., *Micro and nano-structuration of silicon by femtosecond laser: Application to silicon photovoltaic cells fabrication.* Thin Solid Films, 2007. **516**: p. 6791-6795.

35. Gervinskas, G., et al., *Black-Si as a platform for sensing.* Proc. of SPIE, 2013. **8923**.

36. Keiser, G., *Optical fiber communications*. Electrical Engineering Series, ed. M.-H.I. Editors. 2000, Singapore: McGraw Hill.

37. Stoddart, P.R. and D.J. White, *Optical fibre SERS sensors.* Anal. Bioanal. Chem, 2009. **394**: p. 1760-1774.

38. Snyder, A.W. and J.D. Love, *Optical waveguide theory*. 1983, Great Britain: J.W. Arrowsmith Ltd., Bristol.

39. Potyrailo, R.A., S.E. Hobbs, and G.M. Hieftje, *Optical waveguide sensors in analytical chemistry: today's instrumentation, applications and trends for future development.* J. Am. Chem. Soc., 1998. **362**: p. 349-373.

40. Han, Y., et al., *Index-guiding liquid-core photonic crystal fiber for solution measurement using normal and surface-enhanced Raman scattering.* Opt. Eng., 2008. **47**(4): p. 040502.

41. Yan, H., et al., *Hollow core photonic crystal fiber surface-enhanced Raman probe.* Appl. Phys. Lett., 2006. **89**(20): p. 204101-3.

42. Zhang, Y., et al., *Liquid core photonic crystal fiber sensor based on surface enhanced Raman scattering.* Appl. Phys. Lett., 2007. **90**(19): p. 193504-3.

43. Komachi, Y., et al., *Micro-optical fiber probe for use in an intravascular Raman endoscope.* Appl. Optics, 2005. **44**(22): p. 4722-4732.

44. Konorov, S.O., et al., *Hollow-core photonic crystal fiber-optic probes for Raman spectroscopy.* Opt. Lett, 2006. **31**(12): p. 1911-1913.

45. Dochow, S., et al., *Multicore fiber with integrated fiber Bragg gratings for background-free Raman sensing.* Opt. Express, 2012. **20**(18): p. 20156-20169.

46. Stadler, J., T. Schmid, and R. Zenobi, *Developments in and practical guidelines for tip-enhanced Raman spectroscopy.* Nanoscale, 2012. **4**(6): p. 1856-1870.

47. Dieringer, J.A., et al., *Surface-enhanced Raman excitation spectroscopy of a single rhodamine 6G molecule.* J. Am. Chem. Soc., 2008. **131**(2): p. 849-854.

48. Maiti, K.K., et al., *Multiplex targeted in vivo cancer detection using sensitive near-infrared SERS nanotags.* Nano Today, 2012. **7**: p. 85-93.

49. Ma, K., et al., *In vivo, transcutaneous glucose sensing using surface-enhanced spatially offset Raman spectroscopy: multiple rats, improved hypoglycemic accuracy, low incident power, and continuous monitoring for greater than 17 days.* J. Am. Chem. Soc., 2011. **83**: p. 9146-9152.

50. Motz, J.T., et al., *Optical fiber probe for biomedical Raman spectroscopy.* Appl. Optics, 2004. **43**(3): p. 542-554.

51. Jayawardhana, S., A.P. Mazzolini, and P.R. Stoddart, *Collection efficiency of scattered light in single-ended optical fiber sensors.* Opt. Lett, 2012. **37**(11): p. 2142-2144.

52. Bridges, T.E., M.P. Houlne, and J.M. Harris, *Spatially resolved analysis of small particles by confocal Raman microscopy: Depth profiling and optical trapping.* Anal. Chem., 2004. **76**: p. 576-584.

53. Jayawardhana, S., et al., *Additional enhancement of electric field in surface-enhanced Raman scattering due to Fresnel mechanism.* Sci. Rep, 2013. **3**.

54. Ma, J. and Y. Li, *Fiber Raman background study and its application in setting up optical fiber Raman probes.* Appl. Optics, 1996. **35**(15): p. 2527-2533.

55. Sato, H., H. Shinzawa, and Y. Komachi, *Fiber-optic Raman probes for biomedical and pharmaceutical applications*, in *Emerging Raman applications and*

techniques in biomedical and pharmaceutical fields, P. Matousek and M.D. Morris, Editors. 2010, Springer: New York. p. 25-45.

56. Viets, C. and W. Hill, *Fibre-optic SERS sensors with angled tips.* J. Molecular. Structure, 2001: p. 515-518.

57. Viets, C. and W. Hill, *Fibre-optic SERS sensors with conically etched tips.* J. Molecular. Structure, 2001: p. 163-166.

58. Zheng, X., et al., *Photochemical modification of an optical fiber tip with a silver nanoparticle film: A SERS chemical sensor.* Langmuir, 2008. **24**: p. 4394-4398.

59. Kostovski, G., et al., *Nanoimprinted optical fibres: Biotemplated nanostructures for SERS sensing.* Biosens. Bioelectron., 2009. **24**: p. 1531-1535.

60. Rogers, K., *Bacteria and viruses*. 2011: Britannica Educational Publishing.

61. Boundless. *Boundless Biology: Introduction*. 04 Sep 2014 [cited 2015 22 Jan]; Available from: https://www.boundless.com/biology/textbooks/boundless-biology-textbook/cell-structure-4/eukaryotic-cells-60/introduction-313-11446/.

62. Boundless. *Boundless Biology: Components of Prokaryotic Cells*. 14 Jan 2015 [cited 2015 22 Jan]; Available from: https://www.boundless.com/biology/textbooks/boundless-biology-textbook/cell-structure-4/prokaryotic-cells-59/components-of-prokaryotic-cells-312-11445/.

63. Nelson, W.H., *Rapid microbiological analysis*. 1991: VCH Publishers.

64. Schuster, K.C., et al., *Multidimensional information on the chemical composition of single bacterial cells by confocal Raman microspectroscopy.* Anal. Chem., 2000. **72**: p. 5529-5534.

65. Leboffe, M.J. and B.E. Pierce, *A photographic atlas for the microbiology laboratory*. 1999: Morton Publishing Company.

66. Dasari, S.R., et al., *Gold nanoparticle based label-free SERS probe for ultrasensitive and selective detection of trinitrotoluene.* J. Am. Chem. Soc., 2009. **131**(38): p. 13806-13812.

67. Sylvia, J.M., et al., *Surface-enhanced Raman detection of 2,4-Dinitritoluene impurity vapor as a marker to locate landmines.* J. Am. Chem. Soc., 2000. **72**(23): p. 5834-5840.

68. Vo-Dinh, T., L.R. Allain, and D.L. Stokes, *Cancer gene detection using surface-enhanced Raman scattering (SERS).* J. Raman Spectrosc., 2002. **33**(7): p. 511-516.

69. Klonoff, D.C., *Continuous glucose monitoring.* Diabetes care, 2005. **28**(5): p. 1231-1239.

70. Talian, I. and J. huebner, *Separation followed by direct SERS detction of explosives on a novel black silicon mulifunctional nanostructured surface prepared in a microfluidic channel.* J. Raman Spectrosc., 2012. **44**.

71. Ivanova, E.P., et al., *Bactericidal activity of black silicon.* Nat. Commun. , 2013. **4**: p. 1-7.

72. Vu, T.K.T., et al., *Preparation of metal nanoparticles for surface enhanced Raman scattering by laser ablation method.* Adv Nat Sci Nanosci Nanotechnol. , 2012. **3**.

73. Polwart, E., et al., *Novel SERS-active optical fibers prepared by theimmobilization of silver colloidal particles.* Appl. Spectrosc, 2000. **54**(4).

74. Hildebrandt, P. and M. Stockburger, *Surface-enhanced resonance Raman spectroscopy of rhodamine 6G adsorbed on colloidal silver.* J. Phys. Chem., 1984. **88**(24): p. 5935-5944.

75. Driskell, J.D., et al., *The use of aligned silver nanorod arrays prepared by oblique angle deposition as surfaced enhanced Raman scattering substrates.* J. Phys. Chem. C, 2008. **112**: p. 895-901.

76. Jayawardhana, S., *Development of optical fibre chemical probes by oblique angle deposition*, in *Centre for Atom-Optics and Ultrafast Spectroscopy*2011, Swinburne University of Technology: Hawthorn.

77. Wagner, C.D., et al., *Handbook of X-ray photoelectron spectroscopy*. 1979, Minnesota: Perkin-Elmer Corporation.

78. Gao, X., et al., *Study of structure and optical properties of silver oxide films by ellipsometry, XRD and XPS methods.* Thin Solid Films, 2004. **455-456**: p. 438-442.

79. Nowak, R., et al., *XPS characterization of chromium films deposited from $Cr(CO)_6$ at 248 nm.* Appl.Surf.Sci, 1989. **43**: p. 11-16.

80. Lascovich, J.C., R. Giorgi, and S. Scaglione, *Evaluation of the sp2/sp3 ratio in amorphous carbon structure by XPS and XAES* Appl.Surf.Sci, 1991. **47**: p. 17-21.

81. Ho, K., A.F. Lee, and A. Bismarck, *Fluorination of carbon fibres in atmospheric plasma.* Carbon, 2007. **45**: p. 775-784.

82. Domke, K.F., D. Zhang, and B. Pettinger, *Enhanced Raman spectroscopy: Single molecules or carbon?* J. Phys. Chem. C, 2007. **111**(24): p. 8611-8616.

83. Yeo, B., et al., *A strategy to prevent signal losses, analyte decomposition, and fluctuating carbon contamination bands in surface-enhanced Raman spectroscopy.* Appl. Spectrosc, 2008. **62**(6).

84. Alexson, D.A., et al., *Metal-adsorbate hybridized electronic states and their impact on surface enhanced Raman scattering.* Chem. Phys. Lett., 2009. **477**: p. 144-149.

85. Gartia, M.R., Y. Chen, and G.L. Liu, *Photoluminescence and cathodoluminescence from nanostructured silicon surface.* Appl. Phys. Lett., 2011. **99**(151902): p. 1-3.

86. Kong, D.Y., et al., *Fabrication of silicon pyramid-nanocolumn structures with lowest reflectance by reactive ion etching method.* Jpn. J. Appl. Phys., 2013. **52**.

87. Tomita, N., Y. Kawabata, and S. Adachi, *Characterization of Si(111) surfaces treated in aqueous H_2SiF_6 solution.* Mater. Sci. Eng. B, 2000. **68**: p. 175-181.

88. Parker, J.H.J., D.W. Feldman, and M. Ashkin, *Raman scattering by silicon and germanium.* Phys. Rev., 1967. **155**(3): p. 712-714.

89. Li, B., D. Yu, and S.L. Zhang, *Raman spectral study of silicon nanowires.* Phys. Rev. B, 1999. **59**(3): p. 1645-1648.

90. Loosdrecht, M.C.M., et al., *The role of bacterial cell wall hydrophobicity in adhesion.* Appl. Environ. Microbiol., 1987. **53**(8): p. 1893-1897.

91. Hartley, J.S., S. Juodkazis, and P.R. Stoddart, *Optical fibers for minaturized surface-enhaced Raman scattering probes.* Appl. Optics, 2013.

92. Garg, S., et al., *Improvement in glycemic excursions with a transcutaneous, real-time continuous glucose sensor.* Diabetes care, 2006. **29**(1).

93. Marcuse, D., *Attenuation of unwanted cladding modes.* Bell System Technical Journal, 1971. **50**(8).

94. Kostovski, G., et al., *Sub-15nm optical fiber nanoimprint lithography: A parallel, self-aligned and portable approach.* Adv. Mater, 2011. **23**(4): p. 531-535.

95. Polemi, A., et al., *Local field enhancement of pillar nanosurfaces for SERS.* J. Phys. Chem., 2010. **114**(42): p. 18096-18102

96. Caldwell, J.D., et al., *Plasmonic nanopillar arrays for large-area, high-enhancement surface-enhanced Raman scattering sensors.* ACS Nano, 2011. **5**(5): p. 4046-4055.

97. Jayawardhana, S., et al., *Light enhancement in surface-enhanced Raman scattering at oblique incidence.* Photonic Sensors, 2012. **2**(3): p. 283-288.

98. Galeener, F.L., *The Raman spectra of defects in neutron bombarded and Ge-rich vitreous GeO2.* J. Non-Cryst. Solids, 1980. **40**(1–3): p. 527-533.

99. Murphy, D.B. and M.W. Davidson, *Fundamentals of light microscopy and electronic imaging*. 2013, New Jersey: John Wiley and Sons.

100. Scarmozzino, R., et al., *Numerical techniques for modeling guided wave photonic devices.* IEEE J. Sel. Top. Quant. Electron. , 2000. **6**: p. 150-162.

101. White, D.J. and P.R. Stoddart, *Nanostructured optical fiber with surface-enhanced Raman scattering functionality.* Opt. Lett., 2005. **30**(6): p. 598-600.

102. Joy, D.C. and C.S. Joy, *Low voltage scanning electron microscopy.* Micron. , 1996. **27**(3-4): p. 247-263.

103. Bergmans, L., et al., *Microscopic observation of bacteria: review highlighting the use of environmental SEM* Int. Endod. J., 2005. **38**: p. 775-788.

104. Efrima, S. and L. Zeiri, *Understanding SERS of bacteria.* J. Raman Spectrosc., 2008. **40**: p. 277-288.

105. Sengupta, A., M.L. Laucks, and E.J. Davis, *Surface-enhanced Raman spectroscopy of bacteria and pollen.* Appl. Spectrosc, 2005. **59**(8): p. 1016-1023.

106. Kahraman, M., et al., *Experimental parameters influencing surface-enhanced Raman scattering of bacteria.* J. Biomed. Opt., 2007. **12**(5).

107. Tamer, U., et al., *Gold-coated iron composite nanospheres targeted the detection of Escherichia coli.* Int. J. Mol. Sci, 2013. **14**: p. 6223-6240.

108. Cui, L., et al., *In situ study of the antibacterial activity and mechanism of action of silver nanoparticles by surface-enhanced Raman spectroscopy.* Anal. Chem., 2013. **85**: p. 5436-5443.

109. Wang, Y., K. Lee, and J. Irudayaraj, *Silver nanosphere SERS probes for sensitive identification of pathogens.* J. Phys. Chem., 2010. **114**: p. 16122-16128.

110. Kahraman, M., et al., *Layer-by-layer coating of bacteria with noble metal nanoparticles for surface-enhanced Raman scattering.* Anal. Bioanal. Chem, 2009. **395**: p. 2559-2567.

111. Majumdar, A. and H. Huang, *Development of an in-fiber white-light interferometric distance sensor for absolute measurement of arbitrary small distances.* Appl. Optics, 2008. **47**(15): p. 2821-2828.

112. Kostovski, G., P.R. Stoddart, and A. Mitchell *The optical fiber tip: An inherently light-coupled microscopic platform for micro- and nanotechnologies.* Adv. Mater, 2014: p. 1-23.

Publications

Some of the material presented in this thesis has appeared in the following publications and presentations.

Papers

Jennifer S Hartley, Saulius Juodkazis and Paul R. Stodart, *Optical fibers for miniaturized surface-enhanced Raman-scattering probes,* Appl. Opt., 2014. 52(34): p. 8388-8392.

G. Gervinskas, G. Seniutinas, S.Kandasamy, **J. S. Hartley**, P.R. Stoddart, N.F.Fahim, and S. Juodakazis, *Surface-enhanced Raman scattering sensing on black silicon,* Annalen der Physik, 2013. 525(12): p. 1-8.

R. Kubiliute, K. Maximova, A. Lajevardipour, J. Yong, **J. S. Hartley**, A. S. M. Mohsin, P. Blandin, J. W.M. Chon, A. H. A. Clayton, M. Sentis, P. R. Stoddart, A. Kabashin, R. Rotomskis, S. Juodkazis, *Ultra-pure, water-dispersed Au nanoparticles produced by femtosecond laser ablation and fragmentation,* International Journal of Nanomedicine, 2013. 8(1): p. 2601-2611.

Conference Proceedings

G. Gervinskas, P. Michaux, G. Seniutinas, **J.S. Hartley**, E.L.H. Mayes, R. Verma, B.D. Gupta, P.R. Stoddart, D. Morrish, N.F. Fahim, M.S. Hossain and S. Juodkazis, *Black-Si as a platform for sensing*, Proc. Of SPIE vol8923, 2013.

Conference Presentations

J.S. Hartley, S. Juodkazis, P.R. Stoddart, *Evaluation of optical fibres for surface-enhanced Raman scattering probes,* P.R Stoddart presented at the SPIE Micro+Nano Materials, Devices, and Applications conference (2013)

Pierrette Michaux, Gediminas Gervinskas, Gediminas Seniutinas, **Jennifer S. Hartley**, Paul R. Stoddart, Dru Morrish, Narges F. Fahim, Md. Sohrab Hossain, Saulius Juodkazis, *Black-Si as a platform for sensing*, co-author for presentation at SPIE Micro+Nano Materials, Devices, and Applications conference (2013).